

Hydrocephalus

A. RAYBAUD AND A. JAMES BARKOVICH

Embryology and physiology of CSF dynamics

Choroid plexuses and CSF formation

CSF circulation

CSF absorption

Mechanisms of hydrocephalus

Classical model: obstructive hydrocephalus

Greitz model: communicating hydrocephalus

Classification of hydrocephalus

Obstructive hydrocephalus

Communicating hydrocephalus

Clinical aspects of hydrocephalus

Fetal hydrocephalus

Postnatal hydrocephalus

Radiologic diagnosis of hydrocephalus

The tools

Fetal diagnosis of hydrocephalus

Postnatal diagnosis of hydrocephalus

Specific categories of hydrocephalus

Hydrocephalus resulting from excessive formation of CSF (choroid plexus papillomas)

Hydrocephalus secondary to intraventricular obstruction of CSF

Hydrocephalus secondary to extraventricular obstruction of CSF

Benign enlargement of the subarachnoid spaces in infants

Definition

Clinical manifestations

Imaging

Imaging of treated hydrocephalus and resulting complications

Radiologic assessment of third ventriculostomies

Shunt malfunctions

Shunt infections

Subdural hematoma formation

Slit ventricle syndrome

Imaging of intracranial hypotension

Other complications

Hydrocephalus may be defined morphologically as a process in which the cerebrospinal fluid (CSF) compartment is actively enlarged at the expense of the brain tissue. It is a common disorder in all age groups, especially so in children. The basic issue of hydrocephalus is relatively easy to understand. The ventricles progressively increase in size in conjunction with increasing head size and progressive compression and, eventually, loss of brain tissue. Some CSF must be diverted out of the head in order to preserve the brain. Establishing the diagnosis also is relatively simple in most cases such as increased ventricular size, effacement of the subarachnoid spaces, macrocephaly, and typically an obstruction somewhere along the CSF pathway (e.g., from a posterior fossa tumor or aqueductal stenosis). But some aspects of hydrocephalus are not so easy to understand. Is the ventriculomegaly due to increased intraventricular pressure? If so, why do the ventricles enlarge in communicating hydrocephalus when the "block" to CSF flow is in the subarachnoid spaces? Brain tissue is mainly water and, therefore, is not compressible other than some space provided by the compression of the vascular bed (<4% of the brain tissue) and effacement of the pericerebral spaces. In chronic aqueductal stenosis, it may take months or years for the ventricular size to increase. Therefore, the daily CSF production (estimated at 500 mL) must be somehow resorbed by cerebral parenchyma; why do we see an increase in ventricular size? The best answer (for now) is that the morphological pattern that we call hydrocephalus is probably the end result of many different processes; accordingly, the imaging and pathologic manifesta-

tions of hydrocephalus vary considerably. In this chapter, we discuss many of these processes. In addition, we show that the degree of dilation of the CSF pathways and the amount of damage to the brain depend upon the cause of hydrocephalus, its severity, and the age of the patient at the time when the hydrocephalus develops.

■ EMBRYOLOGY AND PHYSIOLOGY OF CSF DYNAMICS

Closure of the neural tube in man occurs by about 28 postconceptional days (see Chapters 5 and 9). Certain portions of the central lumen of the neural tube then constrict, while others expand to form the basic pattern of the ventricular system such as enlargement of prosencephalic (forebrain), mesencephalic (midbrain), and rhombencephalic (hindbrain) vesicles. Some midline dorsal meningeal mesoderm invaginates into the lumen of the fourth ventricle during the second gestational month followed by similar invaginations into the lateral and third ventricles; these invaginations form the choroid plexus of the ventricular system and secrete the early CSF (1,2). Initially, the plexuses are large relative to the size of the lateral ventricles, filling approximately 75% of the ventricular lumen during the third month of gestation. The size of the choroid plexus relative to the lateral ventricle gradually diminishes as the brain and ventricular system grow.

Choroid Plexuses and CSF Formation

The choroid plexuses have several functions. They secrete multiple proteins that are postulated to stimulate and modulate the growth of progenitor cells in the ventricular zone of the germinal matrices during development (see Chapter 5) (3). They act on diverse chemosensitive areas of the ependyma throughout life (4); these small areas in the walls of the third and fourth ventricle are called the circumventricular organs; they contain specialized ependymal cells called tanycytes that exchange interfaces allowing the brain, mostly the hypothalamus, to react in response to changing CSF composition. In certain hydrocephalic animal models, the progenitor cells in the ventricular walls are less sensitive to the proliferative effects of certain growth factors than controls. Thus, fetal hydrocephalus may adversely affect brain development (3).

The extracerebral CSF spaces appear near the end of the embryonic period, resulting from the expansion of the meningeal extracellular space as the gelatinous primitive mesenchyme that surrounds the brain (meninx primitiva) undergoes a systematic degeneration to become the fluid-filled leptomeninges (5,6). The communication between ventricular and subarachnoid CSF results from thinning and opening of the inferior midline portion of the fourth ventricular roof to create the foramen of Magendie during the 11th or 12th gestational week, followed by opening of the lateral foramina of Luschka (7,8). The function of CSF in the embryo is not completely understood. However, there is essentially no intrinsic brain vasculature when the plexuses develop (9,10), and it is postulated that important chemicals enter the CSF from the blood vessels of the choroid plexuses and circumventricular organs; these chemicals may be vital in controlling the early development of the nervous system along the entire length of the neural tube (11).

In the adult, CSF is secreted at a rate of approximately 0.3 to 0.5 mL/min, resulting in a daily secretion of approximately 500 mL. The choroid plexus produces an estimated 60% to 90% of CSF, with the other 10% to 40% most likely coming from the parenchyma of the brain and spinal cord (13,14). CSF secretion by the choroid plexus uses ATP hydrolysis to generate unidirectional flux of sodium, chloride, and bicarbonate ions across the plexus epithelium, driving the movement of water by osmosis (4). The total volume of CSF was classically assumed to be 40 to 60 mL in infants, 60 to 100 mL in children, and approximately 150 mL in adults (12). However, studies using volumetric magnetic resonance imaging (MRI) to quantify the CSF volume have found higher values, with a volume of ~150 mL in the intracranial subarachnoid spaces and 100 to 120 mL in the spinal subarachnoid spaces (15). In addition, the interstitial fluid of the central nervous system is estimated to contain 100 to 300 mL of CSF (4). CSF and extracellular fluid in the brain and spinal cord are in continuity with each other, and exchanges occur constantly across the pial membrane, the Virchow-Robin perivascular spaces, and the ependyma (16).

CSF Circulation

Classic teaching suggests that CSF flows from the cerebral ventricles through the ventricular foramina and into the subarachnoid spaces, ultimately being absorbed into the venous system (13,14); this movement of water molecules through the ventricles and cisterns is referred to as bulk flow; it results from a hydrostatic pressure gradient between the site of its formation (arterial) and its site of absorption (venous) (17,18). Another mechanism, the coordinated beating of ependymal cells, creates a current of CSF along the walls of the cerebral ventricles that likely contributes to bulk flow (19,20). CSF leaves the lateral ventricles via the foramina of Monro and then circulates

through the third ventricle, into the Sylvian aqueduct and the fourth ventricle. From the fourth ventricle, CSF courses through the foramina of Magendie and Luschka into the cisterna magna and the basilar cisterns, respectively. It is estimated that 80% of flowing CSF then enters the cisternal system, flowing into the suprasellar cistern and cistern of the lamina terminalis, the ambient and superior cerebellar cisterns, and eventually flowing over the cerebral convexities. The remaining 20% of CSF undergoing bulk flow initially enters the spinal subarachnoid space but is eventually recirculated into the cerebral subarachnoid space (21), although some (10%–15%) is absorbed in the spine at the level of the nerve root sheaths (22–24).

Although the concept of bulk flow in the ventricular system is generally accepted and serves as an adequate model for most cases of hydrocephalus, it fails to explain some cases of progressive ventriculomegaly (25). It has been demonstrated that the CSF "flow" through the subarachnoid spaces is quite slow (~35 mL/min) and that subarachnoid CSF motion is nearly entirely pulsatile; that is, the water molecules pulsate back and forth, driven by expansion of the intracranial blood vessels as they fill with blood after each cardiac systole, but very few CSF water molecules actually follow the rules of bulk flow and actually circulate through the subarachnoid space from the outlet foramina of the fourth ventricle to the arachnoid granulations (26). Thus, *it appears that the circulation of CSF results from the combination of two processes*. The secretion-absorption process (bulk flow) is slow and passive, particularly in the subarachnoid spaces, and may be compared to the lymphatic circulation. The separate, pulsatile process is fast (~60–80 pulsations/min at rest) and is driven by pressure waves produced by enlargement of the intracranial arteries as the blood flows into them after each cardiac systole. These pulsations continuously mix the CSF. As the cranial cavity is rigid and the brain tissue not compressible, the pressure waves need to be damped: the force transmitted through the subarachnoid space via CSF is damped by the expansion of the highly elastic spinal thecal sac, while the force transmitted through the vascular system is damped by expansion of the venous sinuses. This dual dampening process constitutes the compliance of the system. The loss of thecal elasticity (or restriction of the access to the spinal subarachnoid space) results in less attenuation of the CSF pressure wave; this force then is fully exerted upon the brain tissue. If the venous pressure is increased, the dampening of the force in the vascular system is lost and the force of the vascular pressure wave is exerted upon the parenchyma. In both instances, the pressure waves cause a progressive loss of brain tissue. Another factor to consider is the anatomic organization: the arteries surround the brain, which surrounds the ventricles. Therefore, the force of each arterial pulsation is transmitted centrifugally via the parenchyma to the ventricle, pushing CSF toward the cisterna magna; it is only partly counter-balanced by the small pulsations of the intraventricular choroid plexuses. Finally, the transmission of the pressure wave after each pulsation is extremely rapid across the noncompressible CSF but is slower through the more elastic vascular bed; as a consequence, the systolic pressure wave results in constriction of the outlets of the bridging veins before pushing blood into the capillary bed. As a result, the vascular bed expands (through the so-called "bagpipe" effect), increasing the perfusion pressure and, consequently, cerebral perfusion (25).

In summary, pressure waves from arterial pulsations are important for normal CSF flow and cerebral perfusion; however, these pressure waves need to be damped for the system to function properly. The compliance of the system depends on the venous pressure and on the elasticity of the dura. If the venous pressure is elevated, or if the pressure waves do not expand the elastic dura, the force of a pressure wave is not dampened and it pulsates against the parenchyma at full strength. This

causes compression of the cerebral tissue, alterations of axonal function and of cerebral blood flow (CBF), and progressive brain injury.

Neonates and young infants have open fontanelles and sutures, so both the cranial and the spinal dura contribute to this elasticity, whereas in the older child and adult, the cranial dura is attached to a rigid calvarium, so only the spinal dura (long and surrounded by fat and veins) contributes to elasticity. Thus, in older children, obstruction of the foramen magnum (which reduces the total elasticity of the CSF-containing spaces) and any other process that reduces the dampening of the pressure wave (arachnoid fibrosis and loculation, spinal cord tumor, suprasellar cyst, high venous pressure) favors the development of hydrocephalus by reducing the dampening efficacy of the system. Any factor that increases the pressure wave (any pulsating mass in the CSF spaces) may also compromise the equilibrium if the compliance reaches its limit, as was demonstrated experimentally (27).

CSF Absorption

According to the most generally accepted model, CSF absorption occurs mainly through the arachnoid villi, evaginations of the subarachnoid space into the lumen of the dural and venous sinuses. This model proposes that the villi behave as one-way valves that have an opening pressure of between 20 and 50 mm of water; drainage is determined by hydrostatic pressure differences between CSF and the venous sinuses (13,14,17). However, several authors have suggested that approximately half of the CSF may drain via other routes. As the CSF space and extracellular spaces are in continuity via the ependymal and pial surfaces and the perivascular spaces, a significant part of the CSF is presumed to be absorbed by the intracerebral veins, possibly even as the primary mode of absorption (28–31). The lymphatic system probably plays a significant role, particularly through the cribriform plate into the lymphatic vessels located in the nasal submucosa (32–34), in the perineural spaces (13,35–37), and through the optic nerves into the orbital lymphatics (38). The anatomical organization of the dural clefts described where cortical veins join the sagittal and cavernous sinuses, suggests that they could be another pathway of egress of CSF into the dural sinuses (39,40). Still others contend that the brain, rather than absorbing CSF, acts as a conduit for fluid to move from the ventricles into the subarachnoid spaces or into the prelymphatic channels of the blood vessels (41). CSF may nourish cerebral vessels through pathways in the adventitia that may be analogous to systemic vasa vasorum. Another possible route of CSF absorption is through the epithelium of the choroid plexus to the fenestrated capillaries (4) and ultimately to the Galenic venous system. Oi and Di Rocco refer to these routes as the "minor pathways" of CSF absorption and to the classic route via the subarachnoid spaces and arachnoid granulations as the "major pathway" (42). Moreover, they and others suggest that CSF absorption in neonates and infants is predominantly via the so-called minor pathways and that the major pathway only becomes an important route of CSF absorption during the middle or end of the first postnatal year (33,42). This proposal is supported by the observation that third ventriculostomy is less effective in neonates and young infants than in older children and adults and becomes progressively more effective with maturation (42). Others suggest that the "minor pathways" are recruited in neonates and infants only as auxiliary mechanisms when intracranial pressures are high (arachnoid villi and granulations are not formed in neonates and are unlikely to be involved in CSF resorption) (33,42). It is likely that many or all of the mechanisms described above function in CSF absorption, some as primary pathways and others as alternate pathways. It is also likely that all of these pathways are involved in the pathophysiology of hydrocephalus when drainage of CSF through them becomes impaired.

MECHANISMS OF HYDROCEPHALUS

Classical Model: Obstructive Hydrocephalus

In this concept, hydrocephalus results from an imbalance between CSF production and absorption. The rate of CSF production tends to be fairly constant within the brain and, with the exception of hydrocephalus secondary to choroid plexus papillomas, overproduction of CSF is not a cause of hydrocephalus. (Some authors suggest that diffuse villous hyperplasia is a very rare cause of hydrocephalus secondary to overproduction (43–45); others claim that these cases represent multiple choroid plexus papillomas (46); if choroid plexus hyperplasia exists, it is very rare and will not be discussed further in this text.) Therefore, hydrocephalus is almost always the result of impaired absorption of CSF. The diminished absorption may result from a blockage of CSF flow within the ventricular system, the cisterna magna, the basilar cisterns, or the cerebral convexities. Alternatively, diminished absorption may result from blockage of the arachnoid villi or the lymphatic channels associated with the cranial nerves, spinal nerves, and adventitia of the cerebral vessels. As the intracranial pressure increases, CSF may be absorbed through the arachnoid membrane, the stroma of the choroid plexus, or may pass through the extracellular space of the cortical mantle to reach the medullary veins or the brain surface (transendymal absorption of CSF) (13,36,47). Because these new absorption pathways open at increased pressure, a new equilibrium can be established between CSF production and absorption at the higher intracranial pressure. This situation is referred to as compensated hydrocephalus.

Stenotic or obstructive changes in small blood vessels in the compressed periventricular white matter of hydrocephalic patients cause neuronal and astrocytic swelling in the deep gray matter and spongiform atrophic changes in the white matter of the cerebral hemispheres (46,48–51). The blood flow and cerebral metabolic rate, as measured by uptake of ¹⁸F-fluorodeoxyglucose on positron emission tomography, are reduced in the periventricular white matter in hydrocephalic infants (52). Blood flow is particularly affected in the distribution of the anterior cerebral arteries, leading to ischemic injury of the basal forebrain and medial cerebral hemispheres (53). Moreover, the cells that normally cover the ependymal surface of the ventricular wall disappear in hydrocephalic states (54), ependymal cells in the wall of the ventricle stretch and degenerate (46), the choroid plexus become fibrotic (48), and the septum pellucidum undergoes fenestration (46).

Greitz Model: Communicating Hydrocephalus

As mentioned above, an interesting new model of CSF dynamics and the development of hydrocephalus has been proposed in a series of articles by Greitz et al. (25,26,30,31,55,56). CSF pulsations have been observed from the early days of neuroradiology (57), and have been explained by the transmission of pulsations from intracranial arteries. These arterial pulsations, occurring in a rigid skull that is filled almost entirely with incompressible water, transmit blood through capillary beds and toward the venous sinuses while, at the same time, displacing some CSF into the spinal subarachnoid spaces, which is encompassed by more elastic, distensible dura that expands to absorb and dampen the pressure waves (see Section "CSF Circulation" above). The CSF displacement is greatest at the craniocervical junction, where it has been measured at 6 mm per stroke in normal individuals, and at 3 mm in communicating hydrocephalus (15). If the spinal dural sac does not expand to dampen the CSF pressure wave (because, e.g., the foramen magnum is obstructed or the spinal meninges have lost their elasticity, or if the dampening through the vascular bed is prevented by high venous pressure, or if the intraventricular choroid plexus pulsates)

an increased, the force of the pulsating arteries is exerted upon the brain parenchyma. This model leads to three main conclusions:

- Even if nothing opposes the bulk flow of CSF, hydrocephalus may develop because the craniospinal meningeal compliance is lost (communicating hydrocephalus).
- Even in cases with obstruction of the bulk flow pathway (obstructive hydrocephalus), part of the problem comes from the fact that the obstruction restricts the compliance of the system by not allowing the pressure waves to reach the spinal dura.
- Even with no obstruction in the ventricles, increased pulsation waves within the ventricles (e.g., from choroid plexus papilloma or choroid plexus hyperplasia) may overcome the compliance of the system and generate hydrocephalus. (Such a situation has been created experimentally (27).)

Thus, normal volume and elasticity of the spinal dura are needed for proper function of the system in older children and adults. As mentioned above, the area of the spinal meninges is small in relation to the volume of the cranium during the first months of life. From the point of view of compliance, however, the increased elasticity of the skull due to open sutures and fontanelles compensates for small size of the spinal canal. The situation in fetuses is not well understood, as the situation is compounded by high pressure of the surrounding amniotic fluid and a blood circulatory system that is different from the postnatal one.

While the bulk flow cannot be detected by noninvasive means, MR phase-contrast imaging has the ability to evaluate the direction and velocity of CSF flow. Quantitative data in healthy adult individuals have been measured (25). Assuming a CBF of 60 mL/100 g/min, at a heart rate of 60 beats/min, the volume of the arterial stroke is 3.6 mL for a 1500 g brain. Of this, 90% flows directly through the vascular bed to the veins, and the expansion of the intracranial arteries corresponds to 1.5 mL (the sum of the systolic stroke volume of CSF displaced at the foramen magnum—0.8 mL—and of blood displaced into the venous sinuses—0.7 mL). The systolic expansion of the brain capillaries is minimal (0.03 mL, only 2% of the arterial expansion) but it is transmitted inwards to the ventricles, and in the aqueduct, the displaced volume of CSF is correspondingly 0.03 mL per beat (25). Given the small section of the aqueduct, this results in a measurable CSF systolic velocity peak. In another report, the MR-measured systolic peak aqueductal CSF velocity has been evaluated at 3.4 to 4.1 cm/s in normal volunteers, corresponding to a mean CSF flow of 0.02 to 0.03 mL/s (58). Using a similar MR phase-contrast imaging method in volunteers also, another group could measure the CSF production rate and found $0.305 \text{ mL/min} \pm 0.145$ (equivalent to about 430 mL/d), which is in good agreement with the data obtained with more invasive methods (58). Using these basic concepts, Greitz et al. have reconsidered the way of approaching hydrocephalus and have devised a new model that differs from the traditional one. These concepts may be useful in understanding cases of hydrocephalus that cannot be explained

by the traditional models. Examples of the utility of these concepts are discussed in the section on "Normal Pressure Hydrocephalus."

CLASSIFICATION OF HYDROCEPHALUS

Although the pathogenesis of hydrocephalus is complex, it is useful from a clinical and therapeutic point of view to differentiate between obstructive and communicating hydrocephalus (Table 8-1).

Obstructive Hydrocephalus

Hyperacute obstructive hydrocephalus develops in hours from a sudden occlusion of the CSF pathways, with rapid increase of the intraventricular pressure. This may occur after severe head trauma, shunt obstruction or, rarely, granulomatous meningitis. The brain parenchyma has no time to accommodate the increase in ventricular pressure by loss of tissue, so the ventricles are rounded but minimally increased in size, making morphological diagnosis difficult. As neither the parenchyma nor the CSF is instantaneously compressible, the only part of the brain in which volume is lost is the vascular bed. This hypoperfusion is worsened by the fact that any expansion of the brain, even slight, may compress superficial draining veins against the calvarium, while the deep veins are compressed by high intraventricular pressure, resulting in further increase of parenchymal and intracranial pressure. This vicious circle leads to absence of perfusion of the brain. Only tapping the ventricles allows relief of the ventricular tamponade.

Progressively acute obstructive hydrocephalus typically develops over weeks or months, usually from the growth of an intraventricular tumor. CSF outflow is progressively impeded, due to impaired bulk flow, so the ventricles progressively enlarge. If the head enlarges as well, the cerebral volume may be partly preserved; if not, the ventricular enlargement will be at least partially due to loss of brain tissue, with the degree of tissue loss depending on the age of the patient and on the speed of onset of hydrocephalus. The increased ventricular pressure results in compression of the subependymal veins; this, in turn, prevents the normal absorption of interstitial fluid from the deep white matter, resulting in development of periventricular interstitial edema and (often) parenchymal injury, but does not reflect any increased absorption by the parenchyma (50). If not treated, progressively acute hydrocephalus will cause brain herniation and/or circulatory arrest.

Chronic obstructive hydrocephalus can be a result of many causes, such as chronic aqueductal stenosis or leptomeningitis. This chronic condition causes only mild clinical signs of increased intracranial pressure (i.e., headaches) and no periventricular interstitial edema, as the secretion of CSF is presumably compensated by sufficient fluid absorption via capillaries. However, the ventricles and, typically, the skull slowly enlarge and the brain slowly loses volume over the years. An acute decompensation may occur, after trauma for example. The terms "arrested" and "compensated" hydrocephalus are used when no

TABLE 8-1 Classification of Obstructive Hydrocephalus

	Timing	Vasc. Bed	Ventr. Size	Interst. Edema	Skull	Outcome
Hyper-acute	Sudden	↓	=	No	=	Arrest
Progressive	Weeks/months	=	↑	Yes	=/↑	Decompensates
Chronic	Years	=	↑	No	↑	Slow ↑
Arrested	Years	=	↑	No	↑/=	Stable?

progression can be detected clinically or by imaging over long periods of time; this seems to be an uncommon occurrence.

Communicating Hydrocephalus

The term communicating hydrocephalus describes cases in which no clear obstruction to CSF flow can be demonstrated; no morphologic finding explains the development of progressive ventricular dilation with clinical symptoms of hydrocephalus and good response to CSF diversion. Commonly assumed to be related to obstruction or fibrosis of the arachnoid granulations, it is better explained by the Greitz model introduced in Section "Greitz Model: Communicating Hydrocephalus" (25). As explained earlier, free movement of the CSF is impaired by arachnoid pathology (e.g., fibrosis from a previous history of meningeal infection or bleed, or brain trauma) or impaired elasticity of the spinal dura. As a result, the propagation of pulse pressure waves through the CSF is impaired, and their force is exerted against the brain tissue. It is tempting to extend this concept to other disorders such as segmental restriction of the meningeal space (significant spinal degenerative changes in adults, achondroplasia or mucopolysaccharidoses in children, spinal cord tumors) or the Chiari I deformity where the obstruction of the foramen magnum may be considered a CSF pathway obstruction that causes a loss of compliance. This new concept brings into question the use of the term "normal" pressure hydrocephalus, as many physiological studies have shown in adults that the amplitude of the arterial-CSF pulsation pressure wave (if not the mean pressure) is characteristically increased (59–62).

CLINICAL ASPECTS OF HYDROCEPHALUS

The most important and most consistent clinical finding in pediatric hydrocephalus is an excessive rate of head growth. A large head circumference in a child is not, in itself, of concern (it actually allows some preservation of brain volume). Serial head circumference measurements showing an excessive rate of head growth as compared with normal standards, however, should raise clinical suspicion of developing hydrocephalus. Several factors influence the clinical course of hydrocephalus. The most important of these are the age of the patient at the onset of hydrocephalus and the duration of the disease (younger age and longer duration imply worse prognoses). The rate of increase of intracranial pressure and the presence of associated structural lesions are also associated with poor prognosis (63,64).

Fetal Hydrocephalus

Ventriculomegaly is a common indication for fetal MRI or level 3 fetal sonograms (65–67). Fetuses with small heads are unlikely to have hydrocephalus. However, fetal hydrocephalus is not always associated with macrocephaly in utero and, thus, normocephalic fetuses may have hydrocephalus. Associated malformations of the central nervous system (CNS) or non-CNS viscera are identified in 41% to 78% of fetuses or neonates in whom hydrocephalus is detected (68,69). The most common of these are myelomeningoceles, aqueductal stenosis, and callosal anomalies. Excluding myelomeningoceles, Garel et al. (69) found brain abnormalities in 44% of fetuses with ventriculomegaly, with many causes including callosal anomalies (9.5%), ischemic injury (7%), and posterior fossa anomalies (7%). If treated *in utero* (by cephalocentesis or ventriculo-amniotic shunt), only 38% to 55% of survivors will have normal cognitive function (68,70) and average survival is a little more than 4 years. It is not known whether the associated brain damage is the result of the presence of hydrocephalus in the developing brain, whether a prenatal injury may have caused both the hydrocephalus

and the associated malformation, or whether the hydrocephalus may merely be one component of a malformation syndrome.

Postnatal Hydrocephalus

Prior to the age of 2 years, hydrocephalus is almost always accompanied by progressive head enlargement. The Chiari II malformation, aqueductal stenosis, and aqueductal gliosis account for 80% of hydrocephalus in this age group, and 60% of all hydrocephalus regardless of age (48,71). Other relatively common causes of hydrocephalus in infancy include intrauterine, perinatal, and neonatal infection, and perinatal/neonatal hemorrhage. Rare causes of hydrocephalus include other malformations, congenital midline tumors, choroid plexus papillomas, and vein of Galen malformations (48).

In infants with hydrocephalus, the head tends to grow at an abnormal rate, producing macrocephaly within the first few months of life. The forehead is disproportionately large (frontal bossing), the skull is thin, the sutures are separated, the anterior fontanelle is tense, and the scalp veins are dilated. Ocular disturbances are frequent and include paralysis of upward gaze, abducens nerve paresis, nystagmus, ptosis, and diminished pupillary light response. Spasticity of the lower extremities is common, resulting from disproportionate stretching and shortening of the corticospinal axons that arise from the medial parts (leg area) of the motor cortex. These axons have a longer distance to travel and are more directly exposed to pressure from the dilated lateral ventricle than the more lateral corticospinal and corticobulbar axons that supply the upper extremities and the face (48,72,73).

Children older than 2 years tend to present with neurological symptoms resulting from increased intracranial pressure or with deficits referable to the primary lesion; these symptoms occur due to significant changes in the head size. The most common cause of hydrocephalus in this age group are posterior fossa neoplasms (see Chapter 7) and obstruction of the aqueduct. Although each of these specific lesions that result in hydrocephalus have some special features, certain clinical characteristics are common to all hydrocephalic patients. In most patients, the increased intracranial pressure results in an early morning headache that improves after being upright for a while (allowing CSF to re-equilibrate). Papilledema and strabismus are frequent. Pyramidal tract signs are more marked in the lower extremities, as described above. Hypothalamic-pituitary dysfunction is probably caused by compression of the hypothalamus, pituitary stalk, or pituitary gland by the enlarged anterior recesses of the third ventricle. Affected patients may present with small stature, obesity, gigantism, amenorrhea or menstrual irregularities, hypothyroidism, or diabetes insipidus. Perceptual and motor deficits and visual spatial disorientation result from stretched axons of the parietal and occipital lobes around the dilated posterior horns of lateral ventricles (48,72,73). Cognitive disorders may also result from compression of the hippocampus and stretching of the fornices and hippocampal commissure.

RADIOLOGIC DIAGNOSIS OF HYDROCEPHALUS

The Tools

Magnetic Resonance Imaging

MRI is the best tool to investigate hydrocephalus, its causes and consequences. The imaging protocol must be adapted to the patient, but thin section sagittal T1, T2FSE, and FIESTA/CISS sequences show the midline, while coronal T2 best shows the morphology of the lateral ventricles (especially the temporal horns), and axial FLAIR shows parenchymal lesions and interstitial edema (Fig. 8-1). Signal and

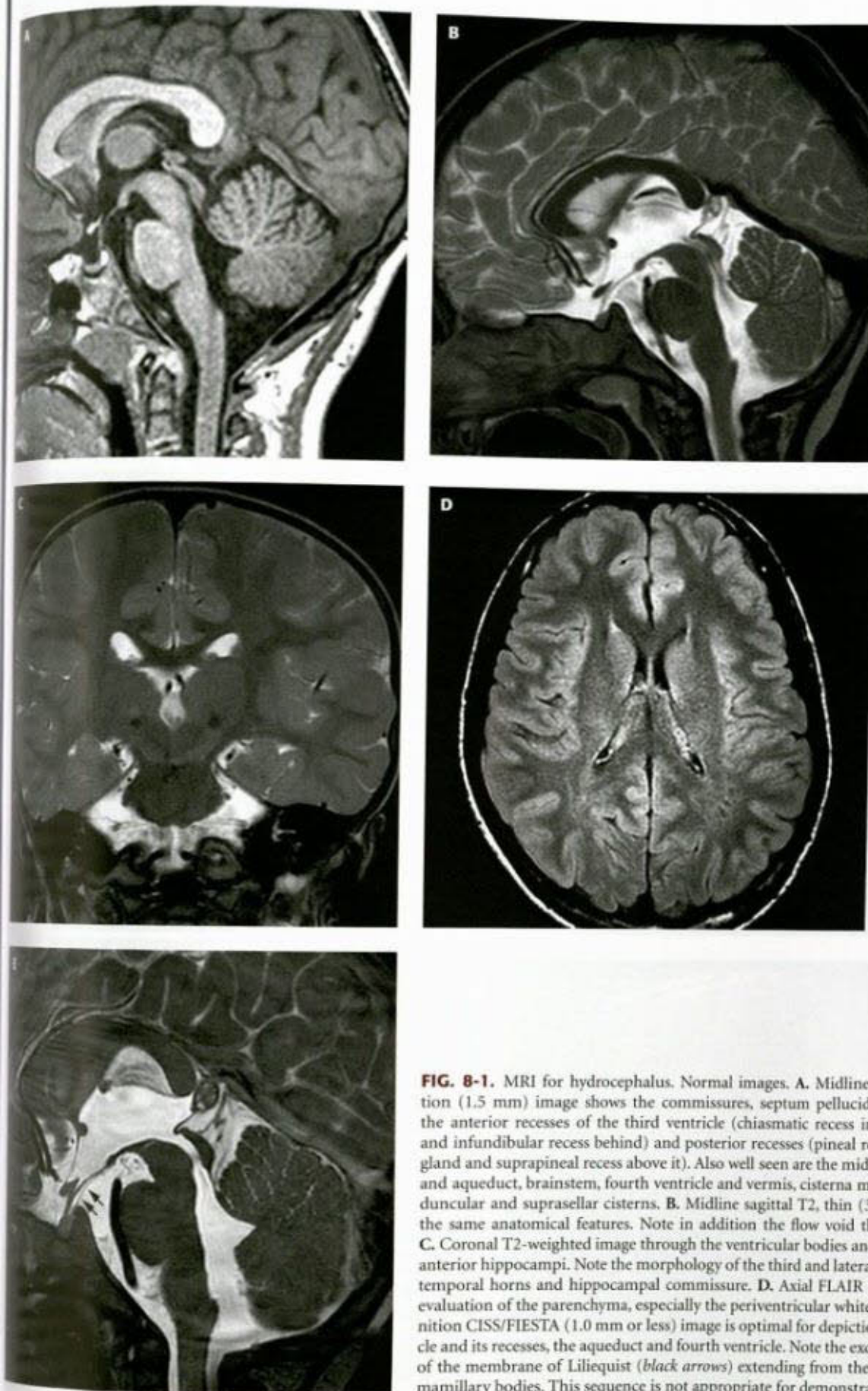


FIG. 8-1. MRI for hydrocephalus. Normal images. **A.** Midline sagittal T1, thin section (1.5 mm) image shows the commissures, septum pellucidum and fornix. Note the anterior recesses of the third ventricle (chiasmatic recess in front of the chiasm and infundibular recess behind) and posterior recesses (pineal recess below the pineal gland and suprapineal recess above it). Also well seen are the midbrain with tectal plate and aqueduct, brainstem, fourth ventricle and vermis, cisterna magna, basilar, interpeduncular and suprasellar cisterns. **B.** Midline sagittal T2, thin (3.0 mm) image shows the same anatomical features. Note in addition the flow void through the aqueduct. **C.** Coronal T2-weighted image through the ventricular bodies and temporal horns and anterior hippocampi. Note the morphology of the third and lateral ventricles, especially temporal horns and hippocampal commissure. **D.** Axial FLAIR image is excellent for evaluation of the parenchyma, especially the periventricular white matter. **E.** High definition CISS/FIESTA (1.0 mm or less) image is optimal for depiction of the third ventricle and its recesses, the aqueduct and fourth ventricle. Note the exquisite demonstration of the membrane of Liliequist (*black arrows*) extending from the dorsum sellae to the mamillary bodies. This sequence is not appropriate for demonstrating the flow voids.

due to rapid CSF flow are seen well on T2FSE sequences; these signal voids can be useful to demonstrate patency of interventricular connections (foramina or aqueduct) or a third ventriculostomy. Remember, however, that although absence of a signal void suggests foraminal occlusion, foraminal narrowing without occlusion increases the velocity and accentuates the signal void. High-definition steady-state (CISS/FIESTA) imaging better demonstrates morphology; stenosis of the aqueduct, cysts and abnormal intraventricular or arachnoid membranes are seen much better than on conventional sequences (Figs. 8-1E and 8-2A).

Contrast administration is useful initially to characterize the cause of hydrocephalus (tumor tissue or infection) but is not useful for following the hydrocephalus itself. Some have safely used intracisternal contrast (74), but it has failed to gain acceptance as the trend in brain imaging now is toward minimal invasiveness. Magnetic susceptibility T2* imaging may demonstrate blood and blood residue. Other MR sequences are not generally useful in the initial work-up.

MR is not commonly used for follow-up imaging of hydrocephalus, as the need for sedation in young children and the relatively limited access to MR have resulted in CT being the usual study of choice.

(As discussed in Chapter 1, a low dose CT technique, which does not allow assessment of subtle parenchymal lesions, is safer for the pediatric patient who will likely have many imaging exams during their lifetime.) "Fast" MR-scanning (using single-shot, ultrafast imaging sequences such as those used in fetal imaging) has been suggested as a potentially useful sequence, as it alleviates the need for sedation/anesthesia and the repetitive exposure to significant ionizing radiation (75). Although these heavily weighted T2 sequences are adequate for assessing the ventricular/cisternal size and morphology, they have poor sensitivity and specificity for parenchymal changes. For various reasons (not easy to implement, limited diagnostic yield, lack of sensitivity/specificity, limited access to MR, necessity to reset the magnetic pressure valve), it has failed to gain wide acceptance.

Occasionally, hydrocephalus may be caused by, or associated with, a spine lesion (tumor or malformation or syringohydromyelia) rather than an intracranial one. The protocol for spinal MRI in these cases should include sagittal T2 sequences of the whole spine, if needed, and T2, and sagittal T1 and possibly contrast-enhanced T1 sequences to be acquired through any region of interest. Use of fat suppression allows better recognition of soft tissue mass, fluid or blood.

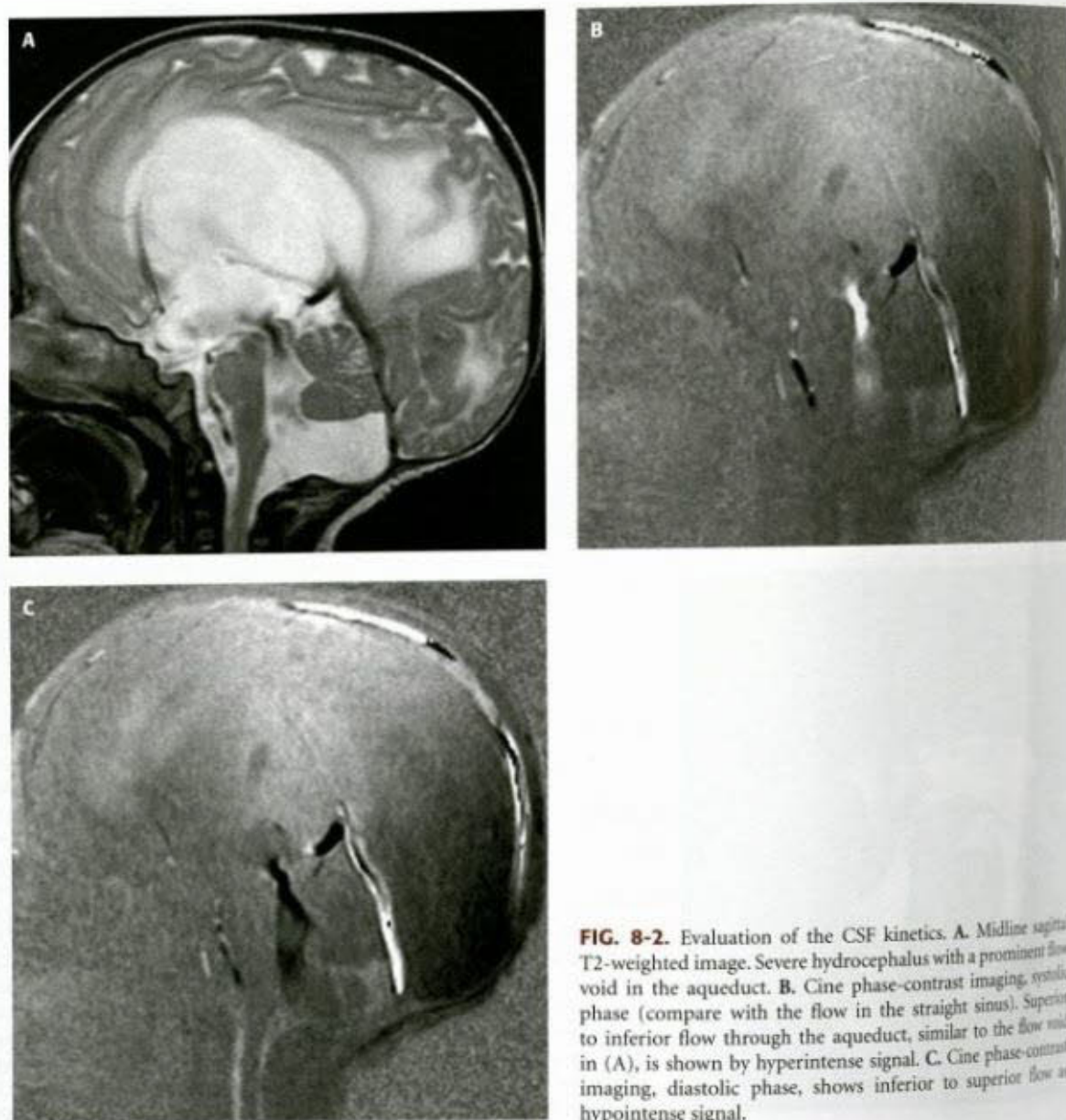


FIG. 8-2. Evaluation of the CSF kinetics. **A.** Midline sagittal T2-weighted image. Severe hydrocephalus with a prominent flow void in the aqueduct. **B.** Cine phase-contrast imaging, systolic phase (compare with the flow in the straight sinus). Superior to inferior flow through the aqueduct, similar to the flow seen in (A), is shown by hyperintense signal. **C.** Cine phase-contrast imaging, diastolic phase, shows inferior to superior flow as hypointense signal.

MR techniques are also able to provide physiologic data on brain metabolism (single- or multivoxel ^1H MR spectroscopy) and brain perfusion (by either arterial spin-labeling or dynamic susceptibility-weighted contrast perfusion imaging, see Chapter 1). Qualitative CSF flow is often demonstrated on routine MR sequences (76–78). On routine spin-echo MR scans, dynamic CSF flow can be detected by signal loss in areas of rapid or turbulent flow (76,77). By use of certain techniques, such as gradient echo and FLAIR, rapidly moving CSF can be made to appear bright while keeping the signal of stationary or slowly flowing CSF dark; the patency of the aqueduct can be assessed in this way (79). Special techniques that take advantage of the relative change in phase angle of moving spins can be used to quantify the flow of CSF through the foramina of Monro, aqueduct, foramen of Magendie, or brainstem cisterns (Fig. 8-2B and C) (80–82). However, CSF motion is dependent on so many physiological factors—arterial stroke (related to blood pressure, perfusion pressure), distal vascular compliance (vascular status, pO_2 , and pCO_2), meningeal compliance, CSF pressure, individual anatomy, etc.—that quantification in

individual patients is rarely useful; such measurements are only valid when obtained from groups of subjects. Practically speaking, functional methods are not useful for individual diagnoses and will not be discussed in this chapter.

CT Scanning

Together with MRI, CT is the most commonly used modality to evaluate hydrocephalus. It is fast and simple and data is easily reformatted in multiple planes (Fig. 8-3). Periventricular interstitial edema is readily apparent on CT, and subarachnoid blood may appear better on CT than on MR. Mass effects responsible for the hydrocephalus are easily recognized and contrast enhancement helps in the characterization of the pathology. However, the diagnostic yield and the versatility of CT are much less than those of MR, and CT can expose children to significant doses of ionizing radiation (see Chapter 1). In our practices, initial evaluation of the brain and CT is used for follow-up assessment only, with implementation of a low-dose technique that limits evaluation mostly to assessment of ventricular size (see Chapter 1).

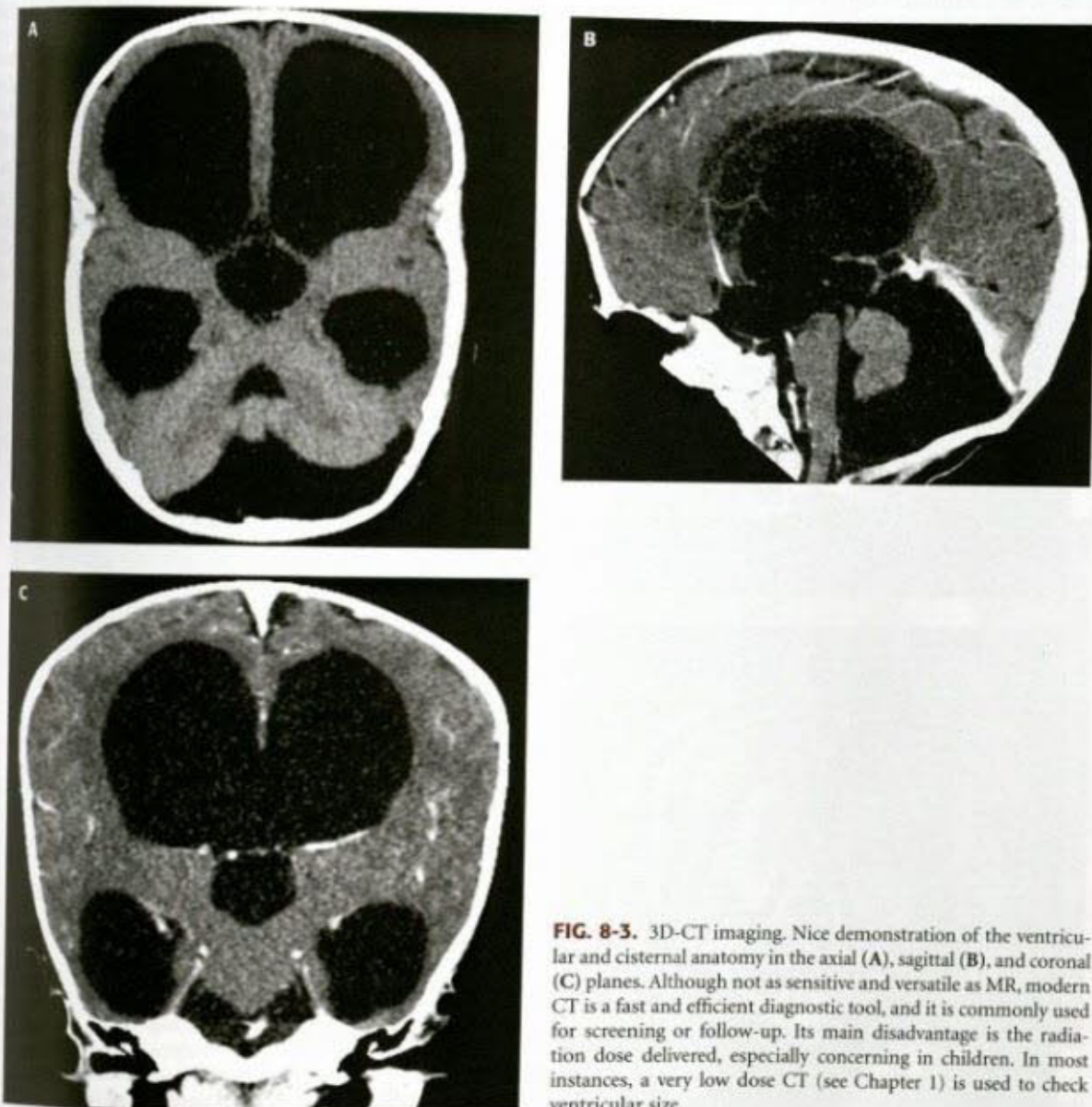


FIG. 8-3. 3D-CT imaging. Nice demonstration of the ventricular and cisternal anatomy in the axial (A), sagittal (B), and coronal (C) planes. Although not as sensitive and versatile as MR, modern CT is a fast and efficient diagnostic tool, and it is commonly used for screening or follow-up. Its main disadvantage is the radiation dose delivered, especially concerning in children. In most instances, a very low dose CT (see Chapter 1) is used to check ventricular size.

Ultrasonography

Head ultrasound is the primary modality of choice for the screening of infants and fetuses suspected of having hydrocephalus. It is noninvasive, can be performed at the bedside, and gives a good evaluation of the ventricular size and morphology. It is also sensitive (if not specific) to parenchymal abnormalities and, when Doppler is used, can give an efficient functional assessment of the vasculature. Its use, however, is limited to the first months of life when the fontanelles are open, and it does not give nearly as comprehensive a presurgical assessment of hydrocephalus as MRI.

Monitoring of intracranial pressure is an important factor in the differentiation of hydrocephalus from atrophy. New innovative approaches with transfontanelle sonography may allow assessment of intracranial pressure noninvasively. Taylor and Madsen (83) studied the hemodynamic response to fontanelle compression in infants with ventriculomegaly. These authors used Doppler sonography to determine resistive indices in the anterior and middle cerebral arteries in premature neonates who had suffered intracranial hemorrhage. Baseline resistive indices without fontanelle compression did not correlate with intracranial pressure. However, a statistically significant correlation was found between the changes in resistive index during fontanelle compression

in children with elevated intracranial pressure. The maximum change in resistive index was significantly higher in infants who subsequently required shunting than in infants who did not ($p = 0.001$) (83). Thus, the need for shunt placement may be determined by assessment of resistive indices with and without fontanelle compression.

Fetal Diagnosis of Hydrocephalus

The prenatal diagnosis of hydrocephalus is currently made almost exclusively by obstetrical sonography. In fact, the fetal sonogram shows ventriculomegaly, not frank hydrocephalus, as many of the radiologic signs of hydrocephalus (see next section) cannot be accurately determined by fetal sonography. The diagnosis of ventriculomegaly is made if the fetal sonogram shows that the atrium of the lateral ventricle is larger than 10 mm (66,84). Fetal MRI gives higher reproducibility and provides better contrast, allowing a more precise measurement of the ventricle (69) (Fig. 8-4). The measurement is best made on coronal images parallel to the brainstem at the level of the choroid plexus (Fig. 8-4C). This measurement obviously does not determine whether the ventriculomegaly is the result of increased intraventricular pressure or destruction of periventricular brain tissue. Thus, some authors have

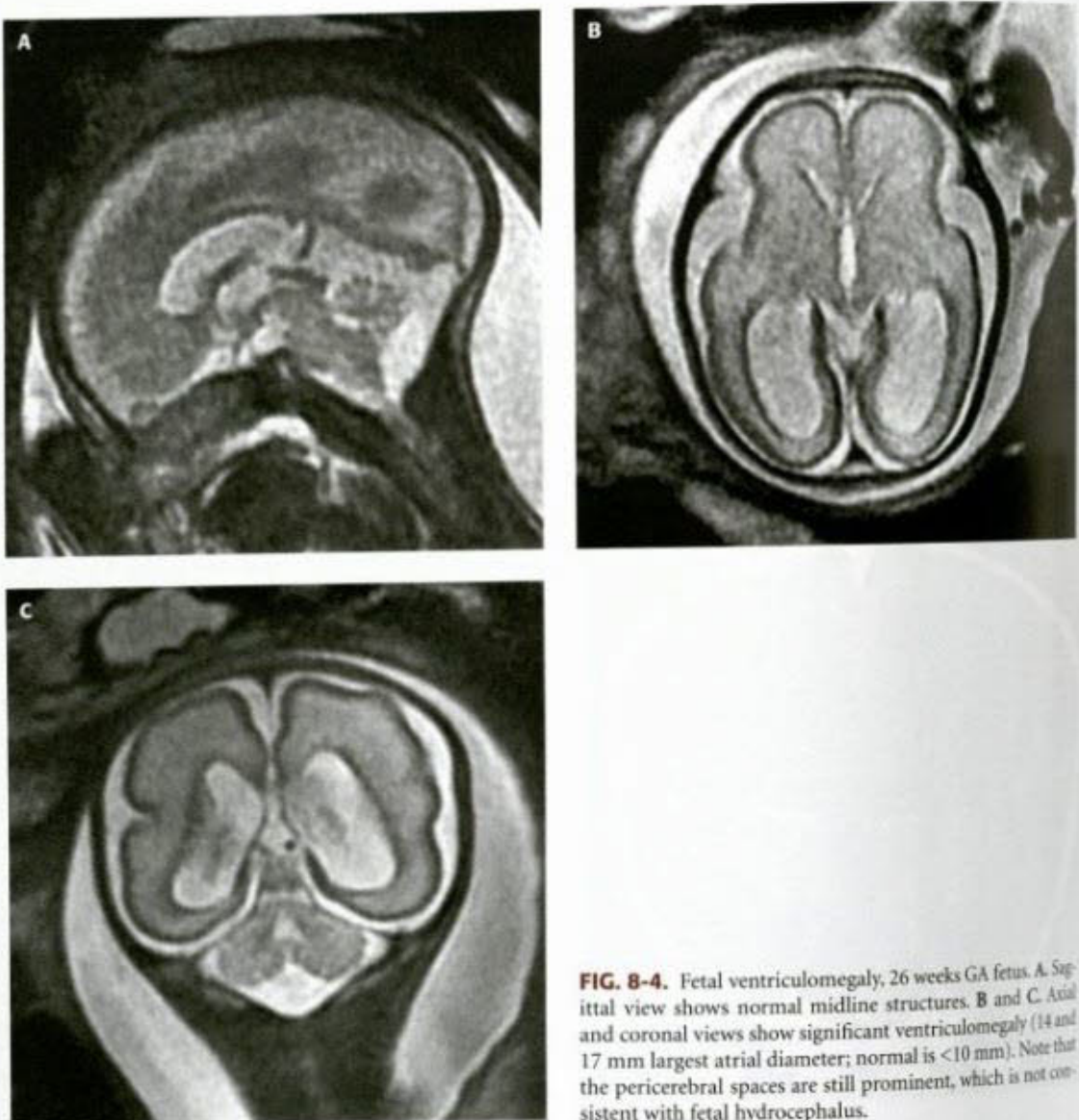


FIG. 8-4. Fetal ventriculomegaly, 26 weeks GA fetus. A. Sagittal view shows normal midline structures. B and C. Axial and coronal views show significant ventriculomegaly (14 and 17 mm largest atrial diameter; normal is <10 mm). Note that the pericerebral spaces are still prominent, which is not consistent with fetal hydrocephalus.

composed use of the ratio between the atrial diameter and the biparietal diameter (atrio-cerebral ratio); this value progressively decreases during gestation (13.6% at 22 weeks, 8% at 38 weeks) (85). Whatever the case, the presence of fetal ventriculomegaly suggests that brain development may be abnormal and is reason to do a more definitive fetal neuroimaging study, either a more sophisticated sonogram or a fetal MRI scan (86). The diameter of the atrium of the fetal lateral ventricle is of some prognostic significance. If the atrium measures larger than 10 mm, it is likely to be abnormal. Moreover, as the size of the ventricle increases, the prognosis worsens (66,84). If the atrium measures 12 mm or less, outcome is normal in 93% (87). If the atrium measures 13 to 15 mm, the child has a 21% to 25% chance of developmental delay (66,87). If the atrium is larger than 15 mm, the chance of developmental delay increases to greater than 40% (84,87). However, male fetuses have bigger ventricles than do female fetuses (88); indeed, some have suggested setting the upper limit of normal ventricular size at 10 mm instead of 10 mm (89). Therefore, the prognosis for male fetuses is worse than that for male fetuses with a similar degree of ventriculomegaly (88). The sizes of the third and fourth ventricles can also be measured in the fetus; typically, they are measured from transverse ultrasound images and from coronal (third ventricle) and sagittal (fourth ventricle) MRI images. The diameter of the third ventricle should be less than 3.5 mm on ultrasound and less than 4 mm on MRI, while the fourth ventricle diameter should be below 4.8 mm on ultrasound and below 7 mm on MRI (90).

Differentiating between simple ventriculomegaly and hydrocephalus is not always easy. Hydrocephalic fetuses often have normal head size (Fig. 8-5A). However, the ventricular expansion effaces the typically prominent subarachnoid space that is normally observed over cerebral convexity in fetuses (Fig. 8-5B, compare with Fig. 8-4B), especially before 32 weeks (this space progressively becomes filled by the growing brain in the last weeks of gestation). The ventricular morphology is also useful; in hydrocephalus the ventricles expand symmetrically and have a rounded configuration, especially the temporal horns. If the hydrocephalus is not too severe, the cellular layering in the cerebral mantle (ventricular zone, intermediate zone, subplate, cortex, as described in Chapter 2) is usually preserved; this layering commonly

disappears in cases of destructive ventriculomegaly (91). Aqueductal occlusion or stenosis is suspected when the posterior fossa appears normal; this can usually be evaluated on sagittal views of the midbrain. One complication of hydrocephalus in the fetus is the pressure erosion of the septum pellucidum, which may be impossible to differentiate from developmental absence of the septum. MRI is useful in excluding associated or causative malformations (holoprosencephaly, callosal agenesis, CRASH syndrome, periventricular nodular heterotopia [92,93]) and in demonstrating the cause of hydrocephalus (aqueductal stenosis, hindbrain malformations, hemorrhages, infection, vein of Galen malformation, torcular AV fistula, or rarely tumor).

Therefore, while sonography will likely remain the initial screening modality for the prenatal detection of ventriculomegaly, MRI of the fetus has been proved a useful adjunct to look for associated destructive lesions or parenchymal malformations that may be associated with the ventricular enlargement (69,85,86,90,92–94).

Postnatal Diagnosis of Hydrocephalus

The Ventricular System

The characteristic triad of hydrocephalus on imaging is the ventricular rounding and dilation, effacement of the pericerebral spaces over the convexity, and (at least in children) macrocephaly. Normal lateral ventricles are typically narrow, encroached upon by the heads of the caudates, the thalamus, the hippocampi, the calcarine sulci, and the collateral sulci (Fig. 8-1). In hydrocephalus the ventricles are dilated (Fig. 8-6) and present a rounded appearance on the axial and mostly the coronal images, notably of the lateral angle (Fig. 8-6C–E). Several features allow the differentiation between hydrocephalus and ex vacuo ventriculomegaly in children (Table 8-2). For the frontal horns, bodies and atria, widening and rounding are not really specific as they can be similar in atrophy. The appearance of the temporal horns, however, is quite specific: in atrophy, the roof and the floor of the horn remain roughly parallel, whereas in hydrocephalus, the horn is rounded with the choroidal fissure becoming enlarged and the hippocampus being compressed and displaced inferomedially (95) (Fig. 8-6C and D). The temporal horns dilate less than the bodies of the lateral ventricles in

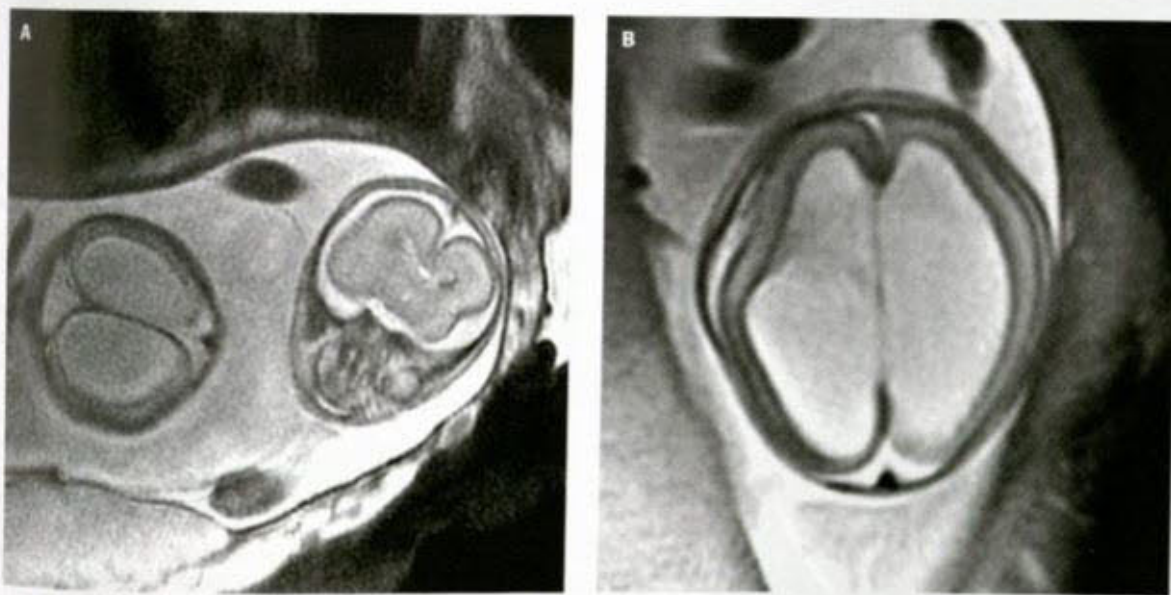


FIG. 8-5. Fetal hydrocephalus, twin pregnancy, 21 weeks GA fetuses. **A.** This image shows the two fetal heads, one which is normal, and the other hydrocephalic. Note that the head diameter is similar in both, but the pericerebral spaces of the hydrocephalic fetus are effaced and the ventricles enlarged. **B.** Axial image of the hydrocephalic brain shows the pericerebral effacement.

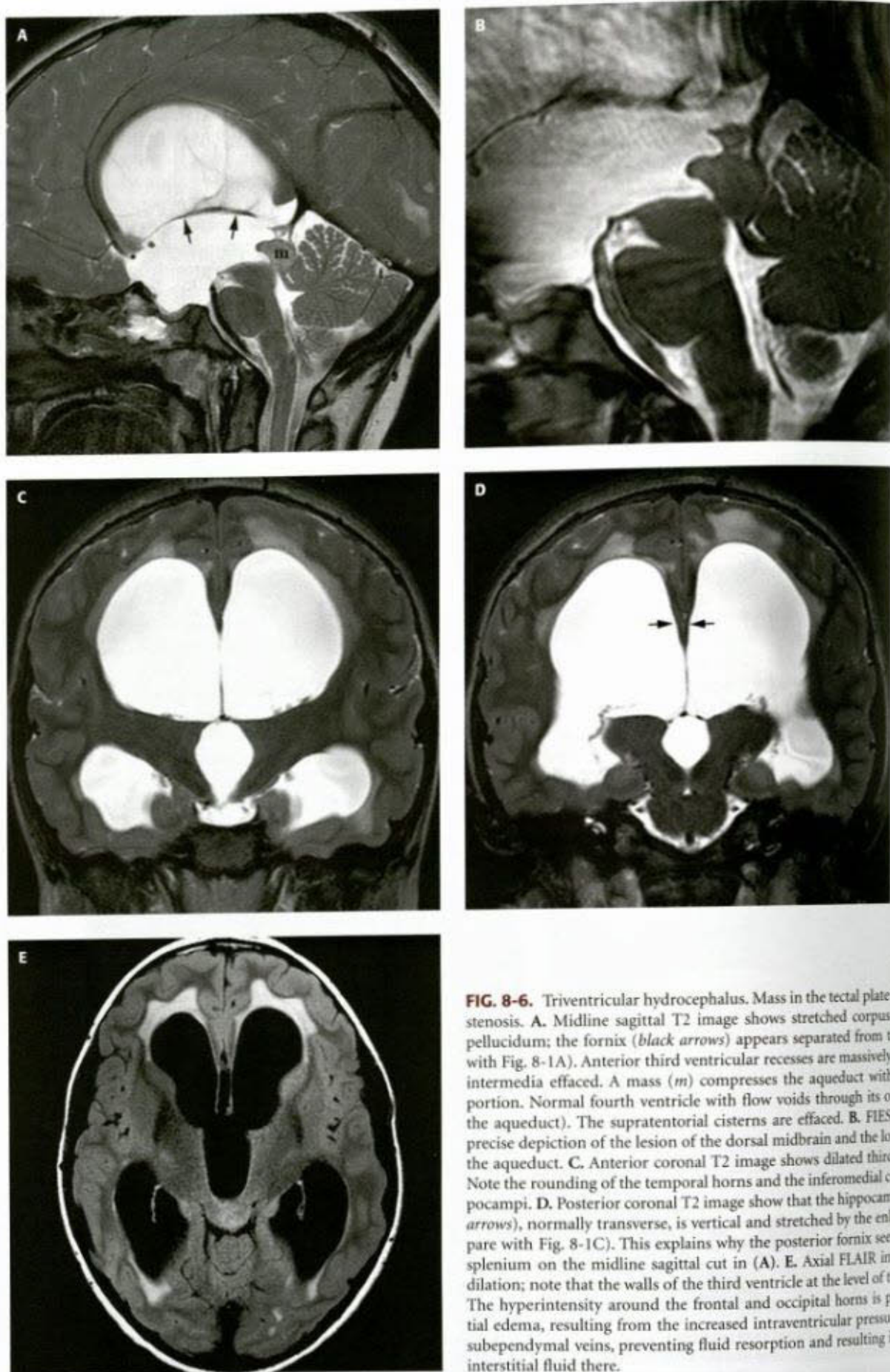


FIG. 8-6. Triventricular hydrocephalus. Mass in the tectal plate with severe aqueductal stenosis. **A.** Midline sagittal T2 image shows stretched corpus callosum and septum pellucidum; the fornix (black arrows) appears separated from the splenium (compare with Fig. 8-1A). Anterior third ventricular recesses are massively dilated, and the rostral intermedia effaced. A mass (*m*) compresses the aqueduct with dilation of its rostral portion. Normal fourth ventricle with flow voids through its outlet (but not through the aqueduct). The supratentorial cisterns are effaced. **B.** FIESTA thin imaging for precise depiction of the lesion of the dorsal midbrain and the location of narrowing of the aqueduct. **C.** Anterior coronal T2 image shows dilated third and lateral ventricles. Note the rounding of the temporal horns and the inferomedial compression of the hippocampi. **D.** Posterior coronal T2 image shows that the hippocampal commissure (black arrows), normally transverse, is vertical and stretched by the enlarged ventricles (compare with Fig. 8-1C). This explains why the posterior fornix seems separated from the splenium on the midline sagittal cut in (A). **E.** Axial FLAIR image shows ventricular dilation; note that the walls of the third ventricle at the level of the thalamus are periventricular. The hyperintensity around the frontal and occipital horns is periventricular edema. The hyperintensity around the frontal and occipital horns is periventricular edema, resulting from the increased intraventricular pressure that compresses the subependymal veins, preventing fluid resorption and resulting in the accumulation of interstitial fluid there.

TABLE

8-2 Imaging Characteristics of Hydrocephalus (Given in Order of Utility)

- Enlargement of the anterior or posterior recesses of the third ventricle
- Downward convexity of the floor of the third ventricle (results in decreased mamillopontine distance)
- Commensurate dilatation of the temporal horn with the lateral ventricles
- Narrowing of the ventricular angle
- Widening of the frontal horn radius
- Effacement of cortical sulci

The first three are the most useful signs. Although many measurements can be derived from these signs (e.g., spleniochiasmal distance, third ventricular glial distance, mamillocommissural distance [109]), these measurements are unnecessary.

patients with cerebral atrophy, and the hippocampus is not displaced (Fig. 8-7). The rather small size of the temporal lobes and, in particular, the relatively small volume of white matter in the temporal lobes, is almost certainly the reason for this (98). The presence of temporal horn enlargement is not reliable in children with significant temporal lobe atrophy, such as those with Down syndrome. *The Sylvian fissures should always be studied to assess the degree of temporal lobe atrophy before enlargement of the temporal horns is used to make a diagnosis of hydrocephalus.* If the Sylvian fissures are enlarged, or other evidence of temporal lobe atrophy is present, enlarged temporal horns are not a reliable sign of hydrocephalus.

The ventricular index is the ratio of the ventricular diameter at the frontal horns to the diameter of the brain at the same level (Fig. 8-8A). The ventricular angle (Fig. 8-8C) measures the divergence of the frontal horns. The angle between the anterior or superior margins of the frontal horns at the level of the foramina of Monro is diminished by concentric enlargement of the frontal horns (96). The diminution of the angle may be appreciated on either axial or coronal images. The concentric enlargement of the frontal horns eventually causes them to become rounded, producing an appearance of "Mickey Mouse ears" on axial scans. This concentric enlargement of the frontal horns also causes enlargement of the so-called frontal horn radius (Fig. 8-8D), which is determined by measuring the widest diameter of the frontal horns taken at a 90° angle to the long axis of the frontal horn (96). Ventricular rounding may be the single feature identified in hyperacute hydrocephalus (within hours), when the volume of brain tissue is still preserved, or even becomes swollen.

The dilation and tension of the lateral ventricles modifies the appearance of the midline. As the lateral ventricles are more dilated than the third ventricle, the latter is pushed downward. The corpus callosum is stretched, thinned, arched upward, more than the columns of the fornix, so that the distance between them increases (Fig. 8-6A); the septum pellucidum is stretched and may even be torn (Fig. 8-6B). The part of the fornix that forms the hippocampal commissure (the psalterium), normally transverse, becomes verticalized on each side of the midline (Fig. 8-6D, compare with Fig. 8-1C), which explains why the posterior part of the fornix seems to be detached from the undersurface of the splenium on the midline sagittal cut (Fig. 8-6A, compare with Fig. 8-1A).

In rare cases of chronic severe obstructive hydrocephalus (usually aqueductal stenosis) the ventricular anatomy may be compounded by a ventricular diverticulum, inferior expansion of the medial wall of the ventricular atrium through the choroid fissure behind the thalamus, into the supracerebellar and quadrigeminal cisterns (Fig. 8-9) (99–102). The inferomedial atrium is affected because it is the thinnest portion of the atrial wall and has the largest surface of the ventricular

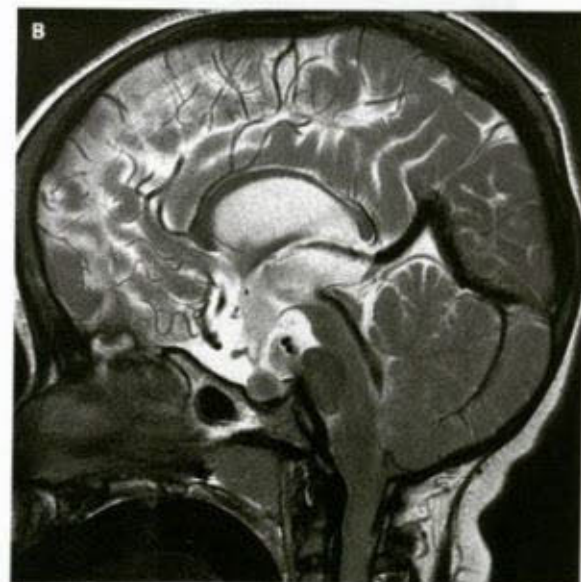
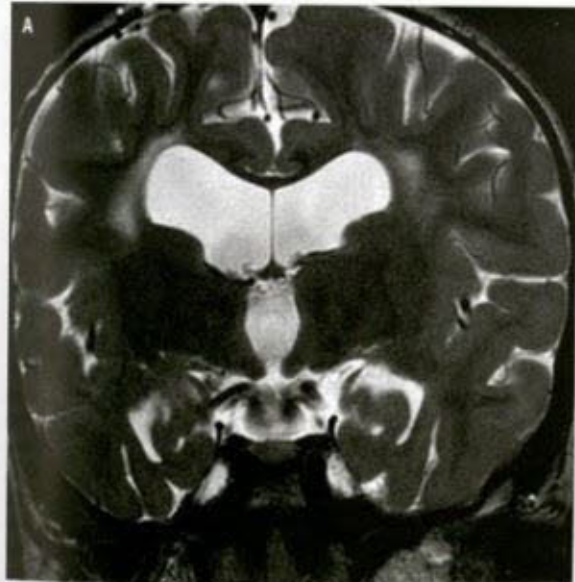


FIG. 8-7. Brain atrophy in a 4-year-old child, with head circumference below the 25th percentile. **A.** The third and lateral ventricles are wide with rounding of the lateral angles. However the temporal horns, although large, are small compared to the bodies of the lateral ventricles; they retain their normal shape and the hippocampi are not displaced medially. The pericerebral spaces are patent, notably the sylvian fissures. **B.** The corpus callosum is thin and the fornix appears lowered. However, the anterior third ventricular recesses are not dilated, the lamina terminalis and the tuber cinereum are both concave. The pineal recess is prominent, but this may be a normal variant. The suprasellar cisterns are prominent.

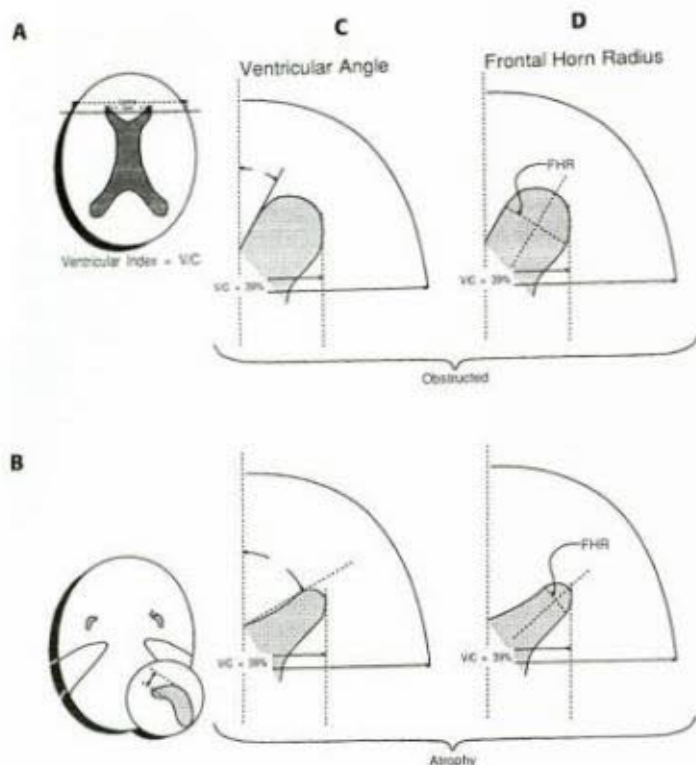


FIG. 8-8. Various methods in the radiographic diagnosis of hydrocephalus. **A.** The ventricular index is the ratio of the ventricular diameter at the level of the frontal horns to the diameter of the brain measured at the same level. This is not a very sensitive or specific measurement in the detection of hydrocephalus because the ventricular index is enlarged in cerebral atrophy as well as in hydrocephalus. **B.** Enlargement of the temporal horns commensurately with the bodies of the lateral ventricles is probably the most sensitive and reliable sign in the differentiation of hydrocephalus from atrophy. There is significantly less dilatation of the temporal horns than the bodies of the lateral ventricles in cerebral atrophy. **C.** The ventricular angle measures the divergence of the frontal horn. In theory, the angle made by the anterior or superior margins of the frontal horn at the level of the foramina of Monro is diminished when concentric enlargement of the frontal horns occurs. Compare the illustration of hydrocephalus (top) with that of atrophy (bottom). The ventricular index in both instances is 39%; however, the ventricular angle is markedly reduced in hydrocephalus. **D.** The frontal horn radius measures the widest diameter of the frontal horns taken at a 90° angle to the long axis of the frontal horn. The usefulness of this measurement is demonstrated by the markedly increased frontal horn radius in the patient with hydrocephalus (top) as opposed to the patient with atrophy (bottom). Overall, no one measurement is completely accurate in the diagnosis of hydrocephalus; the size of the temporal horns, ventricular angle, the frontal horn radius, and the size of the ventricles as compared to the cortical sulci should all be assessed. (This figure courtesy Dr. E. Ralph Heinz, Durham, NC.)

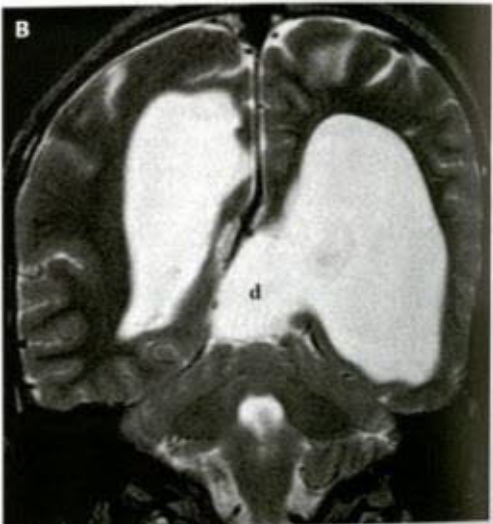


FIG. 8-9. Ventricular diverticulum. Axial FLAIR (A), coronal T2 (B), and sagittal T2 (C) images show expansion of the left lateral ventricle with the posteromedial aspect of it evaginating through the choroidal fissure into the ambient cistern behind the third ventricle. This diverticulum (*d*) compresses the adjacent structures such as the tectal plate and the top of the vermis. On sagittal cuts it may be mistaken for an arachnoid cyst, but the continuity with the ventricle is well shown on axial and coronal planes.

and, therefore, has the highest wall tension. If not treated, these diverticula can compress the mesencephalic tectum with the risk of significant neurological complications; they can be mistaken for arachnoid cysts in the region of the quadrigeminal cistern (Fig. 8-9C). Coronal images are very helpful in the evaluation of these patients, demonstrating the continuity of the trigone of the lateral ventricle with the diverticulum (Fig. 8-9B).

The third ventricle is normally slit-like, mildly wider anteriorly than posteriorly. It is enlarged both in atrophy and hydrocephalus, but in hydrocephalus, it commonly develops rounded recesses: anteriorly the chiasmal (supraoptic) and infundibular recesses and posteriorly the suprapineal recess. This feature is best appreciated on sagittal images (Figs. 8-6A, B and 8-10A), in which the anterior wall of the third ventricle, normally concave anteriorly, becomes straightened, and the floor of the third ventricle, usually concave downward, becomes straightened or convex downward. The enlargement and inferior displacement of these recesses can compress the infundibulum and diminish flow within the hypothalamic-pituitary portal venous system, resulting in hypothalamic-pituitary dysfunction (103). When the aqueduct or the outlet of the fourth ventricle are occluded, the tuber cinereum is characteristically hugely dilated and bulges into the interpeduncular cistern (Figs. 8-6A, B and 8-10A) sometimes wrapping the head of the basilar artery.

The suprapineal recess of the third ventricle is another common site of ventricular herniation. The dilated recess expands into the posterior incisural space, displacing the pineal gland inferiorly and, occasionally, elevating the vein of Galen. When large, diverticula sometimes extend inferiorly to compress the quadrigeminal plate, with consequent shortening of the tectum in the rostral-caudal direction (104) (Fig. 8-10A). The short, thick tectum should not be mistaken for a neoplasm; isointensity with normal brain tissue on T2/FLAIR images and the absence of contrast enhancement exclude a tumor. The suprapineal recess may also enlarge further posteriorly and compress the tectum from the posterior direction, resulting in thinning of the tectum and narrowing of the aqueduct (104).

The disproportionate enlargement of the recesses of the third ventricle probably results from the relatively small resistance to expansion provided by the thin hypothalamus and the cisterns that surround the walls of the recesses. In contrast, the thalamus, which form the walls of the body of the third ventricle, provide a great deal more resistance to expansion. It is important to note that even with a significant ventricular enlargement, the lateral walls of the third ventricle (i.e., the thalamus) remain parallel to each other (Fig. 8-6E); a rounded, circular third ventricular lumen indicates the presence of a cyst, usually a suprasellar cyst with intraventricular expansion (Fig. 8-11). The anterior (chiasmal and infundibular) recesses seem to enlarge earlier and more severely than the posterior (suprapineal) recess (105). The pulsating dilated anterior third ventricle may be so huge that it erodes the dorsum sellae (Figs. 8-6A and 8-10A). On axial images, the dilated anterior recesses of the third ventricle are best detected by noting that the third ventricle is larger at the level of the optic chiasm (Fig. 8-10B) than at the level of the middle of the ventricle. When hydrocephalus is severe and chronic, the floor of the third ventricle may rupture spontaneously, creating an internal drainage pathway that allows CSF to escape from the ventricular system into the subarachnoid space (106).

The cerebral aqueduct (of Sylvius) is a narrow craniocaudal curved channel that connects the third and fourth ventricles. When narrowed or occluded, obstructive hydrocephalus develops (aqueductal stenosis) (Figs. 8-6 and 8-10). Occlusion may be intrinsic (ependymal, usually postinflammatory) (Fig. 8-12), or extrinsic; the latter may be caused by a tegmental or a tectal mass lesion (Figs. 8-6 and 8-10), or by an extrinsic compression of the midbrain. It has been suggested that, in some instances at least, aqueductal stenosis may result from compression by expanded temporal lobes (Fig. 8-13); in this situation, the hydrocephalus may be primarily communicating in nature with aqueductal narrowing being a result, rather than a cause, of hydrocephalus (104,107,108). In contradistinction, the aqueduct typically is dilated when the fourth ventricle is obstructed, either due to the force exerted by the CSF pressure or the mechanical effect of a mass expanding the ventricular lumen (Fig. 8-14).

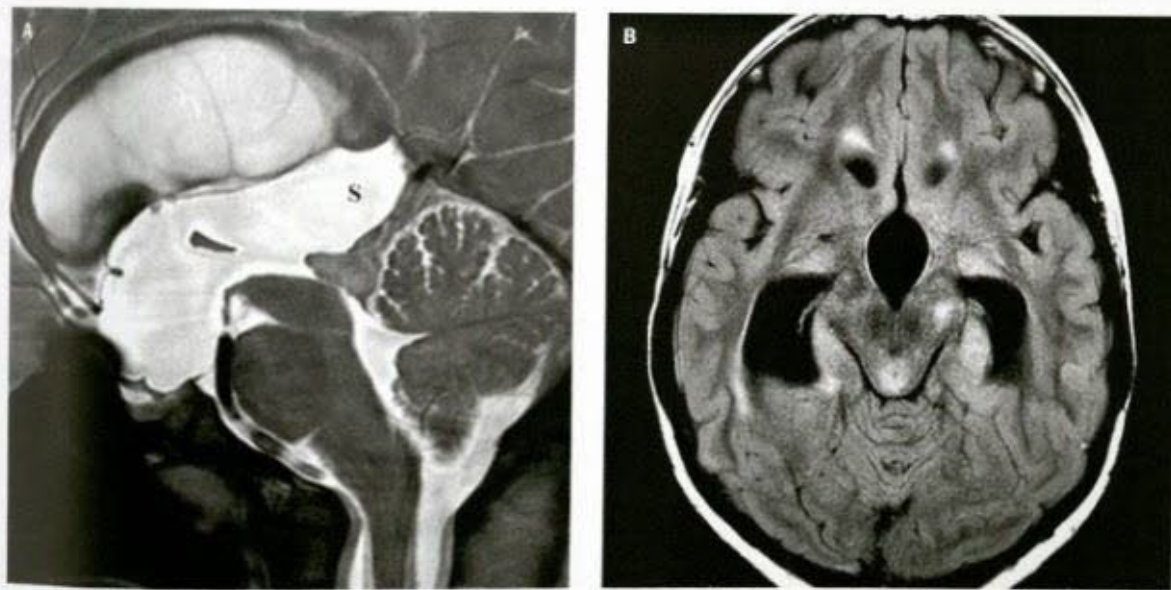


FIG. 8-10. Aqueductal stenosis caused by a tectal mass. **A.** Sagittal T2-weighted image shows severe dilation of the third ventricular recesses, especially the suprapineal recess (S). Dilation of this recess is not consistently seen (see Fig. 8-6A and B); it may depend on a preexisting prominence of the recess (see Fig. 8-7B), or on the duration or early occurrence of hydrocephalus. **B.** The anterior (hypothalamic) portion of the third ventricle presents a more rounded appearance than the more posterior interthalamic portion (see Fig. 8-6E).

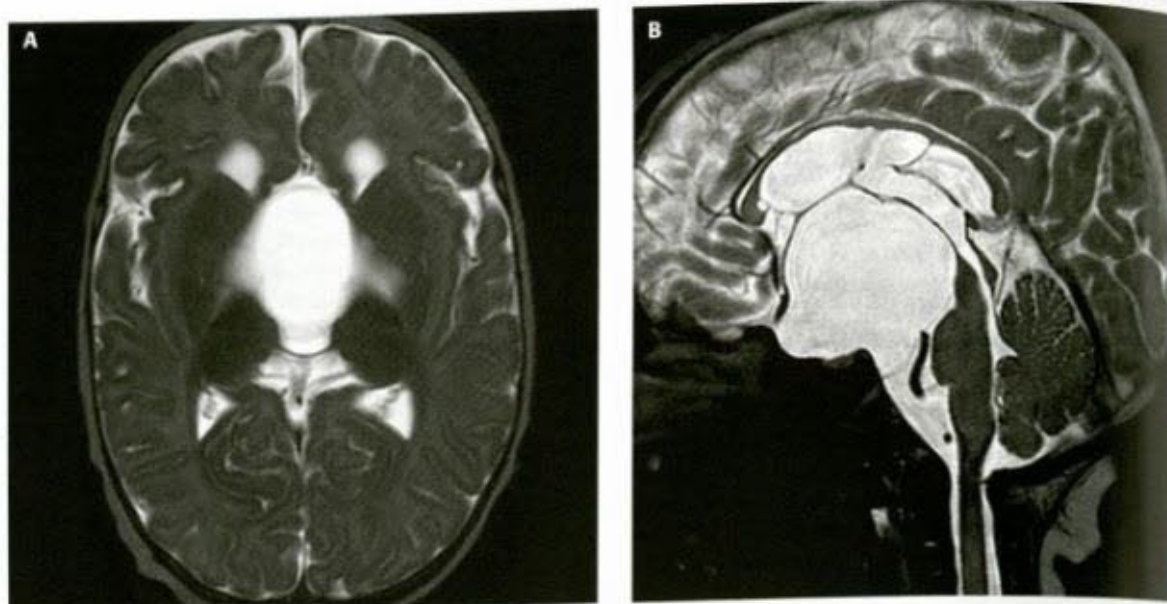


FIG. 8-11. Rounded appearance of the third ventricle; suprasellar cyst. **A.** Axial T2-weighted image shows the whole third ventricle, including its interthalamic portion appearing rounded. **B.** Sagittal FIESTA image shows a huge suprasellar cyst displacing the ventricular floor upward.

Due to the pulse amplitude of the CSF through the normal aqueductal strictures, a striking flow void is normally observed there on the sagittal midline T2 image, extending from the posterior third ventricle to the superior fourth ventricle (76) (Fig. 8-1B). This flow void disappears if the aqueduct is occluded (Figs. 8-6A and 8-12), but its presence does not exclude a stenosis; flow velocity is increased, and therefore signal intensity is decreased, as the aqueductal diameter is diminished (Fig. 8-15). Flow is also increased in cases of decreased meningeal compliance (e.g., in communicating hydrocephalus), even

when the aqueduct is patent or large, because the amplitude of the pulsations is increased (Figs. 8-2A and 8-16 to 8-18).

The fourth ventricle in hydrocephalus ranges from normal to markedly dilated. It is normal in obstructive hydrocephalus when the obstruction is located above it (Figs. 8-6, 8-10, 8-12, 8-13, and 8-15); it is often normal in communicating hydrocephalus, as well (Fig. 8-19), so it must be remembered that *triventricular hydrocephalus does not necessarily mean aqueductal stenosis!* In most cases of communicating hydrocephalus, however, the fourth ventricle is mildly dilated.

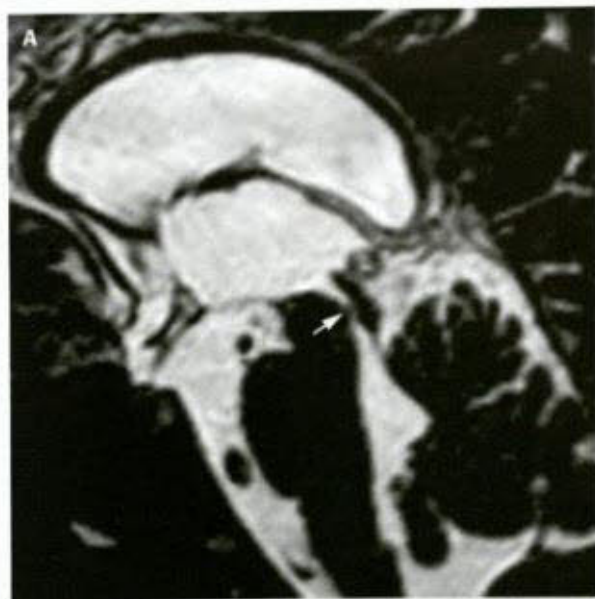


FIG. 8-12. Intrinsic aqueductal stenosis. **A.** Sagittal T2-weighted image in an infant with previous perinatal hemorrhage shows narrowing of the middle portion of the aqueduct (white arrow). Aqueductal stenosis likely develops from ependymal inflammation in the aqueduct. Note adherent recesses in the anterior third ventricle. Normal tectal plate. **B.** Sagittal FIESTA image in congenital hydrocephalus shows obstruction of the aqueduct by a transverse occluding membrane or web (white arrow) in its caudal portion; note widening of the rostral segment and normal tectal plate.

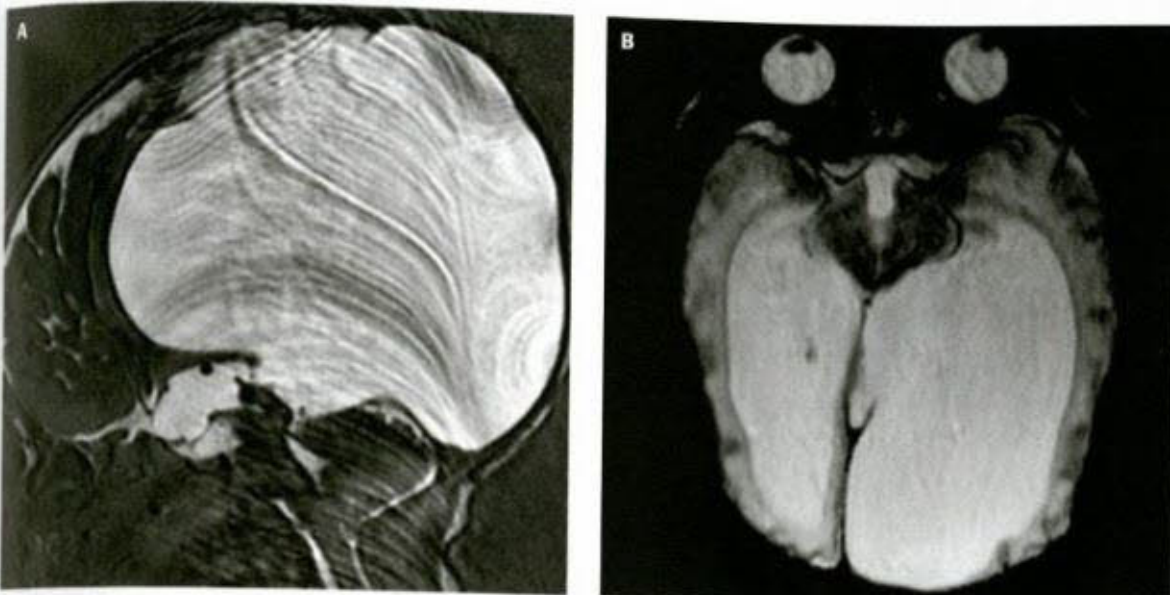


FIG. 8-13. Extrinsic aqueductal stenosis. **A.** Sagittal T2-weighted image in a patient with congenital hydrocephalus. Note huge dilation of the lateral ventricles and to a lesser degree of the third ventricle. Small posterior fossa. The tectal plate appears compressed by the expanded lateral ventricle. **B.** Axial T2. The bilateral ventricular distension results in bilateral compression of the midbrain and deformity of the tectal plate, likely causing the aqueductal occlusion.

(Figs. 8-2, 8-16, and 8-17). Elevated CSF pressure tends to globally increase the volume of the brain, so that all ventricles and cisterns are large (Fig. 8-19A); anatomy normalizes after shunt placement (Fig. 8-19B). When both the fourth ventricle and the cisterna magna are involved, a posterior rotation of the vermis may occur, which is not a malformation but just hydrocephalus. Finally, the fourth ventricle may be hugely dilated when both in-flow and out-flow are occluded, especially if the lateral ventricles are decompressed (isolated fourth ventricle, discussed in more detail in section Specific categories of hydrocephalus of this chapter).

Appearances of the ventricular system usually define the type of obstructive hydrocephalus. These will be discussed in more detail in

Section "Specific Categories of Hydrocephalus," dealing with specific causes of hydrocephalus. Univentricular hydrocephalus occurs when the obstruction sits at one foramen of Monro; the most common cause is SEGA in tuberous sclerosis (see Chapter 6). The affected lateral ventricle is dilated and rounded, and the septum pellucidum bulges toward the normal side. Biventricular hydrocephalus is caused by the obstruction of both foramina of Monro; common causes include bilateral SEGA, colloid cyst of the third ventricular tela choroidea, suprasellar cyst, or tumor. Triventricular hydrocephalus results from when the occlusion is in the distal third ventricle, cerebral aqueduct, or upper fourth ventricle; common causes are inflammatory aqueductal stenosis and midbrain/pineal, posterior third ventricular tumors. Quadriventricular hydrocephalus is seen when the four ventricles are dilated, either because a mass occupies the lower fourth ventricle or because an obstructive process (typically infection) compromises the fourth ventricular outlets. A variant of this ("pentaventricular hydrocephalus") is seen when the outlets of the cisterna magna are occluded (e.g., fibrous arachnoiditis of the posterior fossa cisterns) resulting in a dilated cisterna magna (the "fifth ventricle") together with the four ventricles (Fig. 8-20).

The Cisterns

In hydrocephalus the cisterns may be effaced or dilated, depending on the specific anatomic/hydrodynamic conditions in each patient. When the obstruction is intraventricular the cisterns surrounding the portion of the brain that is hydrocephalic tend to be effaced. In case of aqueductal occlusion, the supratentorial cisterns are effaced, including the suprasellar and ambient cisterns, the interhemispheric cistern, and the subarachnoid space over the convexity (Figs. 8-6 and 8-10). In case of fourth ventricular occlusion, the posterior fossa cisterns (cisterna magna, cisterns around the brainstem and midbrain) are effaced, as well (Fig. 8-20).

When the occlusion is cisternal, the cisterns located between the occlusion and the ventricular outlets are dilated, the cisterns located between the occlusion and the main absorption sites are effaced. However, cisternal obstructions often result from diffuse arachnoid fibrosis



FIG. 8-14. Aqueductal dilation. Large tumor (anaplastic ependymoma) expanding the fourth ventricle and occluding its outlets results in hydrocephalus with a dilated aqueduct.



FIG. 8-15. Incomplete aqueductal stenosis. Midline sagittal T1 (A) and T2 (B) images show aqueductal stenosis; the T2-weighted image demonstrates a striking signal void due to rapid flow. This doesn't mean that the aqueduct is normal, but that the stenosis results in an increased CSF flow velocity, compatible with obstructive hydrocephalus.

with multiple occlusive arachnoid adhesions; the cisterns appear multiloculated and sometimes frankly multicystic.

In case of chronic communicating hydrocephalus, all ventricles and all cisterns tend to be dilated other than the subarachnoid spaces over the cerebral convexities, which are effaced as a result of the expansion of the lateral ventricles. Note that the sylvian fissures may be quite dilated in this situation.

Finally, there are instances of hydrocephalus in which the arachnoid spaces over the convexity are dilated; *benign infantile*

enlargement of subarachnoid spaces (also called external hydrocephalus and extraventricular obstructive hydrocephalus [EVOH]; see section "Benign Enlargement of Subarachnoid Spaces in Infants" of this chapter).

It is generally assumed that increased pressure within the ventricular system causes compression of the brain tissue against the immovable skull and consequent diminution of sulcal size. In pediatric patients, however, this conclusion may be misleading because both *enlargement and hydrocephalus can enlarge both the ventricles and sulci* (Fig. 8-16).



FIG. 8-16. Communicating hydrocephalus with accentuated signal void in widely patent aqueduct. A. Midline sagittal FLAIR image shows a large aqueduct, mildly dilated fourth ventricle and, likely, arachnoid loculations in the suprasellar cistern (note the mass effect upon the tuber cinereum and the pituitary stalk). B. Midline sagittal T2-weighted image shows prominent signal void through the aqueduct, explained by increased pulsatility of the CSF through the aqueduct; restricted cisternal CSF circulation has resulted in reduced compliance.

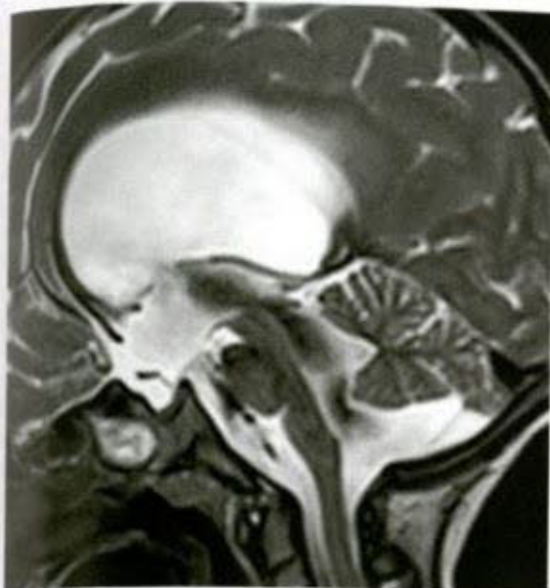


FIG. 8-17. Communicating hydrocephalus. Sagittal T2-weighted image shows hugely prominent flow void through the aqueduct and the mildly enlarged fourth ventricle, down to the cistern magna. According to the Cenni model, this results from a decreased compliance of the theca.

Further complicating the radiologic assessment is the fact that the size of the ventricles and subarachnoid spaces is quite variable over the first years of life (111). In such a case, the final indicator of hydrocephalus is *enlargement of the ventricular system to a degree that is disproportionate to the enlargement of the cortical sulci* (98). The failure of measurements such as the bicaudate index (112,113) and the Evans ratio (114,115) to accurately differentiate hydrocephalus from atrophy reflects this difficulty (116). Knowledge of the head size of the infant is essential; a large or a too-rapidly enlarging head suggests hydrocephalus whereas a small or diminishing head circumference is more compatible with atrophy.

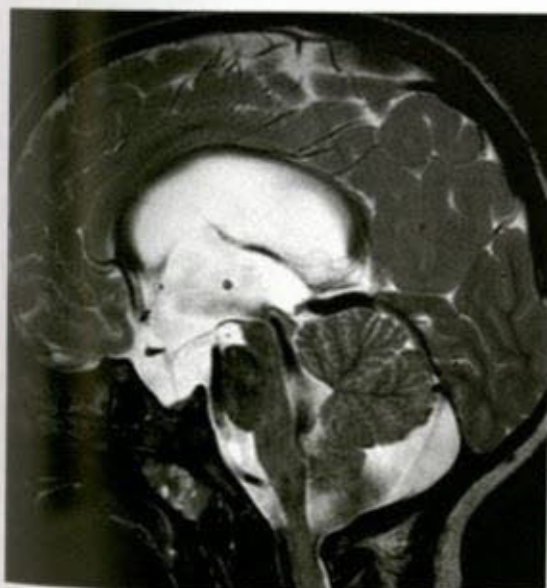


FIG. 8-18. Communicating hydrocephalus. Midline sagittal T2 image shows communicating hydrocephalus with normal fourth ventricle. Note prominent signal void in aqueduct and fourth ventricle.



FIG. 8-19. Cerebral deformities caused by hydrocephalus. Infant with macrocephaly. A. At age of 2 months, midline sagittal T1 shows huge dilation of the posterior fossa cisterns, particularly dorsal to the vermis; a diagnosis of cystic malformation of the posterior fossa was discussed, but finally a ventriculoperitoneal shunt was inserted in the lateral ventricle. B. At age of 8 months, midline sagittal T1 shows normal brain anatomy. Artifact is from the shunt valve.

Acute Parenchymal Changes

Periventricular Interstitial Edema

Acute hydrocephalus is characterized by a periventricular band of low density on CT, of low T1 and high T2/FLAIR signal on MR, which reflects periventricular interstitial edema. Rather than an outflow of fluid from the ventricle to the parenchyma (which in some way would relieve the ventricular pressure) (47,48), this accumulation of fluid in the periventricular white matter is felt to represent a failure of normal parenchymal drainage, with consequent accumulation of fluid within the interstitial spaces of the cerebrum (50). Current thought suggests that free exchange of water between the ventricular cavities and the extracellular spaces of the periventricular white matter is a normal



FIG. 8-20. Quadriventricular hydrocephalus associated with dilated cistern magna, due to occluded cistern magna outlets.

process. Increased intraventricular pressure prevents the normal flow of fluid toward the ventricles, and by compressing the subependymal veins, prevents its absorption by the deep medullary venous channels. Periventricular interstitial edema, therefore, is not seen in hyperacute hydrocephalus (water cannot accumulate in a short period of time) nor in chronic hydrocephalus (the ventricular pressure is not high enough), but only in acute/subacute obstructive hydrocephalus such as from an enlarging midline tumor. *Periventricular interstitial edema, therefore, is a complication of hydrocephalus, not a compensatory process;* it increases the volume of interstitial water, thus increasing the mass effect upon, and causing damage to, the cerebral parenchyma (50,51).

On CT, interstitial edema appears as hypodensity in the periventricular region; the ventricular margins may appear indistinct (Fig. 8-21A and B). On MR, the increase in water appears as a rim of hypointensity and T2/FLAIR hyperintensity surrounding the lateral ventricles (Fig. 8-21C and D). This rim may be difficult to appreciate on heavily T2-weighted sequences, where the high signal intensity is indistinguishable from the ventricular CSF; a proton density or FLAIR image is much more sensitive. Diffusion-weighted images will show increased water motion in the affected areas. Periventricular interstitial edema in neonates and young infants may be masked by the normal high water content of the immature brain.

Structural Parenchymal Changes

With the expansion of the ventricular surface, ependymal cells often maintain the lining but the stretching possibilities are limited, and the ependyma rapidly becomes disrupted, especially over the white matter and the septum pellucidum (50). Choroid plexuses degenerate and become sclerotic, possibly with decreased secretory activity (50). Multiple experimental and animal studies have demonstrated that CBF is compromised in hydrocephalus, and may impede shunt placement (50,117,118); an evaluation of this phenomenon is possible using MR technology (118). Impaired cerebral energy metabolism in experimental hydrocephalus has been demonstrated by MRS and ^1H MRS (119), but the same group could not show similar changes with ^1H MRS in human hydrocephalus (120). Finally, white matter tracts are disrupted in acute hydrocephalus, as the ventricular enlargement stretches the axons of the corpus callosum to the septum pellucidum (which contains the limbic fibers that connect the septal cortex to the cingulate cortex), the fornices, the hippocampal commissure, the occipitofrontal, inferior longitudinal and corticospinal tracts, and the optic radiations. Histologically this stretching has been shown to be associated with axonal degeneration (50). MRI with Diffusion Tensor Imaging (DTI) DTI has demonstrated microstructural changes reflecting compression of the tracts in the white matter lateral to the ventricles (increased FA, increased longitudinal diffusivity but unchanged ADC) but not in the corpus callosum (decreased

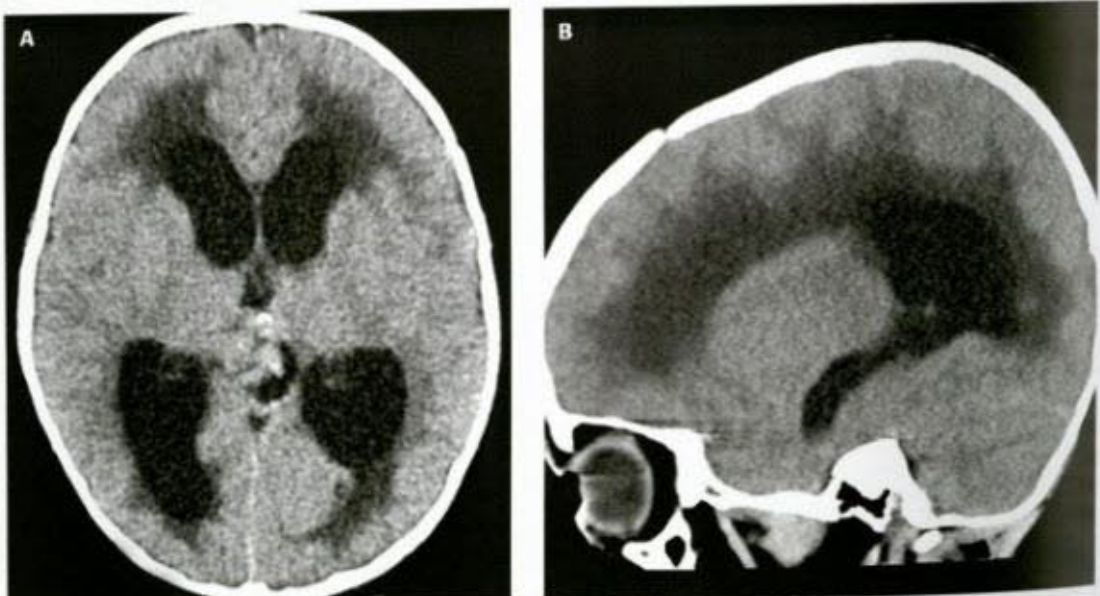


FIG. 8-21. Progressive/acute hydrocephalus due to posterior third ventricular tumor: effects on the parenchyma. A and B. Axial and parasagittal CT. Markedly enlarged lateral ventricles with low attenuation of the periventricular white matter, reflecting periventricular interstitial edema that results from the compression of the subependymal veins and consequent lack of absorption of the interstitial fluid from the deep white matter. This parenchymal edema develops in addition to the hydrocephalus.

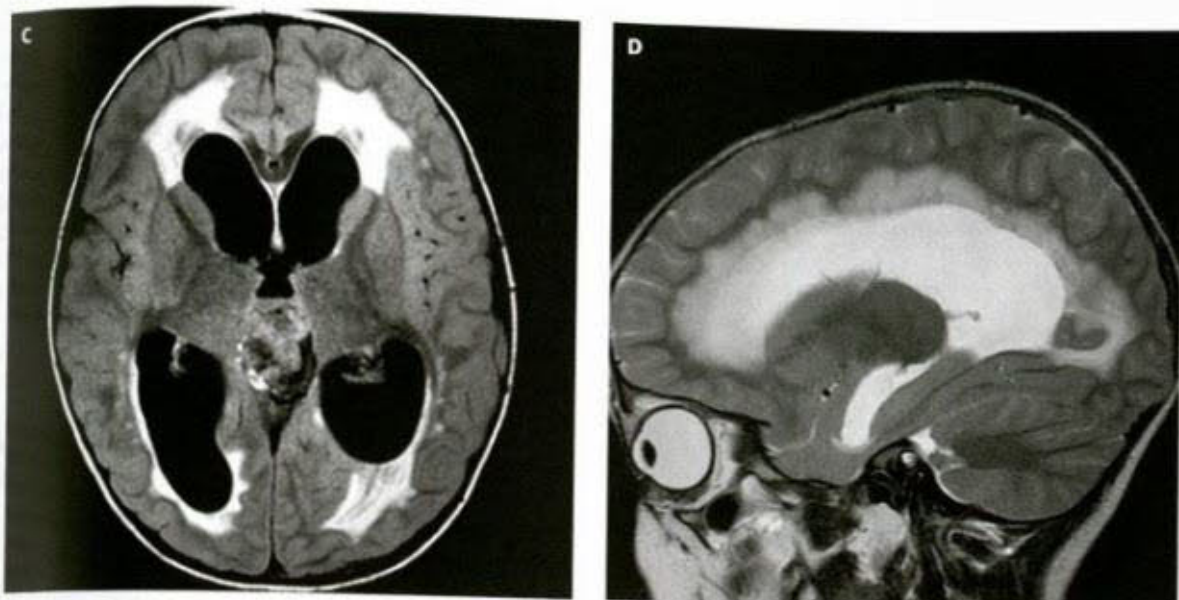


FIG. 8-21. (Continued) C and D. Same case, MRI with axial FLAIR (C) and parasagittal T2 (D) images. The MR changes are similar to the CT changes, but are more easily seen.

with increased ADC) (121). The changes reversed after treatment (121).

Herniation

Increased supratentorial pressure with ventricular dilation may lead to downward herniation of the mesial temporal structures along the free edge of the tentorium toward the posterior fossa. In the process, the midbrain and the aqueduct are compressed, and the vessels in the adjacent cisterns are stretched and compressed with resultant ischemia/infarction. Increased pressure and hydrocephalus occurs in the posterior fossa, so structures may herniate both upward through the tentorial incisura and downward through the foramen magnum, with similar effects on the midbrain and medulla; in addition, occlusion of the foramen magnum results in a rapid, tamponade-like increase of intracranial pressure.

Circulatory Arrest

Because neither CSF nor brain parenchyma is compressible, the main implication of a rapid increase of intraventricular/intracranial pressure is vascular compression: the subependymal veins are compressed within the ventricles, the cortical veins are compressed against the ependyma, and the engorged intracerebral capillaries are compressed in between. The resulting increased capillary pressure causes brain edema and consequent herniations; herniated tissue fills the tentorial incisura and/or the foramen magnum, increasing the pressure even more and leading to intracranial circulatory arrest as the perfusion pressure cannot overcome the intracranial pressure. This situation may occur early, in hyperacute hydrocephalus, or as a later, terminal complication of progressive hydrocephalus. In hyperacute hydrocephalus, the ventricles remain small but rounded. In both situations, the pericerebral spaces are effaced, the parenchyma becomes edematous with loss of gray-white matter contrast and, if administered, intravenous contrast pools in the surface vessels but is not able to penetrate the parenchyma.

Chronic Parenchymal Changes

Although many of the acute changes noted in progressive hydrocephalus (interstitial edema, demyelination, vascular compromise, axonal loss) are reversible if shunting is performed in a timely fashion, some (ependymal damage, gliosis, and abnormal myelination, including aberrant

myelination of glial cells) may persist (50). Demyelination and axonal degeneration have a similar MR appearance, a ribbon of bright T2/FLAIR signal in the paraventricular white matter, sometimes accompanied by loss of brain volume. Axonal degeneration however does not necessarily imply neuronal loss (122) and damaged axons may regenerate, resulting in return to a nearly normal appearance of the brain. This may be rather spectacular in infants whose posterior cerebral mantle was compressed to a few millimeters thick before shunting. Subependymal fibrosis and sclerosis is usually found at autopsy (51); it may appear in young infants as a hypointense ventricular wall interposed between the bright CSF and bright periventricular white matter on T2-weighted images.

A rare late complication of chronic hydrocephalus is the local rupture of the ventricular wall and the development of a CSF-filled cleft that dissociates the hemispheric white matter ("ventricular disruption"). Similar changes have been reported in human fetal hydrocephalus (pseudo-schizencephaly) (123).

SPECIFIC CATEGORIES OF HYDROCEPHALUS

Hydrocephalus can be divided into major categories (Table 8-3). The first is overproduction of CSF. Essentially all patients in this category have choroid plexus papillomas, a rare tumor. A very small number may have diffuse villous hyperplasia of the choroid plexus, mentioned earlier in the chapter (43–45). The other major category is obstruction to normal CSF flow and absorption. This second category, termed obstructive hydrocephalus, is generally divided into intraventricular obstructive hydrocephalus caused by intraventricular obstruction of CSF flow, and EVOH, in which there is cisternal obstruction to CSF flow or diminished absorption of CSF. In addition to these categories, the introduction of the Greitz model of CSF hydrodynamics based on the arterial pulsatile pressure wave leads to the concept of purely communicating hydrocephalus, which assumes no physical obstacle to the flow of CSF but an inability of the thecal sac to appropriately buffer the systolic pressure waves.

In this section, various causes of hydrocephalus are presented. For each type of hydrocephalus the most common causes, the mechanisms by which they cause hydrocephalus, the specifics of the radiologic

TABLE 8-3 Categories of Hydrocephalus

A.	Hydrocephalus secondary to overproduction of CSF
	Choroid plexus papillomas
	Diffuse villous hyperplasia of the choroid plexus
B.	Hydrocephalus secondary to disturbance of CSF flow or absorption
	Intraventricular obstructive hydrocephalus
	EVOH
C.	Hydrocephalus secondary to a loss of thecal compliance
	"Normal-pressure" chronic communicating hydrocephalus

appearance of each cause, and the appearance of the associated hydrocephalus will be discussed.

Hydrocephalus Resulting From Excessive Formation of CSF (Choroid Plexus Papillomas)

Choroid plexus papillomas (see Chapter 7) (Fig. 8-22) are large aggregations of choroidal fronds that are microscopically similar to normal choroid plexus; these neoplasms can produce great quantities of CSF (124,125). Choroid plexus papillomas account for 2% to 4% of childhood intracranial tumors. They usually present during infancy with signs of increased intracranial pressure; occasionally, however, they are found incidentally at postmortem examination. In the past, the presence of hydrocephalus was thought to be related to the mass effect of the tumor, the presence of proteinaceous CSF, or intraventricular hemorrhage with subsequent obstruction of CSF flow (obstructive hydrocephalus). More recent preoperative and postoperative studies have supported earlier suggestions that, at least in some cases, oversecretion of CSF by the papilloma produces hydrocephalus (124,125) by overcoming the capacity of the system to absorb the fluid. It has also

been hypothesized that, by pulsating into the ventricular lumen, the papilloma increases the amplitude of the CSF pressure, thus creating communicating hydrocephalus (27). This theory could apply to hydrocephalus associated with choroid plexus hyperplasia as well (Fig. 8-23).

The imaging appearance of choroid plexus papillomas on CT and MR was discussed and illustrated in Chapter 7. Briefly, the tumors are frond-like, enhancing masses that are most commonly located in the trigones of the lateral ventricles, with the bodies and temporal horns of the lateral ventricles, the third ventricle, and the fourth ventricle being the next most common sites. In contrast to adults, in whom the fourth ventricle is the most common site for these tumors, fourth ventricular choroid plexus papillomas are very rare in the pediatric age group. Resection of the tumor cures the hydrocephalus in most patients.

Hydrocephalus Secondary to Intraventricular Obstruction of CSF Flow (Noncommunicating Hydrocephalus)

Tumors and Cysts

Hydrocephalus may result from obstruction of any portion of the ventricular system from the lateral ventricles to the fourth ventricular outflow foramina of Luschka and Magendie. The most common location for obstruction are the locations where the CSF pathway is narrow: the foramina of Monro, the posterior third ventricle, the aqueduct of Sylvius, the fourth ventricle, and the fourth ventricular outflow foramina. Tumors are the most common cause of such obstructions in the pediatric age group.

Tumors and arachnoid cysts can grow into and obstruct the foramina of Monro from a number of locations. Masses originating in the lateral ventricles, such as choroid plexus tumors (Figs. 8-22 and 8-23), ependymomas, astrocytomas, or meningiomas, typically cause obstruction at the foramina of Monro, whereas masses originating in the third ventricle, such as astrocytomas, choroid plexus papillomas, craniopharyngiomas, or pineal region tumors, can grow anteriorly or superiorly to obstruct the foramina of Monro or posteriorly or inferiorly to obstruct the cerebral aqueduct. Suprasellar tumors and arachnoid cysts may occasionally grow upward to the foramina of

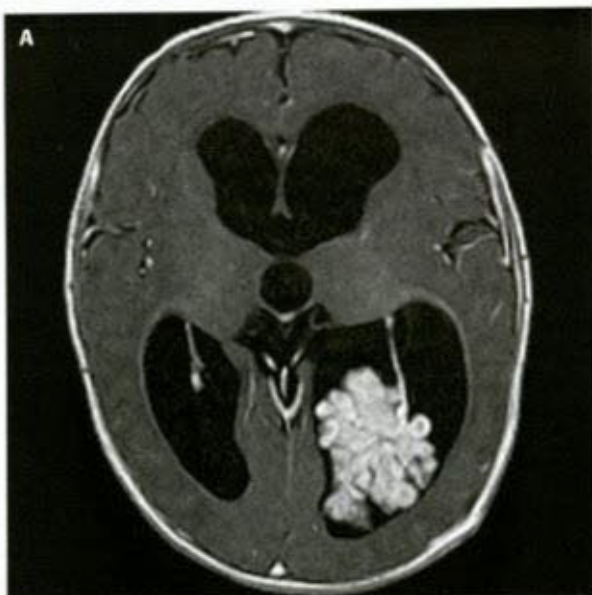


FIG. 8-22. Hydrocephalus and choroid plexus papilloma. Axial (A) and coronal (B) postcontrast T1 images show a dense, avidly enhancing mass in the left atrium. It does not obstruct the ventricle. The bilateral, symmetrical hydrocephalus is tentatively explained by an overproduction of CSF, by the high density of protein usually found in the CSF, and by the increased pulsatility of the tumorous choroid plexus.

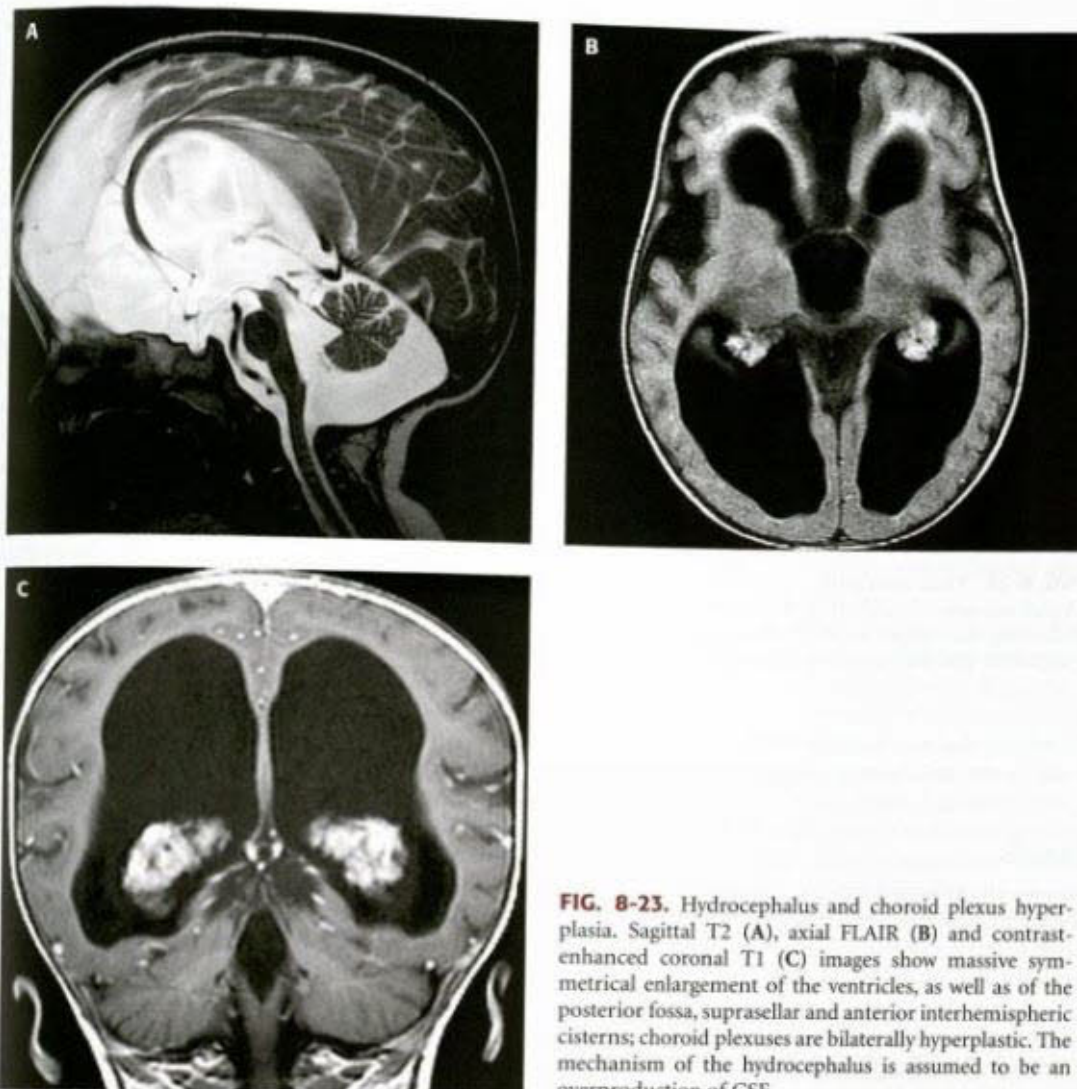


FIG. 8-23. Hydrocephalus and choroid plexus hyperplasia. Sagittal T2 (A), axial FLAIR (B) and contrast-enhanced coronal T1 (C) images show massive symmetrical enlargement of the ventricles, as well as of the posterior fossa, suprasellar and anterior interhemispheric cisterns; choroid plexuses are bilaterally hyperplastic. The mechanism of the hydrocephalus is assumed to be an overproduction of CSF.

Monro, pushing the floor of the third ventricle superiorly (Fig. 8-24). In children with tuberous sclerosis, giant cell tumors, which originate adjacent to the foramina of Monro, often grow medially and obstruct the foramina (see Chapters 6 and 7).

Obstruction of the Sylvian aqueduct is a common cause of hydrocephalus. The most common cause of obstruction at this level in children is a tumor of the pineal region (see Chapter 7). Germ cell tumors (germinoma, endodermal sinus tumor, embryonal cell carcinoma, choriocarcinoma, teratoma), tumors of pineal origin (pineoblastoma, astrocytoma in young adults mostly but also in teenagers), astrocytomas (from the quadrigeminal plate, thalamus, or the tegmentum of the midbrain), meningiomas (from the tentorium), supravermian arachnoid cysts, or varices of the vein of Galen may all cause hydrocephalus from compression of the aqueduct (in vein of Galen arteriovenous malformations, a component of increased venous pressure also contributes to the hydrocephalus). CT identifies most of these lesions; however, astrocytomas of the posterior third ventricle or arising in the quadrigeminal plate are often subtle and difficult to identify on CT. Both are easier to identify by MR because MR has inherently better contrast resolution and the ability to image in the sagittal plane. Posterior third ventricular masses are seen as discrete masses within the ventricle, whereas tumors of the quadrigeminal plate are seen on MR as bulbous tectal masses with prolonged T2 relaxation and poorly defined margins (Fig. 8-6A, B, and E). Thus, MR is essential to differentiate

benign aqueductal stenosis from stenosis secondary to a tumor in children with aqueductal narrowing.

Children with *tumors of the fourth ventricle and cerebellum* frequently have hydrocephalus by the time of presentation. The most common posterior fossa neoplasms in the pediatric age group are medulloblastomas, followed by cerebellar astrocytomas and ependymomas (see Chapter 7). Imaging studies show the tumor in the fourth ventricle, obstructing CSF flow directly (Figs. 8-14 and 8-25), or in the cerebellum compressing the aqueduct and/or ventricle. In contrast to cerebellar or ventricular tumors, hydrocephalus is uncommon in pontine neoplasms.

Rarely, *tumors of the spine and spinal cord* (see Chapter 10) can cause hydrocephalus. It is important to think about spinal tumors in all cases of unexplained new onset hydrocephalus in children and to image their spines accordingly. The cause of the hydrocephalus in these cases is not obvious, but a number of hypotheses have been proposed. Among these are (1) increased viscosity of CSF secondary to elevated CSF protein, (2) obliteration of cisterna magna due to rostral extension of tumor, (3) restriction of the thecal space and poor buffering of the systolic pressure wave, and (4) blockage of spinal subarachnoid pathways of CSF resorption. All of these mechanisms may have a role in some cases, although the fact that Chiari I malformations (see Chapter 5) are inconstantly associated with hydrocephalus makes mechanism (2) rather unlikely. Because almost all reported cases have very high CSF

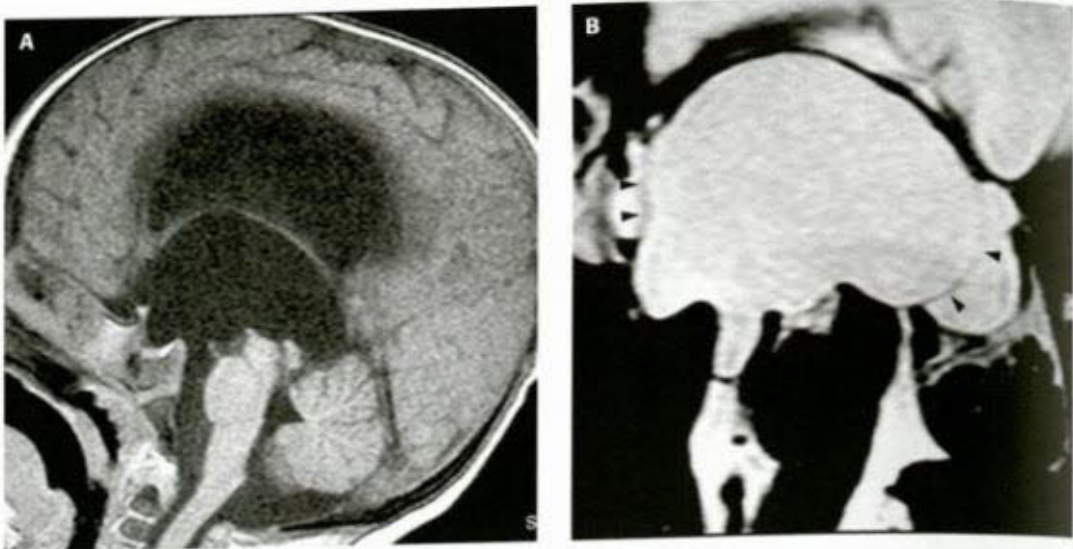


FIG. 8-24. Third ventricular cyst. **A.** Midline sagittal T1 image shows triventricular hydrocephalus suggesting aqueductal stenosis, although the aqueduct looks patent. **B.** Midline sagittal FIELTA shows a thin cyst wall (arrowheads), indicating that a large CSF-filled cyst occupies most of the ventricle, sparing the anterior and posterior portions only. It blocks CSF flow through the rostral end of the aqueduct and the foramina of Monro.

protein content, it is likely that dissemination of tumor through CSF probably plays a role in the development of hydrocephalus in these patients (126).

Aqueductal Stenosis

After the initial closure of the neural tube, its lumen has a relatively uniform dimension throughout the neural axis. As the brain and spinal cord mature, the lumen of the neural tube expands in some areas, such as the cerebral ventricles, but not, or less, in others, such as the spinal canal and Sylvian aqueduct. The lumen of the aqueduct decreases in relative size beginning in the second month of fetal life, continuing until birth (127). This relative narrowing appears to be caused by growth pressures upon the aqueduct from adjacent mesencephalic structures.

Aqueductal stenosis can be developmental or acquired (128–130) and is present in approximately 20% of patients with hydrocephalus. Its incidence ranges from 0.5 to 1 per 1000 births with a recurrence rate in

siblings of 1% to 4.5% (131). The normal mean cross sectional area of the aqueduct at birth is $.5 \text{ mm}^2$ with a range of 0.2 to 1.8 mm^2 (132). Aqueductal stenosis, the aqueduct is focally reduced in size, narrowing generally occurs either at the level of the superior colliculi or at the collicular sulcus (132). In many instances, aqueductal stenosis is accompanied by branching of the aqueduct into dorsal and ventral channels; the dorsal channel is often divided into a group of several ductules. This condition has been termed aqueductal forking (133). Forking of the aqueduct is often accompanied by fusion of the quadrigeminal body, fusion of the third nerve nuclei, and molding or beaking of the tectum. In some patients, the shape of the molded tectum is congruent with the shape of the medial aspect of the adjacent temporal lobes, which are markedly expanded by hydrocephalus. This congruency has motivated some authors to postulate that aqueductal stenosis may be a secondary phenomenon in some patients, resulting from communicating hydrocephalus and secondary compression of the quadrigeminal plate by the dilated cerebral hemispheres (107,108,134) (Fig. 8-13).

The onset of symptoms is usually insidious; it may occur at any time from birth to adulthood. As in all types of hydrocephalus, the symptoms depend upon the cause of the hydrocephalus and the age of the patient at the time of onset.

The CT appearance of benign aqueductal stenosis is dilation of the lateral and third ventricles with a normal sized fourth ventricle. This appearance may be misleading, however, since the fourth ventricle is normal in a significant percentage of patients with communicating hydrocephalus. Moreover, as stated earlier, tectal tumors that are large enough to obstruct the aqueduct can be missed on routine CT scans. In all patients with suspected aqueductal stenosis the posterior third ventricle should be carefully scrutinized for the presence of a mass. *Asymmetry of the posterior aspect of the third ventricle is indicative of an MR study to rule out the presence of a mass in the mesencephalon or posterior thalamus.* The MR findings in aqueductal stenosis are non-specific but are nonetheless quite variable. Patients with severe hydrocephalus generally have a stenosis in the proximal aqueduct, either at the level of the superior colliculi or at the entrance to the aqueduct immediately inferior to the posterior commissure (104). In patients with mild hydrocephalus, the level of obstruction is more often in the distal portion of the aqueduct. When the distal aqueduct is stenotic,



FIG. 8-25. Fourth ventricular tumor. Midline sagittal postcontrast T1 image shows triventricular hydrocephalus due to the large fourth ventricular medulloblastoma.

the dilated proximal aqueduct tends to displace the quadrigeminal plate posteriorly. MR can nearly always differentiate benign aqueductal stenosis from neoplastic aqueductal stenosis. Tectal and tegmental gliomas that compress and obstruct the aqueduct appear as bulbous masses that have high signal intensity on T2/FLAIR images (Fig. 8-6E). These tumors uncommonly enhance (135).

A special case of distal aqueductal stenosis is the aqueductal web. An aqueductal web is a thin membrane of brain tissue situated in the distal aqueduct, restricting the flow of CSF into the fourth ventricle. It has been suggested that the membrane may be the result of a small glial inclusion of the caudal aqueduct that becomes an attenuated sheet of tissue secondary to prolonged pressure from and dilatation of the canal above it (136). The imaging appearance is characteristic, consisting of a thin membrane of tissue separating a dilated aqueduct from a normal-sized fourth ventricle (Fig. 8-12B). The importance of recognizing aqueductal webs is that a third ventriculostomy (see section on "Imaging of treated Hydrocephalus and Resulting Complications") is likely to result in complete resolution of the hydrocephalus. There also exists a possibility of perforating the membrane via fiberoptic ventriculostomy (137–139), another means of obviating the need of an shunting shunt. Indeed, in some centers endoscopic aqueductoplasty is now being performed for aqueductal stenosis of many causes with promising results (139).

X-linked Hydrocephalus (HSAS, CRASH Syndrome)

X-linked hydrocephalus, also known as Bickler-Adams syndrome, X-linked aqueductal stenosis and hereditary stenosis of the aqueduct of Sylvius (HSAS), is a rare hereditary disorder with variable symptoms that include mental retardation, hydrocephalus secondary to aqueductal stenosis, spasticity of the lower extremities, and clasped, adducted thumbs (140). The disorder is caused by mutation of the L1CAM gene that has been localized to Xq28 (141,142). Identification of this disorder is important, not only because of the potential for future siblings being similarly affected, but also because affected patients have poor neurological outcome despite early shunting (143,144). This complex malformation is allelic with (has the same chromosomal location as) the so-called MASA syndrome, which consists of mental retardation, obesity, shuffling gait, and adducted thumbs (145). Some affected

patients have Hirschsprung disease, as well, while others may not have hydrocephalus (146). Because the malformation is so complex, and because hydrocephalus seems to be only one small part of the disorder, Fransen et al. (147) have suggested that the disorder be renamed the CRASH syndrome (corpus callosum hypoplasia, retardation, adducted thumbs, spastic paraparesis, and hydrocephalus) and others have suggested that L1CAM should be investigated in any X-linked disorder associated with corpus callosum anomalies (146). As with many genetic disorders, the site of mutation within the L1 protein correlates with the severity of the disease (148,149).

Pathologic studies show that, in addition to hydrocephalus, affected patients have malformations of cortical development (see Chapter 5) with poor differentiation and maturation of cortical neurons being identified on histologic examination of the brain (143,144). Of interest, some authors have suggested that the aqueduct is narrowed by compression and is not primarily stenotic (150,151). Other pathologic features include absence or diminution of the size of the corticospinal tracts, fusion of the thalamus, fusion of the colliculi, and absence of the septum pellucidum. The corpus callosum is typically small and may be absent (46,152) (see Chapter 5).

Very few reports of MR studies in X-linked hydrocephalus have been published. The only series of patients with this disorder indicates that affected patients have enlargement of the massa intermedia (thalamic fusion), abnormal flattening of the mesencephalic tectum, a small brainstem, and diffuse hypoplasia of cerebral white matter. Interestingly, according to this report, the Sylvian aqueduct is usually patent (153). Others have reported similar findings of large lateral ventricles, hypoplastic cerebral white matter, thin cerebral cortex with abnormal sulcation, fused thalamus, and hypoplasia/hypogenesis/agenesis of the corpus callosum. The authors have seen very few cases of X-linked hydrocephalus and, in those cases, the findings were similar (Figs. 8-26 and 8-27).

Aqueductal Gliosis

Aqueductal gliosis is a postinflammatory process that is usually secondary to a perinatal infection or hemorrhage (128,133,154). It is becoming more prevalent as newborns with bacterial meningitis or intracranial hemorrhage survive at increasing rates. As in benign aqueductal

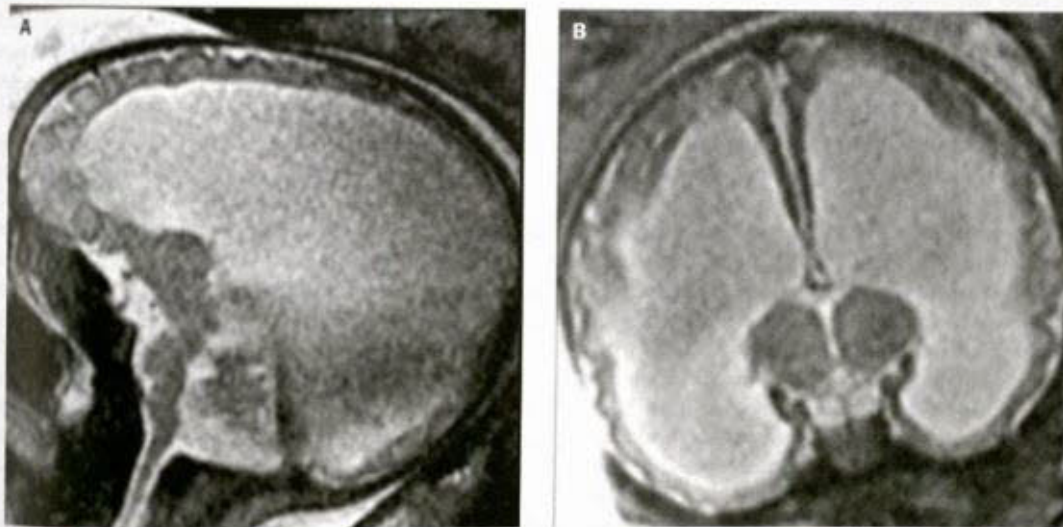


FIG. 8-26. CRASH syndrome, formerly known as X-linked hydrocephalus. Fetal T2-weighted images, sagittal (A) and coronal (B), show severe ventricular dilatation, thin cerebral mantle, absent or extremely hypoplastic corpus callosum, compressed aqueduct, and small posterior fossa. The syndrome is related to a developmental failure of the axons to fasciculate; as a consequence, the white matter is extremely hypoplastic. Hydrocephalus still may develop due to compression of the midbrain.

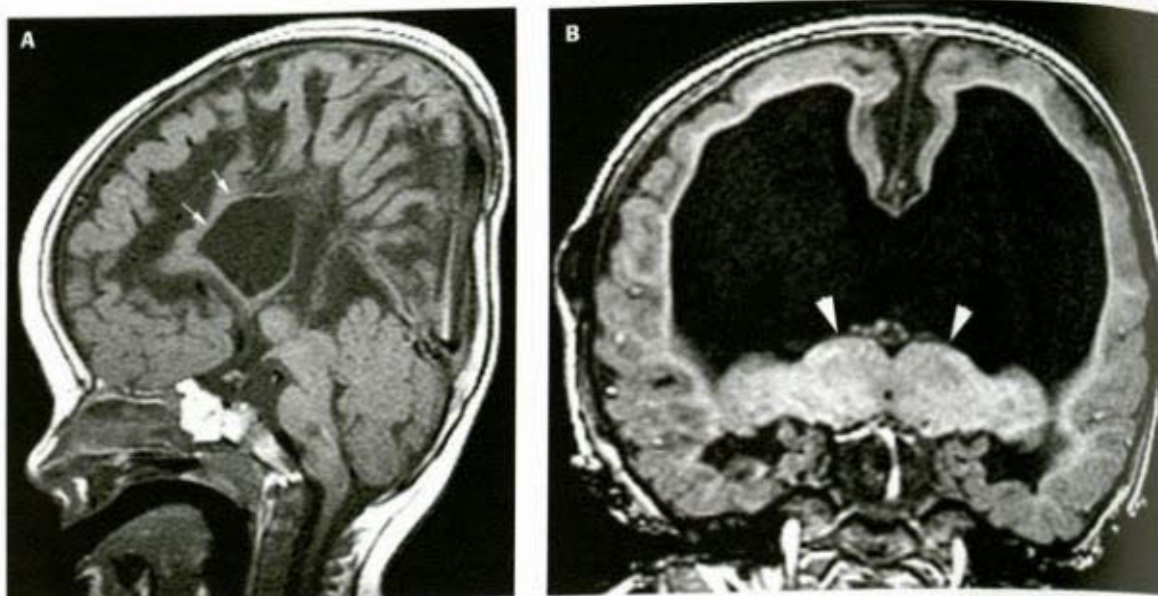


FIG. 8-27. CRASH syndrome, formerly known as X-linked hydrocephalus, in an older child. **A.** Midline sagittal T1. Small, dysmorphic brainstem, with a narrow aqueduct. The lateral ventricles are too large, and the corpus callosum (*arrows*) is thin and incompletely formed. **B.** Coronal T1. The thalamus (*white arrowheads*) are small and incompletely separated. The volume of cerebral white matter is markedly diminished and the cortex has an abnormal gyral pattern with too many sulci that are too shallow.

stenosis, the onset of symptoms, which are those of hydrocephalus, is insidious. The ependymal lining of the aqueduct is destroyed and marked fibrillary gliosis of adjacent tissue is evident at autopsy.

On imaging studies, differentiation of aqueductal stenosis from aqueductal gliosis is not possible. The appearance of the two entities is identical on ultrasound, MR, and CT.

Congenital Anomalies

Among congenital malformations of the brain, two anomalies are, by far, the most common causes of hydrocephalus. The more common of these, the Chiari II malformation, has been extensively discussed in Chapter 5 (Section "Chiari II Malformations") and will therefore be covered only briefly in this section. The Chiari II malformation accounts for approximately 40% of all hydrocephalus in children (71). Although there is still some dispute as to the cause of hydrocephalus in these patients, the most generally accepted theory is that of Russell (133). Russell demonstrated that adequate flow of CSF exists between the ventricles and the spinal canal in patients with Chiari II malformations, but that the connection between the lumbar subarachnoid space and the subarachnoid space over the cerebral convexities is poor. The implication is that disturbance in CSF flow is most likely the result of the abnormal location of the exit foramina of the fourth ventricle below the foramen magnum, within the cervical spinal canal. Since the spinal canal absorbs much less CSF, hydrocephalus develops. Recent experience showing improvement in both posterior fossa herniation and in the degree of fetal ventriculomegaly after fetal myelomeningocele repair does not contradict this theory (155,156).

It is an important clinical concept that patients with the myelomeningocele/Chiari II malformation who develop occipital headaches at night probably have a shunt malfunction. Fatal shunt malfunctions may result in brainstem compression and consequent apneic spells. Symptoms of brainstem compression in patients with the Chiari II malformation are often interpreted as resulting from compression of the medulla by the neural arches of C-1 and C-2 or by the foramen magnum. These patients may be subjected to unnecessary decompressions of the foramen magnum and C-1 and C-2 instead of adjustment or replacement of the ventriculo-peritoneal shunt. It is important to

recognize that the fourth ventricle is normally a thin vertical slit in Chiari II malformation (see Figs. 5-162 and 5-163). The presence of a normal-appearing or enlarged fourth ventricle in these patients suggests a shunt malfunction or an isolated fourth ventricle that resists CSF diversion (see Fig. 5-165).

Hydrocephalus is present in 70% to 80% of patients with the Dandy-Walker malformation (see Chapter 5, Section "Overview of Midbrain and Hindbrain Development") (157,158). It is also common in children with cobblestone cortex disorders (Chapter 5, Section "Malformations of cortical development") and rhombencephalosynapsis (Chapter 5, Section "Classification of Midbrain-Hindbrain Malformations").

The Isolated (Trapped) Fourth Ventricle

When both the aqueduct of Sylvius and the fourth ventricular outflow foramina are occluded, the fourth ventricle becomes isolated from the remaining ventricular system and from the CSF circulation of the subarachnoid space. Continued CSF production by the choroid plexus of the fourth ventricle leads to progressive cystic dilatation of the ventricle; the dilated ventricle can then act as an expanding mass in the posterior fossa. The trapped fourth ventricle appears after shunting of the lateral ventricles and seems to result from mechanical or inflammatory changes that obstruct the aqueduct and the fourth ventricular outlet foramina (159). Thus, CSF from the fourth ventricle cannot drain proximally through the shunt catheter or distally through normal CSF pathways; the ventricle becomes "isolated."

The clinical presentation depends upon the baseline neurological status of the patient. In those patients who have moderate to severe preexisting neurological deficits, the isolated fourth ventricle accentuates preexisting deficits without causing prominent posterior fossa signs or symptoms. Patients with normal or near normal baseline neurological examinations tend to present with signs and symptoms of a posterior fossa mass. A history of a recent ataxia, diplopia, or increasing drowsiness is common (160). Occasionally, patients are mildly symptomatic or asymptomatic and the isolated fourth ventricle can be an incidental finding (159). In these asymptomatic patients, a stable state is presumably reached between production and absorption of the

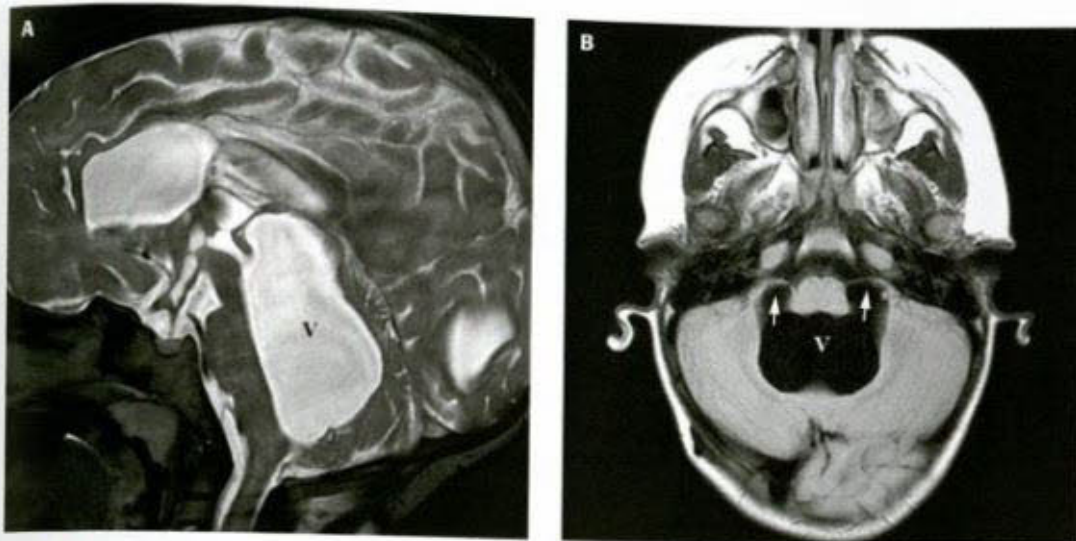


FIG. 8-28. Isolated (trapped) fourth ventricle resulting from previous septic meningitis. **A.** Midline sagittal T2. Huge, elongated fourth ventricle (*V*) that herniates toward the supratentorial space; it seems to communicate with the caudal aqueduct, but not with the cistern magna. Note the multiple loculations in the third ventricle. **B.** Axial FLAIR. The dilation of the fourth ventricle (*V*) extends into both lateral recesses (*white arrows*) presumably because of the obstruction of both foramina of Luschka.

within the fourth ventricle, resulting in the absence of signs of increased intracranial pressure. Close follow-up however is justified as complete lack of evolutivity is uncertain and acute decompensation may occur.

On imaging studies, the isolated fourth ventricle appears as a rounded or pear-shaped midline cystic structure (Figs. 8-28) in the posterior fossa (159–161). In some cases the lateral recesses may be ballooned (Fig. 8-28B) (162). The lateral and third ventricles are small or only moderately enlarged if the ventriculo-peritoneal shunt is functioning. The aqueduct may be completely occluded or the distal aqueduct may be dilated (Fig. 8-28A). Treatment is the installation of a fourth ventricle to peritoneal shunt; endoscopic therapy is currently experimental (138), as is stenting of the fourth ventricle to allow communication with the subarachnoid space (163). After shunting, there is rapid reversal of posterior fossa signs, if they had been present or progressive. In children with preexisting neurological deficits, a return to baseline is generally observed. Occasionally, further treatment, such as posterior fossa decompression, may be necessary (159,160).

Hydrocephalus Secondary to Extraventricular Obstruction of CSF

This represents approximately 30% of all childhood hydrocephalus (171). After leaving the foramina of the fourth ventricle, CSF normally enters the cisterna magna and basilar cisterns and then progresses into the cerebral and cerebellar subarachnoid spaces. Normal CSF drainage is impaired if the normal CSF pathways are obstructed by thickened arachnoid or meninges (Fig. 8-29). (The Greitz model would hypothesize that the obstruction of the cisterns compromises the dampening of the ventricular pressure wave, and that the full force of the wave is then exerted against the parenchyma (25,55); see the theory section earlier in this chapter.) CSF drainage is also impaired if the dural venous sinuses are obstructed or if pressure in the sinuses becomes elevated. Unless venous thrombosis is present, it is usually not possible to determine the level of the extraventricular obstruction to CSF flow from imaging studies.

Impaired flow of CSF through the subarachnoid spaces (or reduced compliance [55]) may result from recent or remote intracranial

hemorrhage, bacterial infections, or granulomatous meningitis. Certain features seen on imaging studies can help to differentiate the different causes of the hydrocephalus. For example, hemorrhage often leaves a transient hemosiderin staining of the parenchyma, ependyma, or pia-arachnoid (superficial siderosis). The hemosiderin will appear black on T2-weighted spin-echo images (Fig. 8-30B–D) (164,165) and especially so on T2*-weighted gradient-echo or susceptibility-weighted images (166,167). Although hemosiderin will remain at the site of hemorrhage for months or years after parenchymal hemorrhages, it is absorbed much more quickly from the ependyma and arachnoid. Both infectious and carcinomatous meningitis may result in meningeal enhancement (Figs. 8-31 and 8-32) after administration of intravenous contrast (168–170). Differentiation of subarachnoid tumor from infection, however, is not possible at this time by radiologic methods.

Hemorrhage

Intraventricular hemorrhage is common in neonates, particularly in babies with a gestational age of 32 weeks or less (see discussion in Chapter 4), with hydrocephalus being a frequent complication. Acute posthemorrhagic hydrocephalus is most commonly the result of red blood cells obstructing the ventricular system or the arachnoid villi; this acute hydrocephalus has no prognostic implications. Scarring and fibrosis begin to appear in the subarachnoid spaces approximately 10 days after the hemorrhagic event (171). The fibrosis tends to be most prominent in the region of the cisterna magna. This adhesive arachnoiditis is the cause of the subacute hydrocephalus that occurs after germinal matrix hemorrhage in premature infants (Fig. 8-30). The presence of subacute hydrocephalus imparts a poor functional prognosis to the infant. However, it is important not to mistake *ex vacuo* ventricular enlargement secondary to periventricular white matter injury for ventricular enlargement secondary to impaired CSF circulation. Therefore, it is important to look for evidence of periventricular white matter injury in all such cases. Irregularity of the ventricular margins, cavitation in the periventricular white matter and T1 and T2 shortening within the periventricular white matter (see Chapter 4) all suggest that brain injury has occurred. Of course, as with all potential cases of pediatric hydrocephalus, correlation with head circumference measurements is vital.

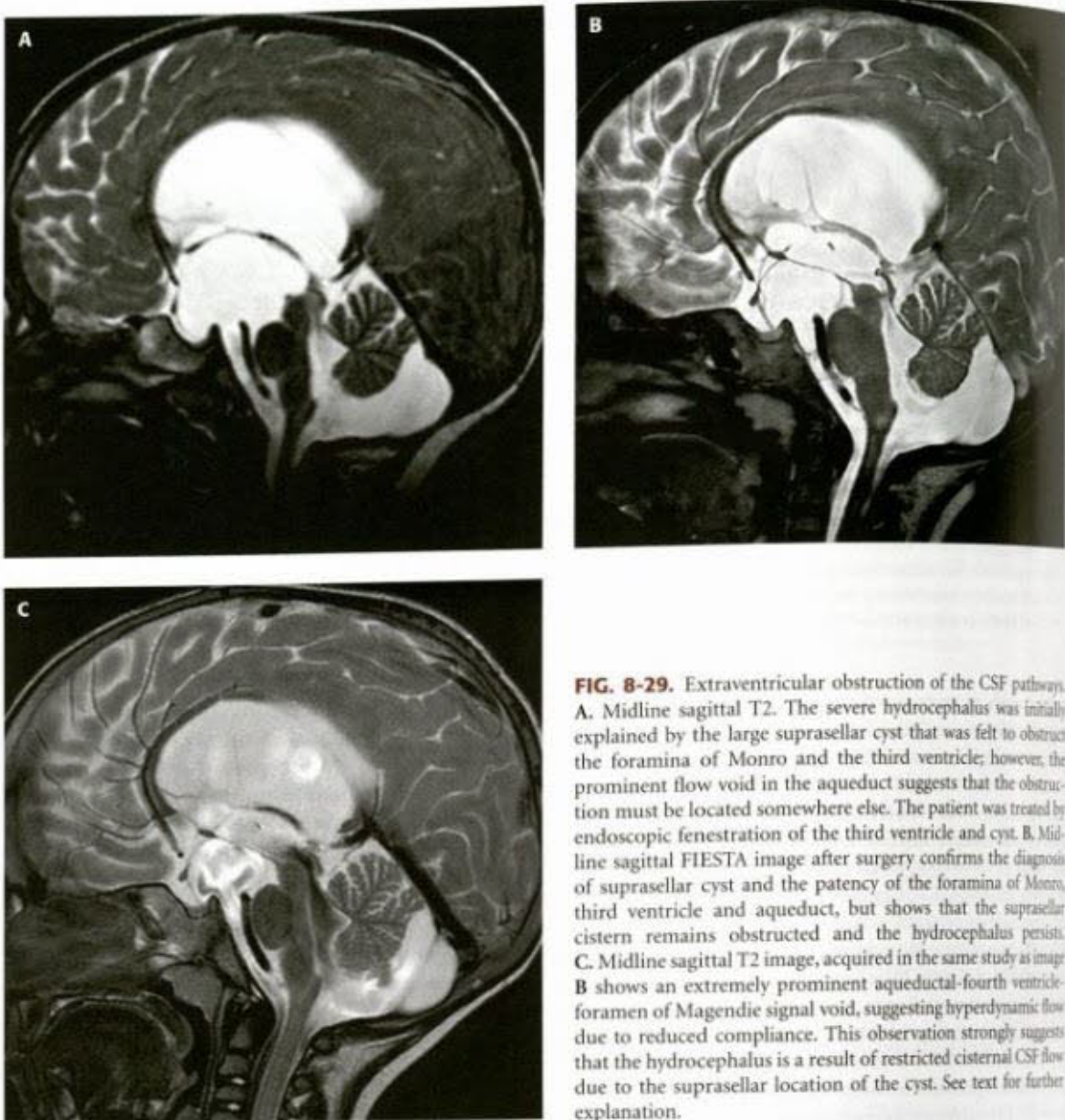


FIG. 8-29. Extraventricular obstruction of the CSF pathway. A. Midline sagittal T2. The severe hydrocephalus was initially explained by the large suprasellar cyst that was felt to obstruct the foramina of Monro and the third ventricle; however, the prominent flow void in the aqueduct suggests that the obstruction must be located somewhere else. The patient was treated by endoscopic fenestration of the third ventricle and cyst. B. Midline sagittal FIESTA image after surgery confirms the diagnosis of suprasellar cyst and the patency of the foramina of Monro, third ventricle and aqueduct, but shows that the suprasellar cistern remains obstructed and the hydrocephalus persists. C. Midline sagittal T2 image, acquired in the same study as image B shows an extremely prominent aqueductal-fourth ventricle foramen of Magendie signal void, suggesting hyperdynamic flow due to reduced compliance. This observation strongly suggests that the hydrocephalus is a result of restricted cisternal CSF flow due to the suprasellar location of the cyst. See text for further explanation.

Subarachnoid hemorrhage in full term infants is most often caused by trauma (see Chapter 4). The causes of acute and chronic hydrocephalus in these infants are similar to the causes of hydrocephalus in premature infants with intraventricular hemorrhage; however, the prognostic value of the hydrocephalus is not as great in term infants as in premature infants.

Meningitis

Inflammation of the leptomeninges may lead to obstruction the CSF pathways (see Chapter 11, Section "Meningitis"). In the acute phase, hydrocephalus is caused by blockage of the CSF flow pathways by purulent fluid. Another component of acute hydrocephalus may be inflammation of the arachnoid granulations (46,172). In the chronic phase, organization of exudate and blood results in fibrosis of the subarachnoid spaces with subsequent obstruction to normal CSF flow and resultant hydrocephalus (46,172).

Clinically significant hydrocephalus is less common in bacterial meningitis than in granulomatous and fungal meningitides. Indeed, hydrocephalus is almost always present at the time of presentation in

granulomatous and fungal meningitis. Hydrocephalus appears to be related to the duration and severity of the meningeal infections; in general, the longer the delay in treatment, the worse the prognosis for the patient. As a general rule, bacterial meningitis tends to produce cisternal cortical arachnoiditis, whereas granulomatous or parasitic meningitides produce cisternal obstruction (Fig. 8-31) (46). Viral meningitides may result in obstruction at either point, albeit rarely. Ventricular dilatation, which presumably results from transiently diminished CSF absorption, is the most common finding on ultrasound, CT scan, or unenhanced MR scans in patients with bacterial meningitis. Contrast enhanced MR scans often show localized or diffuse meningeal enhancement in bacterial and fungal meningitides (see Fig. 8-31 and example in Chapter 11) (169). Arachnoidal scarring from meningitis may also result in arachnoid loculations, which may be indistinguishable from arachnoid cysts.

CSF Seeding of Tumor

A number of neoplastic processes can involve the subarachnoid space diffusely (see Chapter 7). The most common of these in children are



FIG. 8-30. Post hemorrhagic hydrocephalus in a former premature infant. **A.** Midline sagittal FIESTA image shows severe hydrocephalus, dehiscent septum pellucidum, and an obstructed aqueduct. Low signal intensity around the brainstem and inferior vermis suggests hemosiderin from intraventricular hemorrhage. **B–D.** Axial T2*-weighted images show hypointensity (black arrows) from magnetic susceptibility effects of blood on the surface of the brainstem and cerebellum (**B**), choroid plexuses and walls of the lateral ventricles (**C** and **D**).

neuroblastoma, germinoma, leukemia, and lymphoma; it can also be seen in a variant of pilocytic astrocytoma, the pilomyxoid astrocytoma (173). This is in contrast to adults where adenocarcinoma is the most common tumor to show diffuse meningeal involvement (174).

Older patients with CSF seeding of tumor (also called carcinomatous meningitis) typically present with headache, stiff neck, and cranial nerve palsies. Hydrocephalus occurs only later in the course of the disease. As with infectious meningitis, ventricular enlargement is the most common manifestation of this process on ultrasound, CT, and unenhanced MR scans. Occasionally, diffuse meningeal enhancement may be seen on contrast-enhanced CT scans. Significant enhancement of the subarachnoid spaces and cranial nerves (particularly cranial nerves 3 and 8) is typically seen on contrast-enhanced MR scans (Fig. 8-32) (175,176,177).

Venous Hypertension

Obstruction of the cerebral veins and sinuses is thought to be a cause of communicating hydrocephalus in infants (176–178). It appears that the increased intracranial venous pressure may produce either hydrocephalus or pseudotumor cerebri, depending upon the patient's age (176). Hydrocephalus is more likely if the patient is less than 18th months of age, whereas pseudotumor cerebri is noted if the patient is more than 3 years of age. This difference is thought to result from an expandable calvarium and softer, less myelinated parenchyma in the infant; both of these factors allow greater ventricular dilatation under high pressure (179–182). Once the cerebrum is myelinated and the sutures are fused or the calvarium is otherwise prevented from expanding, intracranial hypertension occurs without ventricular enlargement and results in pseudotumor cerebri (176,179). The hydrodynamic theory

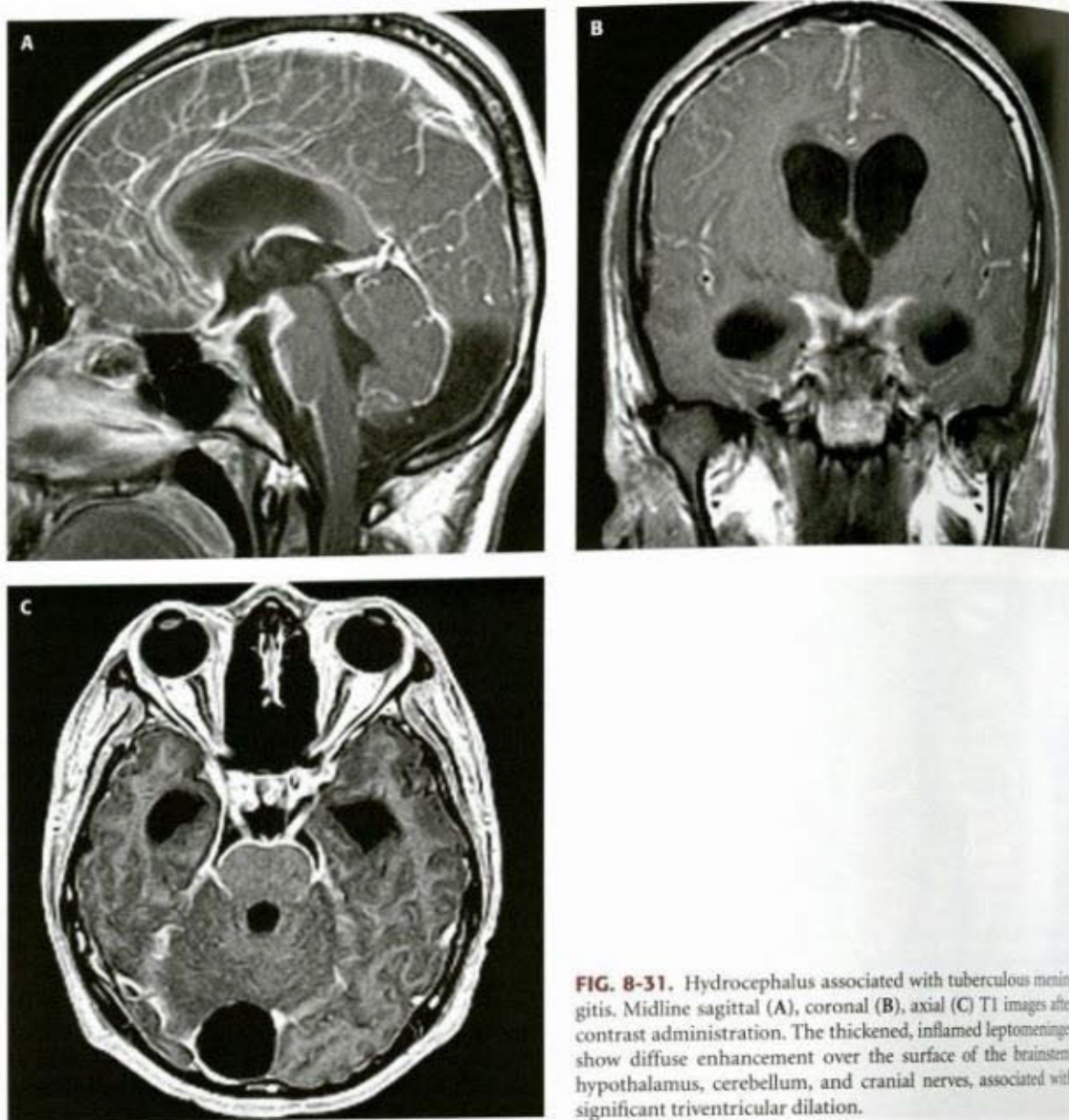


FIG. 8-31. Hydrocephalus associated with tuberculous meningitis. Midline sagittal (A), coronal (B), axial (C) T1 images after contrast administration. The thickened, inflamed leptomeninges show diffuse enhancement over the surface of the brainstem, hypothalamus, cerebellum, and cranial nerves, associated with significant triventricular dilation.

of Greitz would suggest that, in infant with an elastic skull, CSF would accumulate immediately above the obstruction, in the pericerebral subarachnoid spaces, much more than in the ventricles (25).

Ventricular enlargement results from skull base abnormalities in a number of syndromes. These include achondroplasia (183,184) (Fig. 8-33), craniofacial syndromes that result in multisutural craniosynostosis (Apert syndrome, Carpenter syndrome, Pfeiffer syndrome, Crouzon syndrome, and others described in Chapter 5, Section "Craniosynostosis"), and the Marshall-Smith syndrome (a syndrome of accelerated osseous maturation and CNS malformations) (178,185–187). It has been postulated that the ventricular enlargement in all of these syndromes results from diminished venous outflow through the small jugular foramina that, in turn, result from hypoplasia of the skull base (188) (Fig. 8-33D). These theories are supported by experimental evidence in the case of achondroplasia (189,190) and Crouzon syndrome (191). The mechanism of this ventricular enlargement is believed to be an increase in superior sagittal sinus pressures, leading to a decreased pressure gradient across the arachnoid villi, from the subarachnoid spaces to the superior sagittal sinus. (The hydrodynamic theory would suggest that

the arterial systolic inflow not being properly buffered because of the increased pressure in the dural sinuses and, thus, the compliance of the system is decreased (25).) The resultant increased intracranial pressure results in expansion of the calvarium and ventricles in infants until the pressure normalizes (186,187) or the hydrocephalus becomes compensated (192). Typical imaging signs of hydrocephalus are not visible in these patients. For example, temporal horn enlargement results from expansion of the middle cranial fossa and frontal horn enlargement may be the result of the enlarged anterior fontanelle, not necessarily from increased intraventricular pressure. Also, because of the sutural synostosis, the bodies and trigones of the lateral ventricles may not enlarge until a cranial expansion has been performed (193). The indication for shunting in these patients seems to be based primarily on the presence of severe ventricular dilation or evidence of persistent intracranial hypertension such as papilledema (193). A recent study suggests that the intracranial pressure normalizes in patients with craniosynostosis syndromes at the age of approximately 6 years as a result of the enlargement of stylomastoid emissary veins (transcalvarial veins that allow venous drainage into the stylomastoid venous plexus) (194).

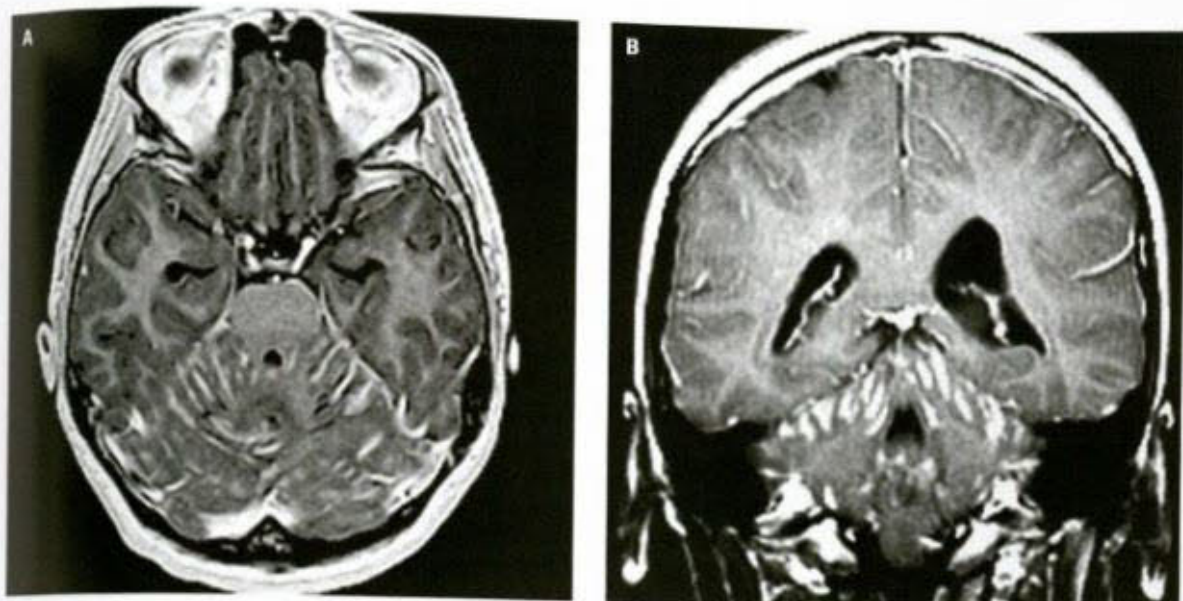


FIG. 8-32. Hydrocephalus associated with leptomeningeal tumoral dissemination (high risk medulloblastoma). Postcontrast T1-weighted axial (A) and coronal (B) images show a thick enhancing layer of leptomeningeal carcinomatosis (carcinomatous meningitis), mainly overlying the cerebellar folia.

Progressive head enlargement in infants can also result from thrombosis of the dural venous sinuses, presumably via the same mechanism. MR venography can be helpful to detect obstruction of the dural venous sinuses in children with increased CSF pressures with no other obvious cause. As two-dimensional (2D) time-of-flight MR venography may show apparent narrowing of the distal transverse and sigmoid sinuses that are caused by complex flow (sometimes by the presence of an arachnoid granulation or flow from the vein of Labbé) in those areas, time-resolved contrast-enhanced MR venography (see Chapter 1, Section "Magnetic Resonance Angiography and CT Angiography") is the study

of choice to evaluate the venous sinuses. However, MR venography cannot determine pressure differential across foci of narrowing in the dural venous sinuses. In difficult cases, it may be necessary to do a catheter venogram and measure pressures in the sinuses.

Normal Pressure Hydrocephalus

Normal pressure hydrocephalus (NPH) is a form of hydrocephalus in which a pressure gradient exists between ventricle and brain parenchyma, despite the fact that CSF pressure is within the normal range at the time of lumbar puncture. Intermittently high pressure probably



FIG. 8-33. Hydrocephalus from venous hypertension in a 15 month old infant with achondroplasia. A. Midline sagittal T1-weighted image shows the frontal bossing characteristic of the disease. Supratentorial ventricles are large, the posterior fossa is small, the crano-vertebral junction and cervical spinal canal are narrow. B. Coronal T2 image shows supratentorial ventricular dilation with typical rounding of the temporal horns compressing the hippocampi, and a prominent suprapineal recess (black arrow).

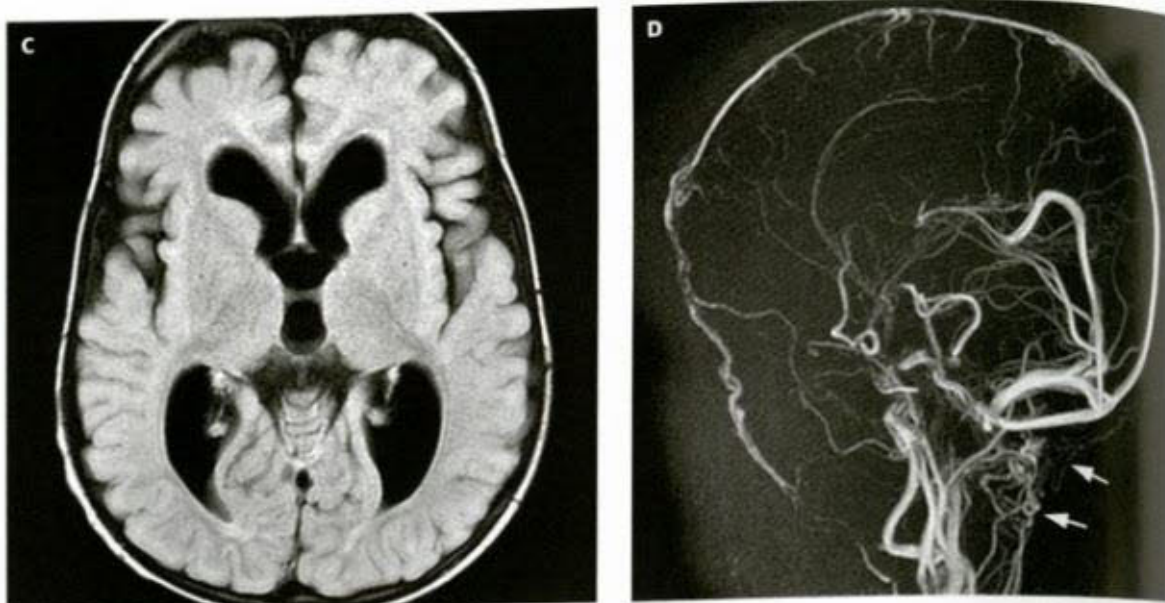


FIG. 8-33. (Continued) C. Axial FLAIR image shows diffuse ventricular dilation with prominent subarachnoid spaces over the frontal lobes and anterior interhemispheric fissure (associated subarachnoid enlargement). D. MR venogram shows both sigmoid sinuses to be interrupted in the jugular foramina. Prominent collateral venous flow can be seen through emissary veins and the venous plexuses around the foramen magnum (white arrows).

results in a compromise of normal compensatory pressure mechanisms (195,196); this is called a loss of compliance in the hydrodynamic theory (25). The fluctuating high pressures may combine with impaired regional CBF to cause ventricular enlargement and parenchymal destruction (131). The most common cause of NPH is communicating hydrocephalus with unidentified arachnoidal damage interfering with normal CSF dynamics, or loss of elasticity of the dural sac. Primary events leading to NPH include neonatal intraventricular hemorrhage, spontaneous subarachnoid hemorrhage, intracranial trauma, infections, and surgery (197). Among the pediatric population, it is most commonly seen in those who have underlying neurological pathology such as complications of meningitis or germinal matrix/intraventricular hemorrhage (198). NPH, therefore, is not merely a disease of adults but occurs in children, as well.

The ultrasound, CT, and MR appearance of NPH in children is indistinguishable from that of other forms of communicating hydrocephalus. However, measurements of CSF flow with flow-sensitive MRI methods have demonstrated that the CSF stroke volume (volume of CSF displaced with each cardiac systole) is reduced by 50% at the craniocervical junction and the venous stroke volume is reduced by 33% in the dural sinuses in communicating hydrocephalus. At the same time, intracranial pressure monitoring reports a 6-fold increase of the CSF pulse pressure (25). This association of decreased stroke volume and increased pressure wave reflects the loss of compliance. It means that the arterial expansion resulting from cardiac systole is decreased and that the arterial pulse wave, instead of being transmitted to the CSF, is transmitted directly to the vascular lumen. Thus, the intravascular pressure is increased in capillaries and veins, preventing the appropriate absorption of CSF by the parenchyma. Because the pulse wave is transmitted into the vessels rather than via the pericerebral CSF, the brain expands, compressing the cerebral ventricles. The ventricular compression, in turn, causes increased amplitude of the pressure wave within the ventricles and, especially, in the aqueduct. The increased pressure in both the vessels and the ventricles results in a slowly progressive loss of brain tissue. In addition the compression of the draining veins by the pericerebral CSF pulse pressure is lost;

therefore, the venous backpressure that keeps open the veins in capillaries is lost, compromising the optimal perfusion and existing conditions that prevailed between the vessels and the brain (25). This model has been confirmed by several reports in which the regimen of the velocity curve at the aqueduct using cine phase-contrast imaging in cohorts of patients demonstrated a significant increase of the stroke amplitude as compared with normal controls (39–61). On conventional diagnostic this is expressed by a significantly increased signal void at the aqueduct on sagittal T2 FSE/TSE imaging.

BENIGN ENLARGEMENT OF THE SUBARACHNOID SPACES IN INFANTS

Definition

A pattern of enlarged CSF spaces with normal to slightly increased ventricular size in infants (Fig. 8-34) is fairly common. These children are usually neurologically normal infants without evidence of prior brain injury (199). This appearance rarely causes clinical concern and, indeed, is rarely noticed unless the infant has macrocephaly or rapid head growth; under these circumstances, the large CSF spaces often raise concerns for hydrocephalus (200–203). The phenomenon of large CSF spaces in developmentally and neurologically normal children with macrocephaly has been variously called benign extra-axial collections of infancy, benign idiopathic extra-hydrocephalus, EVOH, benign subdural effusions of infancy, benign macrocephaly of infancy, and benign enlargement of the subarachnoid spaces (200,202,203). The term benign enlargement of the subarachnoid spaces probably is most appropriate and can be applied to neurologically normal infants with large CSF spaces whether macrocephaly is present or not.

Clinical Manifestations

In the absence of other anomalies, children with benign enlargement of the subarachnoid spaces develop normally (203). If macrocephaly is

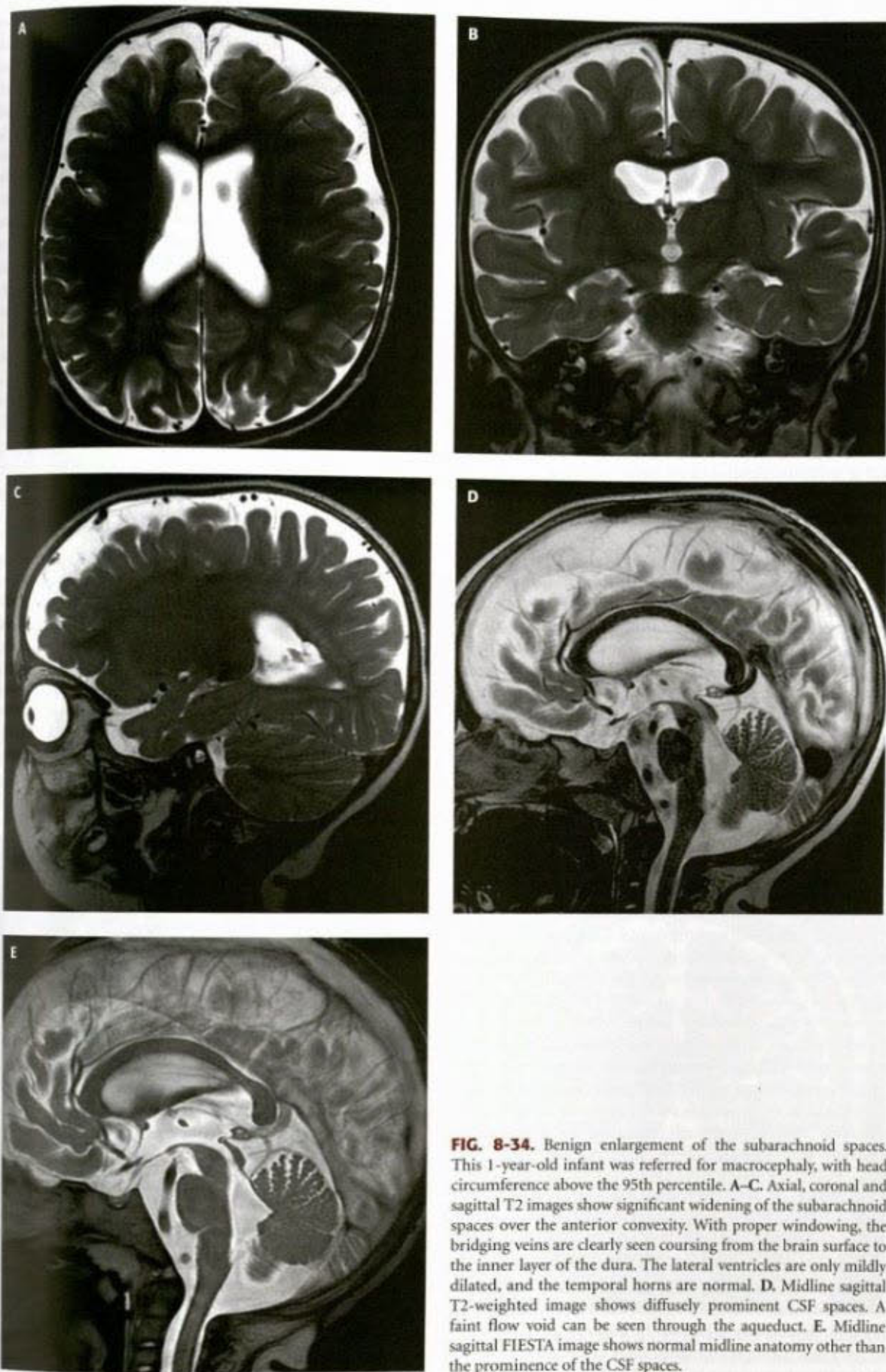


FIG. 8-34. Benign enlargement of the subarachnoid spaces. This 1-year-old infant was referred for macrocephaly, with head circumference above the 95th percentile. A–C, Axial, coronal and sagittal T2 images show significant widening of the subarachnoid spaces over the anterior convexity. With proper windowing, the bridging veins are clearly seen coursing from the brain surface to the inner layer of the dura. The lateral ventricles are only mildly dilated, and the temporal horns are normal. D, Midline sagittal T2-weighted image shows diffusely prominent CSF spaces. A faint flow void can be seen through the aqueduct. E, Midline sagittal FIESTA image shows normal midline anatomy other than the prominence of the CSF spaces.

present, the head circumference tends to be in the high normal range at birth and increases rapidly during the first few months of life; it is generally well above the 95th percentile at the time of presentation (usually between the ages of 2 and 7 months). It is important to recognize that this rapid head growth does not necessarily represent hydrocephalus or the presence of subdural hematomas, particularly in the absence of developmental delay or signs or symptoms of increased intracranial pressure. In fact, when followed without intervention, the head growth curve of affected infants tends to stabilize along a curve parallel to the 95th percentile by the age of 18 months. Both the size of the subarachnoid spaces and the head circumference typically return to normal after the second birthday (202). Cisternography has demonstrated slow flow over the cerebral convexities in these patients (201); the enlarged subarachnoid spaces, therefore, are proposed to result from delayed maturation of the arachnoid villi or other absorption sites such as the nasal mucosal-lymphatic pathway underlying the cribriform plate (34,40). The fact that this same pattern of enlarged subarachnoid spaces may be found also in association with high venous pressure lends credence to this tentative explanation. In most cases, however, benign enlargement of the subarachnoid spaces is idiopathic; it is sometimes familial (204). Histologic examination in affected patients has shown thickening of the arachnoid, which may be a normal developmental phenomenon or perhaps a reactive change that helps to increase resorption of CSF (205).

Imaging

The mere presence of enlarged subarachnoid spaces is not sufficient to make this diagnosis. Enlarged subarachnoid spaces can be caused by a number of factors, including ACTH and corticosteroid therapy (206,207), dehydration, malnutrition (208), total parenteral nutrition, and cancer chemotherapy, in addition to the mechanisms discussed previously in this chapter. The presence of these factors should be ruled out before the diagnosis of benign enlargement of the subarachnoid spaces (or atrophy, or hydrocephalus) is considered.

Typical imaging findings in patients with benign enlargement of the subarachnoid spaces include slightly enlarged lateral and third ventricles, and subarachnoid space that is wider than normal in frontal region, anterior interhemispheric fissure, and Sylvian fissures (Fig. 8-34) (199). The chiasmatic cistern is also typically enlarged (Fig. 8-34D and E). The degree of dilation of the lateral ventricles is roughly proportional to the width of the frontal subarachnoid space. Imaging studies may not be helpful in the distinction of benign enlargement of the subarachnoid spaces from hydrocephalus or, for that matter, from atrophy. As discussed earlier, scrutiny of the anterior and posterior recesses of the third ventricle and the temporal horns (see figures in the early sections of this chapter) may be helpful in the differentiation from hydrocephalus. Symmetry of the extraparenchymal fluid is an important finding, especially on CT; asymmetry is unusual in benign macrocephaly and may indicate the presence of traumatic subdural collections (209). Both MR and ultrasound can differentiate subdural collections from enlarged subarachnoid spaces by visualization of cortical veins (Fig. 8-34A–C). On MR, examining the first echo of a T2-weighted sequence or a FLAIR image is optimal. In benign enlargement of the subarachnoid spaces, veins are identified as curvilinear structures that are adjacent to the inner table of the calvarium; with subdural collections, the veins are displaced from the inner table. Also most subdural collections have high protein content and have higher signal intensity than CSF on T2-weighted or FLAIR images. On cranial ultrasound, differentiation is made by angling the transducer to follow the veins into the superior sagittal sinus. In infants with subdural collections, the echogenic pia-arachnoid is displaced from inner

table with veins medial to it. In patients with enlarged subarachnoid spaces, the veins course directly into superior sagittal sinus (210,211).

Occasionally, patients with clinical courses and CT scans suggestive of benign enlargement of the subarachnoid spaces have had bloody subdural collections, superimposed upon large subarachnoid spaces, detected on MR scans or ultrasound (208,210) (Fig. 8-35). Wilms et al. have reported that infants with bloody subdural collections have a higher incidence of difficult births or postnatal trauma incidents and are more likely to have symptoms of increased intracranial pressure, such as vomiting and somnolence (210). However, some reports describe infants with mildly hemorrhagic subdural collections superimposed upon large subarachnoid spaces in which extensive investigations have revealed no evidence of significant trauma (212–214). It is postulated that the large CSF spaces in these patients may make these infants more susceptible to subdural hematoma formation secondary to rather mild trauma, similar to the condition encountered in patients with middle cranial fossa arachnoid cysts (215,216). All babies with hemorrhagic subdural collections should, nonetheless, be carefully screened by child protective services, as most will be found to have suffered some sort of trauma (217).

IMAGING OF TREATED HYDROCEPHALUS AND RESULTING COMPLICATIONS

As discussed in Sections Classification of hydrocephalus and Clinical aspects of hydrocephalus, severe long-lasting hydrocephalus will cause damage to the brain. In dogs, the brain is not permanently damaged until the cerebral mantle is compressed to a thickness of less than 1 mm (218). Persistent compression of the brain results in gliosis, cortical distortion, damage to neurons, tearing of axons in the internal capsule, and myelin destruction (46,218,219). Therefore, treatment of uncompensated hydrocephalus is mandatory.

In hyperacute hydrocephalus, ventricular tapping with external ventricular drainage relieves the ventricular tamponade and prevents the circulatory arrest caused by the compression of the vasculature (see section Clinical aspects of hydrocephalus). Follow-up imaging

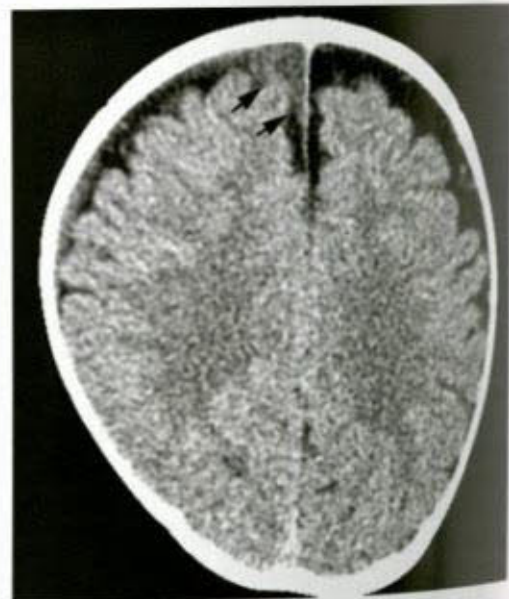


FIG. 8-35. Benign enlargement of the subarachnoid spaces with small subdural hematoma. Axial CT of a 1-year-old infant with head circumference above the 95th percentile shows prominent subarachnoid spaces over the frontal convexity. The right frontal subdural collection of intermediate attenuation (black arrows) is highly suggestive for a subdural hematoma.

typically restricted to the acute period, assesses the ventricular size, the morphological features associated with high intraventricular pressure, and the related condition of the parenchyma.

In less acute situations, hydrocephalus may be treated by endoscopic third ventriculostomy or by CSF diversion in the form of a ventriculo-peritoneal or a ventriculo-atrial shunt. Third ventriculostomy is a popular treatment because it eliminates the necessity of having an shunting shunt, which can become obstructed and can be the cause of hemorrhage, infections, foreign body reactions, slit ventricle syndrome, and other complications listed in this section. In third ventriculostomies, a fiberoptic endoscope is used to create a hole in the floor of the third ventricle, immediately anterior to the mamillary bodies. This hole allows the intraventricular CSF access into the interpeduncular and suprasellar cisterns, from where it can flow laterally and upward over the cerebral convexities to sites of CSF resorption. Thus, the obstructions are bypassed. Third ventriculostomies appear to be most useful in obstructive hydrocephalus; as discussed earlier, obstructive hydrocephalus in children is most often the result of obstruction in the region of the Sylvian aqueduct, fourth ventricular outflow foramina, cisterna magna, or basal cisterns. Third ventriculostomy may also be used in cases of communicating hydrocephalus, as by-passing the cerebral ventricular channels (aqueduct, fourth ventricle) might increase the compliance (220). However, third ventriculostomy is not effective when loculations are present in the subarachnoid spaces, such as the prepontine, interpeduncular or suprasellar cisterns. Studies have shown that third ventriculostomies result in successful resolution of hydrocephalus in 80% of children so treated (221). If the third ventriculostomy does not result in adequate resolution of hydrocephalus, ventricular shunt is placed. Advantages of endoscopic third ventriculostomy include a more physiologic CSF circulation, lower incidence of infections, and better response of infection to antibiotic therapy.

Third ventriculostomies are less useful in young infants, in whom a higher incidence of parenchymal injury and vascular injury is reported; in addition, the communication through the floor of the ventricle is more likely to spontaneously close (222). In countries where appropriate follow-up of patients is difficult for economic or geographic reasons, third ventriculostomy associated with cauterization of the

choroid plexuses is the procedure of choice, provided the cisterns are patent (223,224).

Shunt systems are composed of a ventriculostomy tube, a reservoir (optional), a valve, and a peritoneal tube. The ventriculostomy tube is inserted either into the frontal or occipital horn of the lateral ventricle through a small hole in the calvarium. This is attached to the reservoir, which lies subcutaneously over the calvarial defect. The valve is set to a certain pressure that must be attained before drainage occurs; the presence of the shunt system restores the compliance of the system and allows both dampening of the systolic pressure wave and drainage of the accumulated fluid. Some valves are pressure-adjusted with an external magnetic device; although these magnetic devices are not a contraindication to MRI, it is almost always necessary to reset the valve after the study. The peritoneal tube is run subcutaneously from the valve into the peritoneal cavity. The radiologist is usually asked to assess the function of the shunt by determining the position of the tip of the ventriculostomy tube and the reduction in ventricular size resulting from its placement. In general, the tip of the ventriculostomy tube should lie within the lateral ventricle in the region of the foramen of Monro. The tube is hypointense on T1- and T2-weighted and FLAIR MR images (Fig. 8-36A-C) and has high attenuation on CT (Fig. 8-36D). Some diminution in ventricular size should be apparent soon after the placement of a shunt; if the ventricular size is unchanged after 2 to 3 days, the patency of the shunt system should be questioned. It has been shown that if the cerebral mantle measures 2 cm or more in thickness after shunting, patients usually attain average intellectual development (46).

Surgical cannulation of the aqueduct was proposed in the 1970s to 1980s for treating aqueductal stenosis (128,225) and reintroduced in the past decade using fiberoptic ventriculoscopy, with or without stenting (139,226). It is uncommonly used and the reader is unlikely to encounter such cases.

Radiologic Assessment of Third Ventriculostomies

Although sonography, CT, or MR can be used to assess shunted hydrocephalus, MR is the study of choice for the assessment of patients

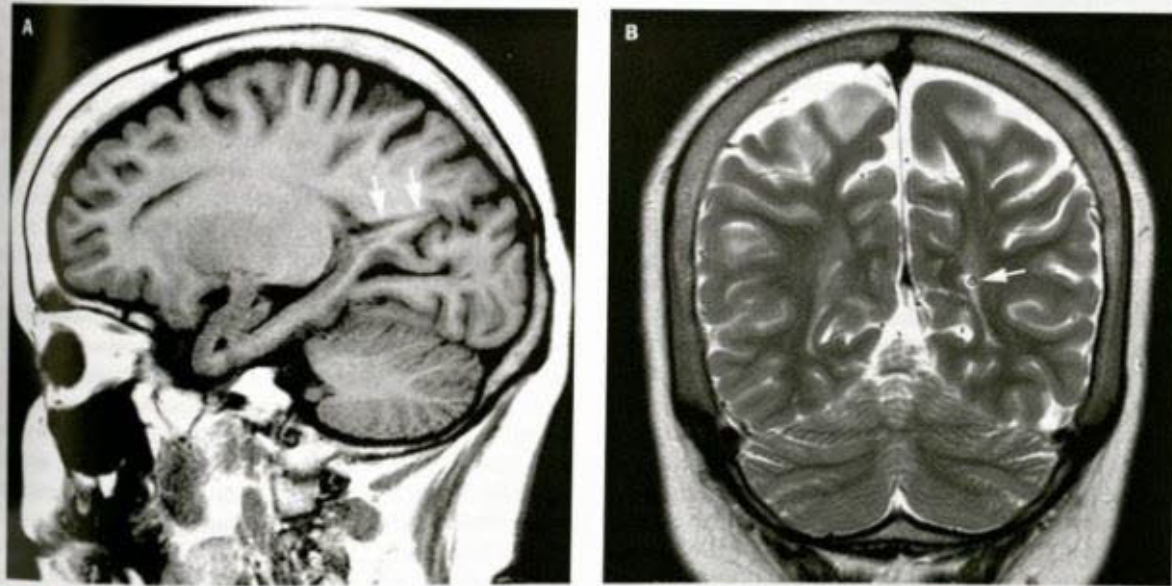


FIG. 8-36. Appearance of a ventriculoperitoneal shunt (white arrows) on MR (A and C) and CT (D). On MR the shunt appears as a hypointense linear structure extending from the ventricle to the extracranial soft tissues. It appears as a high attenuation linear structure on CT.

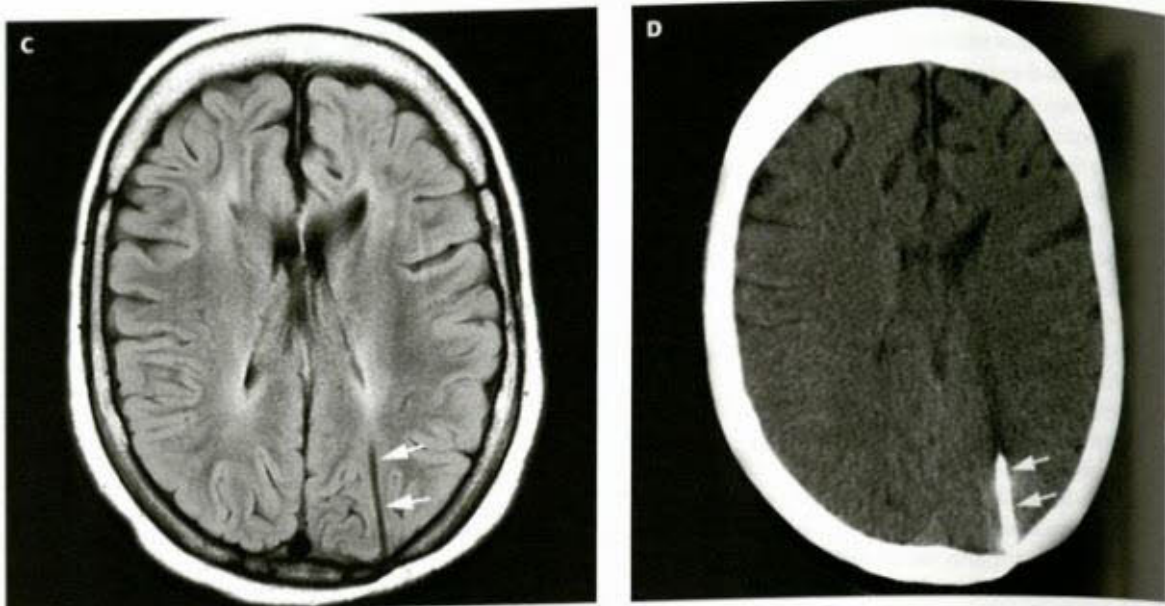


FIG. 8-36. (Continued)

treated with third ventriculostomy, as only by MR can one assess the surgically induced defect in the floor of the third ventricle and the CSF pulsing through it.

In children who have undergone successful third ventriculostomies, the reduction in ventricular size is usually slower and less dramatic than in those who have been treated using ventricular shunts (227). The ventricular size after third ventriculostomy usually decreases over several months, instead of several days as in patients with ventricular shunt catheters (228). On follow-up, the ventricles remain larger than they would usually be after shunt placement. This difference in magnitude of ventricular size reduction is likely related to the fact that indwelling ventriculostomy catheters dampen the pulsations of CSF emanating from the choroid plexus or possibly to a reduced absorption capacity in the affected children (229).

Imaging assessment of the third ventriculostomy is aimed at demonstrating flow passing through the hole in the floor of the third ventricle. This can be best accomplished noninvasively by the use of MR. Lev et al. used phase-contrast MR flow studies to determine ratios of CSF flow velocities in patients with third ventriculostomies (230). They found that the ratio of velocity of CSF in the prepontine space to that in the anterior cervical spinal subarachnoid space was significantly higher in patients with patent third ventriculostomies than in normal patients. Those patients with velocity ratios lower than normal needed revisions (230). Fischbein et al. found that sagittal 3 to 4 mm fast spin-echo sequences show hypointensity in the region of the ventriculostomy secondary to rapid pulsatile flow. In their study, the fast spin-echo studies were as sensitive as cine phase-contrast studies (227) (Fig. 8-37). Kim et al. used a combination of T2-weighted images and phase-contrast images (228). Hoffman et al. used a steady-state free precession sequence and consistently found loss of the steady state (and consequent loss of signal) in the inferior third ventricle and suprasellar cistern in patients with patent third ventriculostomies but no loss of the steady state (persistent high signal intensity in the inferior third ventricle) in patients with occluded third ventriculostomies (231) (Fig. 8-38). As all of these techniques rely on detecting flow in the inferior third ventricle and suprasellar/interpeduncular/prepontine cisterns, it is likely that all of them work. Therefore, choice of the precise technique to be used should depend upon which techniques are available on the MR scanner being used and with which technique(s) the imaging

physician is most comfortable. In addition, detailed morphologic analysis can be provided by using CISS/FIESTA submillimeter imaging. This sequence is not sensitive to flow but demonstrates the ventriculostomy well and can identify occlusive septations in the surrounding cisterns better than flow-sensitive sequences.

Shunt Malfunctions

Shunt malfunctions are manifested clinically by symptoms of increased intracranial pressure, persistent bulging of the anterior fontanel, excessive rate of head growth in the infant, or seizures (131,232). On imaging studies, shunt malfunction is usually manifested by increasing ventricular size (Fig. 8-39A and B). In infants, this is usually assessed by sonography. In older children, CT is the standard study but development of fast imaging (half-Fourier single-shot RARE sequences or PROPELLER sequences) now allow rapid assessment of ventricular size by MR without sedation and without ionizing radiation (233-236). If time is available on the MR scanner, serious consideration should be given to using these techniques. Shunt failure does not always result in ventricular enlargement, however. Some patients have considerable scarring in and around the ventricular walls, causing decreased compliance of the brain and no enlargement or minimal enlargement of the ventricular system in the presence of shunt malfunction (see subsequent section on the "Slit Ventricle Syndrome" [237,238]). The most common cause of malfunction is occlusion of the ventricular catheter by choroid plexus or glial tissue that grows into the lumen of the catheter. This diagnosis can only be inferred from imaging studies, which will show enlarging lateral ventricles in spite of a well-placed ventriculostomy tube and intact connections of the shunt system.

Disconnection of the shunt components can occur at any point within the system; it most commonly occurs where the various components are joined. Although the site of shunt malfunction (ventricular portion versus peritoneal portion) can often be determined clinically, plain film studies of shunt components (Fig. 8-39C), positive contrast plain film radiography, or radionuclide studies are sometimes necessary (239-243). If radionuclide studies are performed, both dynamic and static studies should be obtained (239). The "scout" film from a CT scan will sometimes show a disconnection at the valve that is not appreciated on the axial images; therefore, the scout film should always

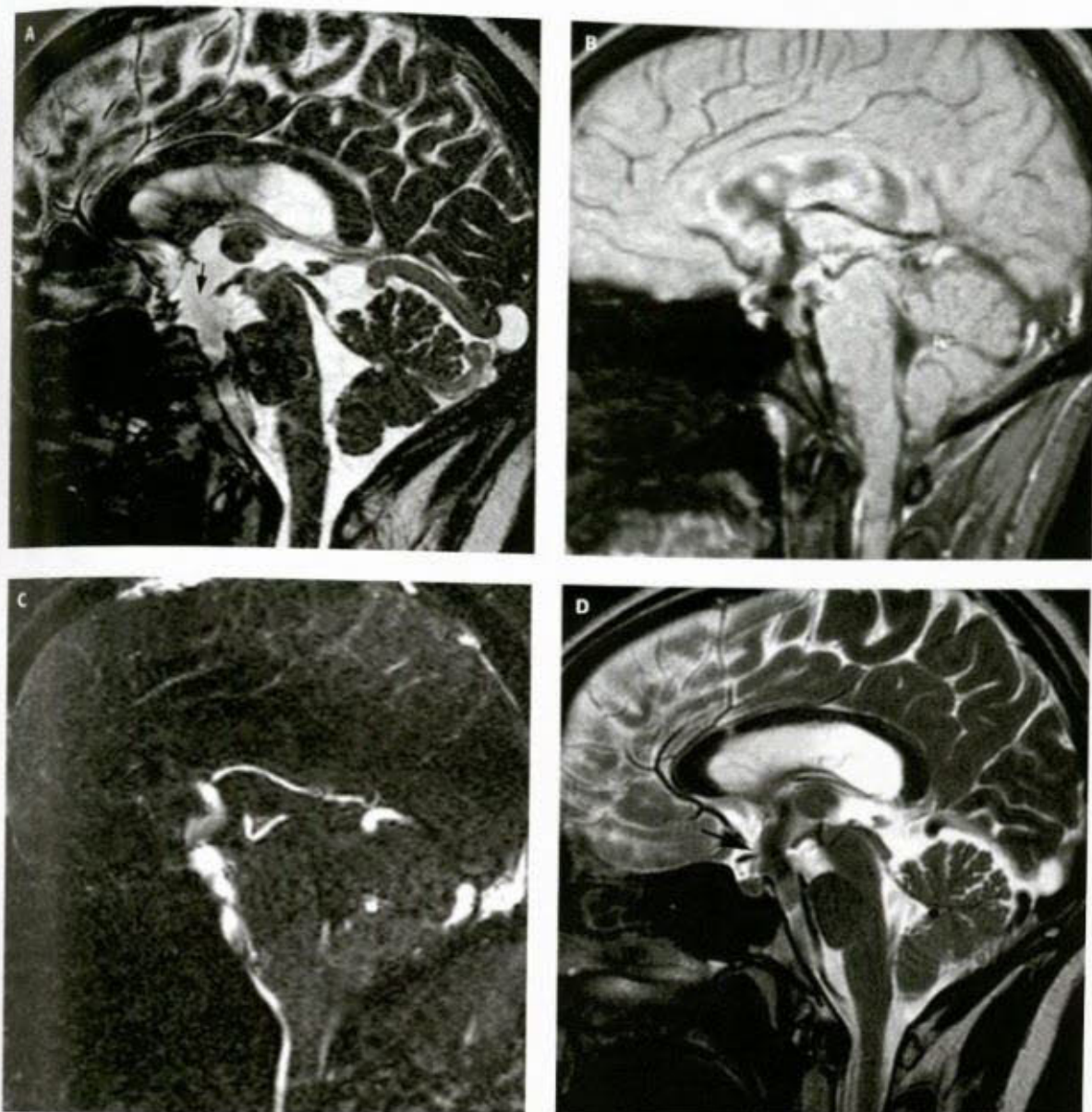


FIG. 8-37. Endoscopic third ventriculocisternostomy (ETV) efficacy assessment. **A.** Midsagittal FIESTA image shows a wide defect (black arrow) in the anterior part of the floor of the third ventricle. **B** and **C.** Cine phase-contrast imaging demonstrates good CSF flow (hypointensity in [B], hyperintensity in [C]) across the defect in the floor of the ventricle. **D.** Sagittal T2-weighted image demonstrates a prominent signal void (black arrow) at the ventriculostomy site. FSE T2 is felt to be similarly diagnostic as cine phase-contrast imaging for evaluating the patency of an ETV.

analyzed. In addition to showing the location of obstruction or disconnection, shunt function studies are of value when symptoms of shunt malfunction are vague and clinical testing of shunt function is equivocal. Note that the reservoir is not always radio-opaque and, therefore, may appear as a discontinuity of the shunt system on plain radiographs. It is essential to communicate with the treating neurosurgeon to perform a positive contrast or radionuclide study in order to differentiate a disconnection from the presence of a radiolucent shunt component.

Using special techniques described in Chapter 1, CSF flow can be analyzed by MR techniques (81,82). When used properly, the CSF flow techniques can be used to analyze flow in ventricular catheters and in connecting tubing (244,245); when done properly and calibrated

carefully, flow rates within the shunt can be calculated (246). Parameters are set to detect flow with velocity greater than a certain minimum. If flow is seen within the shunt tubing, therefore, one may confidently conclude that a rate of flow above that minimum is present within the shunt system. However, CSF production and, therefore, CSF flow, vary from minute to minute (247); therefore, a negative study (a study showing no flow) is indeterminate. CSF may be flowing through the shunt at a velocity below the minimum detectable rate (245). In addition, the amount of CSF flowing through the shunt may vary with position (e.g., upright versus supine). As a result of these considerations, a lack of detection of CSF flow on an MR study is not necessarily diagnostic of shunt failure. Therefore, if no flow is detected, a more conventional radionuclide or positive contrast study becomes necessary.

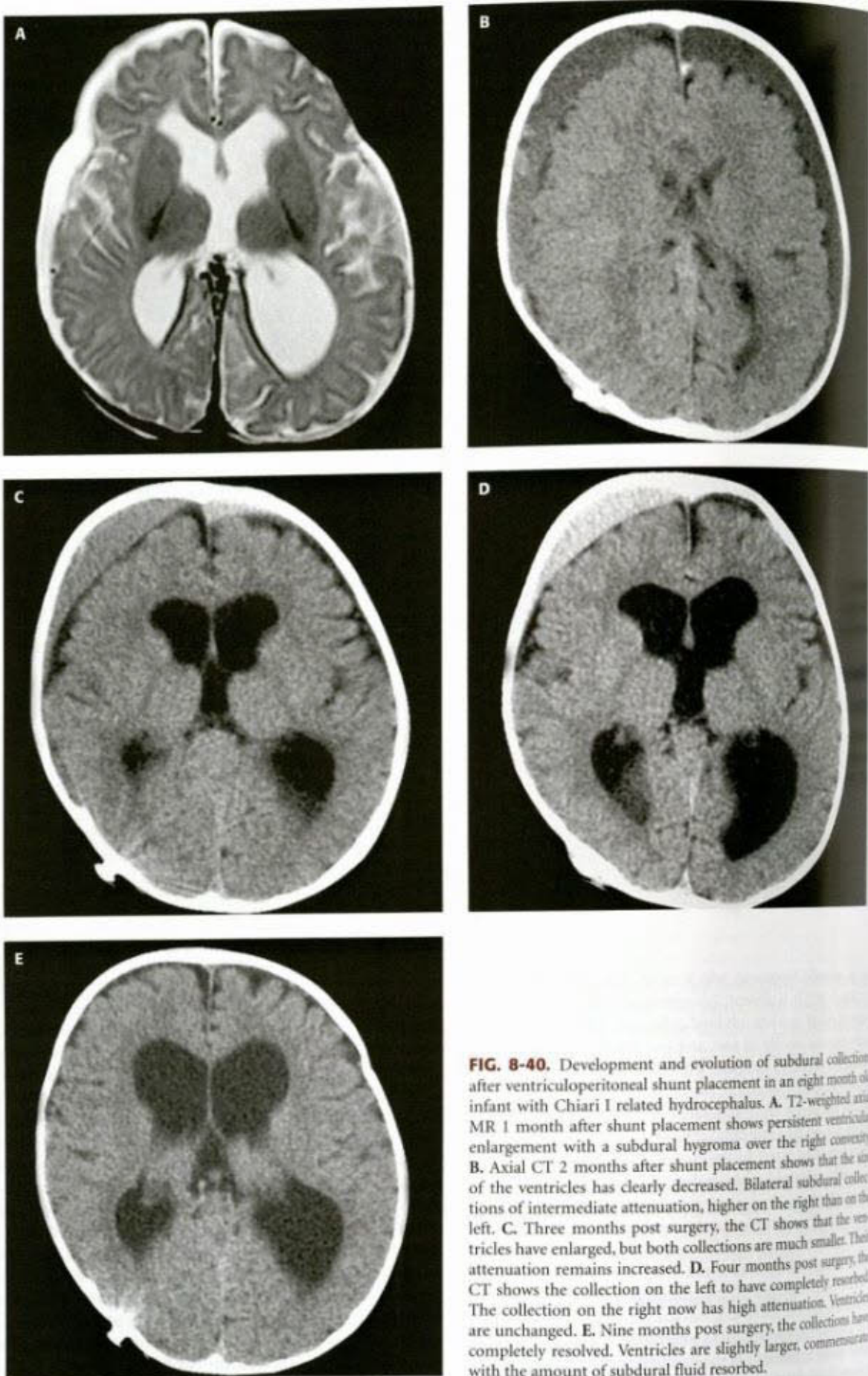


FIG. 8-40. Development and evolution of subdural collections after ventriculoperitoneal shunt placement in an eight month old infant with Chiari I related hydrocephalus. A. T2-weighted axial MR 1 month after shunt placement shows persistent ventricular enlargement with a subdural hygroma over the right convexity. B. Axial CT 2 months after shunt placement shows that size of the ventricles has clearly decreased. Bilateral subdural collections of intermediate attenuation, higher on the right than on the left. C. Three months post surgery, the CT shows that the ventricles have enlarged, but both collections are much smaller. Their attenuation remains increased. D. Four months post surgery, the CT shows the collection on the left to have completely resolved. The collection on the right now has high attenuation. Ventricles are unchanged. E. Nine months post surgery, the collections have completely resolved. Ventricles are slightly larger, commensurate with the amount of subdural fluid resorbed.

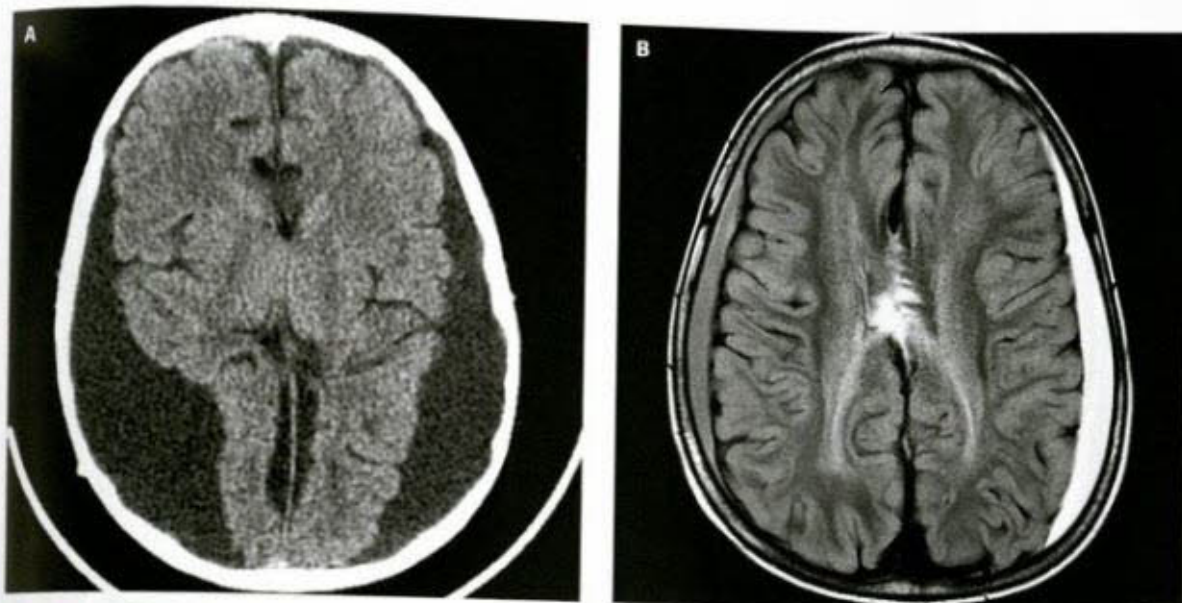


FIG. 8-41. Subdural hematomas after shunt placement. **A.** Axial CT shows bilateral large subdural collections of intermediate attenuation associated with ventricular compression. **B.** Axial MR FLAIR in a different patient shows bilateral moderate-sized collections of different signal intensity, associated with ventricular compression.

meningeal fibrosis enhances dramatically, presumably as a result of vascular granulation tissue intermixed with the collagen bundles in the subdural space (256).

Slit Ventricle Syndrome

Definition

Shunted hydrocephalic patients may become symptomatic from shunt failure without evidence of ventricular enlargement on ultrasound, CT, or MR. Patients who exhibit this phenomenon have been labeled as

having the "slit ventricle syndrome" (238,257–261). Some debate exists as to what constellation of clinical and/or pathological findings define this syndrome (238,262). It has become clear that there are multiple different entities lumped together under this name; therefore, affected patients may require several different treatments (263).

Di Rocco has divided slit ventricle syndrome into three groups: (1) patients with inability of the ventricles to expand due to stiffness at the subependymal level (normal intracranial pressure), (2) patients with chronic low pressure from overdrainage or siphoning of CSF through a shunt catheter or chronic CSF leak (low intracranial

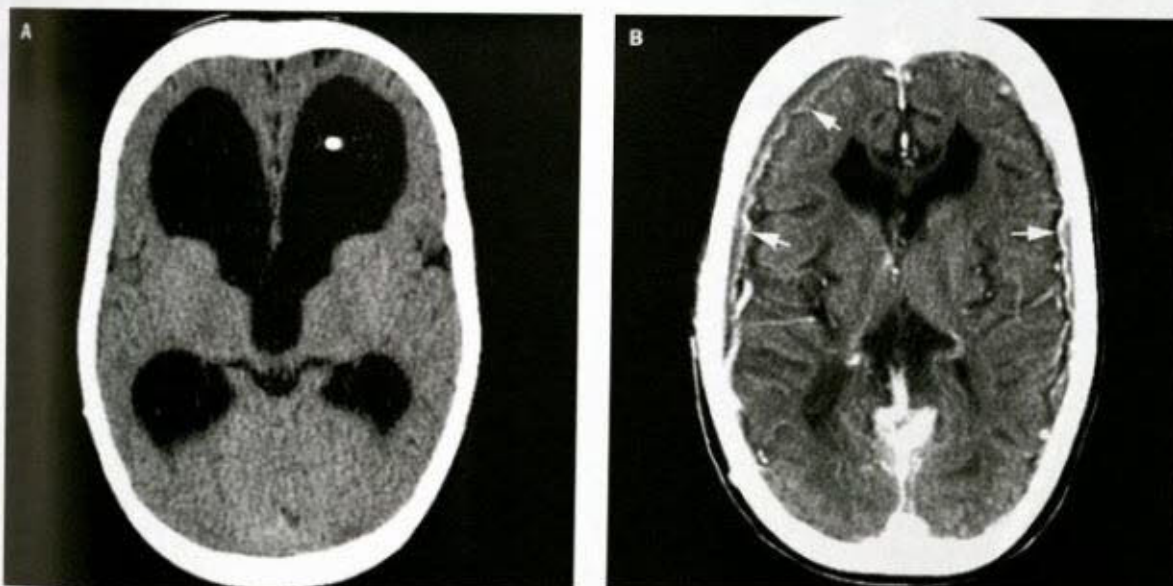


FIG. 8-42. Post shunt meningeal fibrosis and calvarial thickening. Constellation of findings in chronic intracranial hypotension. Child with congenital hydrocephalus. **A.** At 5 years of age, axial CT shows prominent ventricles, but the pericerebral spaces in the sulci and interhemispheric fissure are visible. **B.** At age 7 years, contrast-enhanced CT showed much smaller ventricles. The skull is markedly thicker than at 5 years. There is a thick layer of intermediate density (white arrows) between the subarachnoid space and the skull. It could be mistaken for a fluid collection but its irregular, enhancing inner margin suggests meningeal fibrosis.

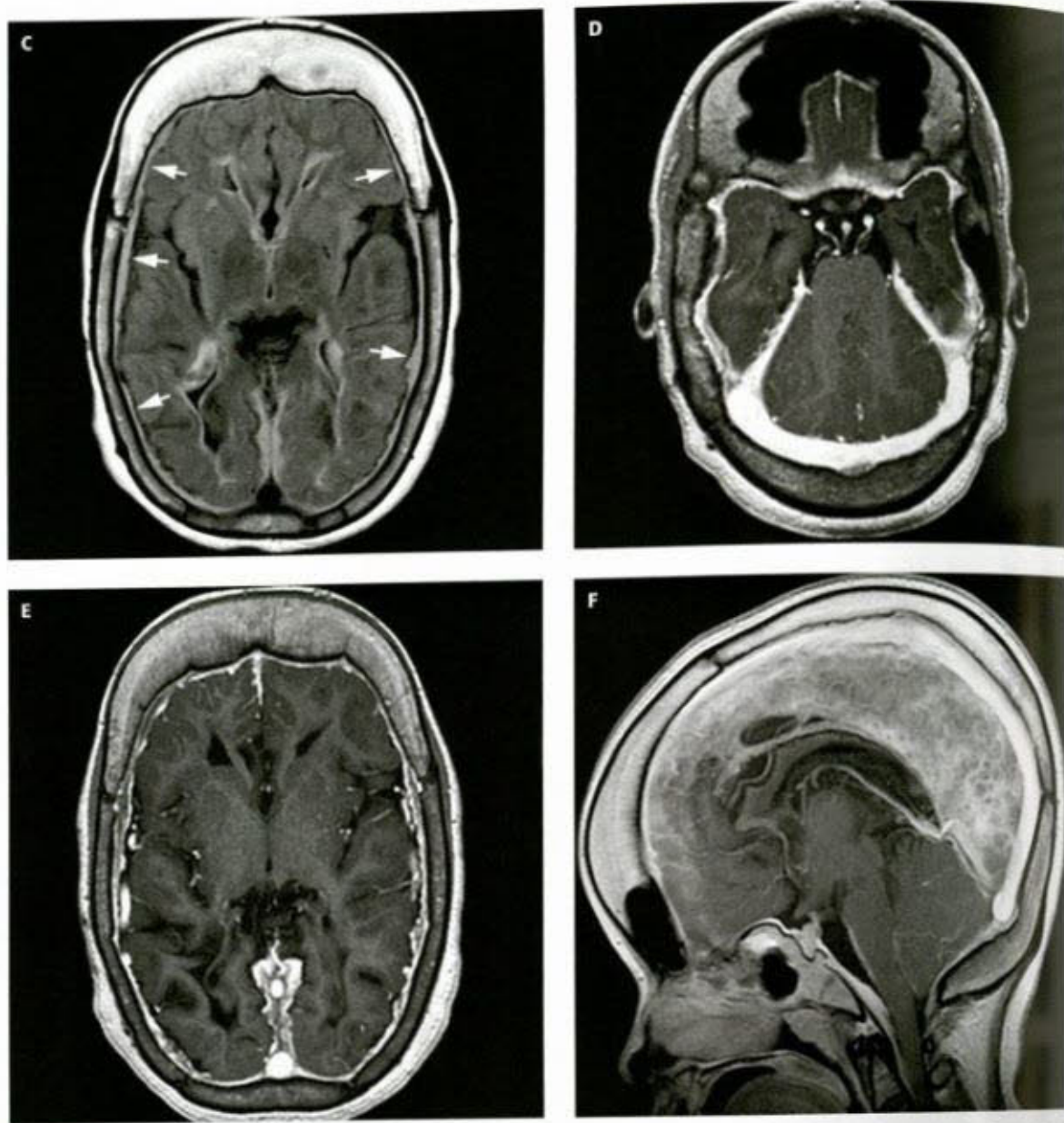


FIG. 8-42. (Continued) C. At the age of 16, axial FLAIR shows marked bone thickening especially the frontal bone. The ventricles are small and surrounded by a thin band of white signal, presumably periventricular gliosis/fibrosis. A thick layer of tissue (white arrows) is interposed between the brain and the calvarium and between the occipital lobes, most likely dural fibrosis. D-E. T1 post contrast axial (D and E) and sagittal (F) images from the same study show that the thick fibrotic calvarial, tentorial, and falcine dura enhances avidly. The dural venous sinuses are prominent. The cerebellar tonsils are low and compressed. The pituitary gland is prominent.

pressure), and (3) patients with craniocerebral disproportion secondary to early suture fusion (high intracranial pressure) (264). Rekate (257) has a different classification of the various disorders composing the slit ventricle syndrome. He divides them into (1) extreme low pressure headaches, probably from siphoning of CSF from the brain by the shunt; (2) intermittent obstruction of the proximal shunt catheter; (3) normal volume hydrocephalus (in which the buffering capacity of the CSF is diminished, see following paragraph); (4) intracranial hypertension associated with working shunts (probably linked to venous hypertension); and (5) headaches in shunted children unrelated to intracranial pressure or shunt function. Thus, shunted patients may experience a number of disorders, with very different treatments,

that can cause headaches without detectable ventricular enlargement. Other than Rekate's category no. 3, which may show calvarial thickening, imaging cannot differentiate these categories. Bruce and Nagy suggest that patients with symptoms of shunt malfunction in the absence of ventricular enlargement require an emergency shunt insertion study, followed by shunt revision with revision of the ventricular catheter and valve (261).

Pathophysiology

The syndrome most commonly referred to by the name "slit ventricle syndrome" is the result of a combination of decreased intraventricular volume; resultant diminished CSF buffering capacity (diminished

ability to compensate for the normal variations in intracranial pressure, diminished brain compliance; and, possibly, intermittent or partial shunt obstruction (237,238). Intracranial volume decreases because shunting causes an immediate reduction in ventricular, and hence brain, size. Thus, the brain expansion that maintains the patency of the cranial sutures is temporarily reversed and the sutures close. By the time the brain grows enough to once again fill the calvarium, the sutures have fused and the calvarium cannot enlarge as rapidly as the brain. When the overlying calvarium is too small, the CSF spaces are not large enough to provide adequate buffering of normal variations in intracranial pressure. Thus, unless the shunt is functioning perfectly, patients have recurrent episodes of increased intracranial pressure. However, because of the small size of the CSF spaces and the compression of the brain, the lateral ventricles do not enlarge significantly during these episodes of increased pressure.

Diagnosis

Affected patients typically present with recurrent, transient symptoms of shunt failure. Imaging studies, however, will show small ventricular size (Fig. 8-43). Shunt function studies show the shunt system to be patent, although flow may be reduced. Treatment is shunt revision or replacement with a valve having higher opening pressure (Fig. 8-43D). If this fails, bilateral temporal craniotomies are performed in order to expand the volume of intracranial CSF. Theoretically, the expanded intracranial space is better able to compensate for the transient changes in intracranial pressure that accompany the variations in CSF production.

One finding on imaging studies that may help in the determination of which patients have diminished buffering capacity is that of progressive calvarial thickening. Such thickening may or may not be associated with premature synostosis of the cranial sutures; either way, the

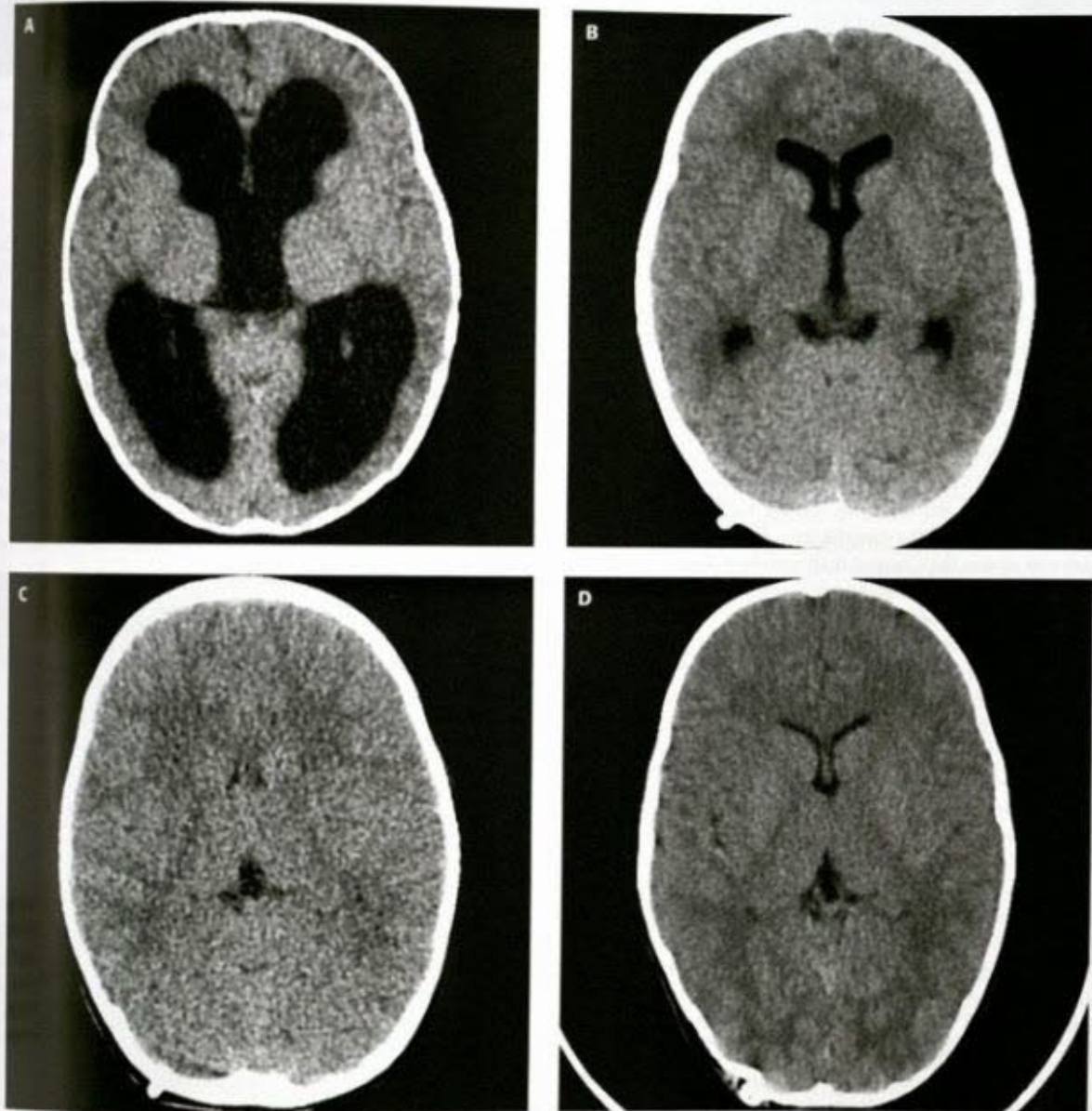


FIG. 8-43. Slit ventricles. A. Initial CT scan demonstrating significant hydrocephalus. B. First post surgery CT shows that the ventricles are still large, with rounded temporal horns but markedly improved. C. Two years later the child complains of headaches. A new CT demonstrates almost completely effaced ventricles and pericerebral spaces (sulci and cisterns). D. After shunt revision, headaches have resolved. The CT shows normal-looking ventricles.

result is a diminished reservoir of CSF to buffer the normal variations in intracranial pressure (238).

It is less important for the radiologist to know all the possible causes of small ventricles in a symptomatic patient than to realize that the presence of very small ventricles after placement of a ventriculo-peritoneal shunt is not diagnostic of, or even suggestive of, the "slit ventricle syndrome." *This syndrome is a clinical, not a morphologic syndrome.* Small ventricles are not, in the majority of cases, a problem; they are the desired result of many surgeons after treatment of hydrocephalus and, even when extremely small, their only implication in the vast majority of patients is that the shunt is functioning.

Imaging of Intracranial Hypotension

Beside the early development of subdural collections and the isolated delayed "slit ventricle", too much depletion of the ventricles may lead to the progressive development of the imaging constellation characteristic of intracranial hypotension, findings identical to those observed in idiopathic cases, iatrogenic cases or cases related to pathologies such as Marfan syndrome. Intracranial hypotension is important to recognize as its clinical symptoms are similar to those of intracranial hypertension, while the therapeutic goals are diametrically opposed. The main symptom is a postural headache exacerbated by standing and relieved by reclining. Other nonspecific neurological manifestations may be observed, including cranial neuropathies and, in severe cases, coma. When the condition is chronic, head MRI is diagnostic, showing a characteristic constellation of nonspecific abnormalities (265) (Fig. 8-42). The most typical findings are diffuse pachymeningeal (dural) enhancement and thickening (PME/PMT) (100%) (Fig. 8-42B, C, E, and F), and the venous distension sign (VDS) (100%) which reflects venous engorgement resulting from the low intracranial pressure (265) (Fig. 8-42D and F). PMT may be seen without contrast administration on FLAIR images. VDS may be recognized on T1 imaging without contrast as well, from observing the convexity of the sinus walls (265); it is the first anomaly to resolve after normalization of the intracranial pressure (265). Other features may include subdural hygromas or hematomas, effacement of the cisterns, and downward brain herniation (which can mimic the Chiari I malformation, Fig. 8-42F). An increased height of the pituitary gland with convex upper border is commonly observed as well (265) (Fig. 8-42F).

Another presentation of chronic intracranial overdrainage is that of the complicated acquired Chiari I malformation (266). As mentioned before, CSF diversion produces a major reduction of intracranial capacity due to calvarial thickening, premature closure of the sutures (possibly induced), and expansion of the paranasal sinuses and mastoid air cells. The craniocerebral disproportion may be further complicated by the development of intracranial hypertension with tonsillar herniation that can only be relieved by a decompressive supratentorial craniotomy (266). Imaging in this situation shows a small posterior fossa with tonsillar herniation through the foramen magnum, small ventricles, markedly reduced pericerebral CSF spaces and prominent thickening of the calvarium (266). As in all instances of intracranial hypotension, there may be a pachymeningeal thickening, avidly enhancing after contrast administration, and prominent widening of the dural venous sinuses. Clinical features suggest intracranial hypertension with symptoms pointing to the lower brainstem (266).

This is different from another variety of "acquired Chiari I malformation" (more accurately, another form of intracranial hypotension) that is a fairly common complication of lumboperitoneal shunting (267) (Fig. 8-44). It is assumed to result from a CSF pressure differential between the cranium and the spine, but this explanation has been challenged (268).

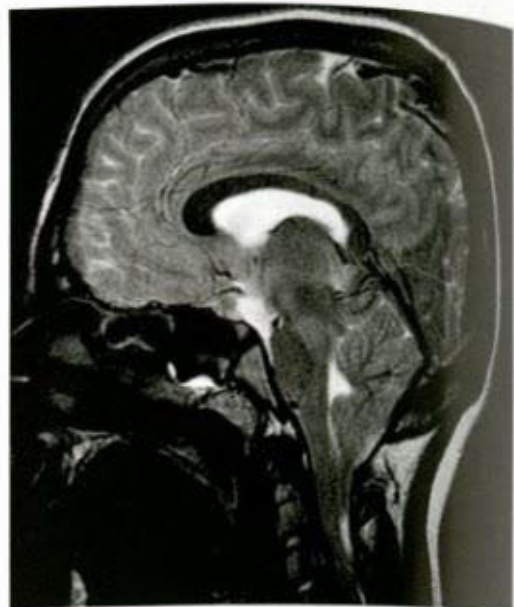


FIG. 8-44. Iatrogenic Chiari I secondary to placement of lumboperitoneal shunt. Midline sagittal T2-weighted image shows elongated tonsils herniating through the foramen magnum.

Other Complications

Other complications resulting from ventriculo-peritoneal shunting are much less common. Complications within the abdomen result from the shunt becoming too short while the child grows, with the peritoneal end remaining in the same area instead of being displaced by the bowel displacements; they include ascites, pseudocyst formation, perforation of a viscus or of the abdominal wall, intestinal obstruction (241,269), and catheter degradation (270). Very rarely, patients develop a granulomatous reaction adjacent to the shunt tube site within or near the ventricle (271). These granulomatous lesions are

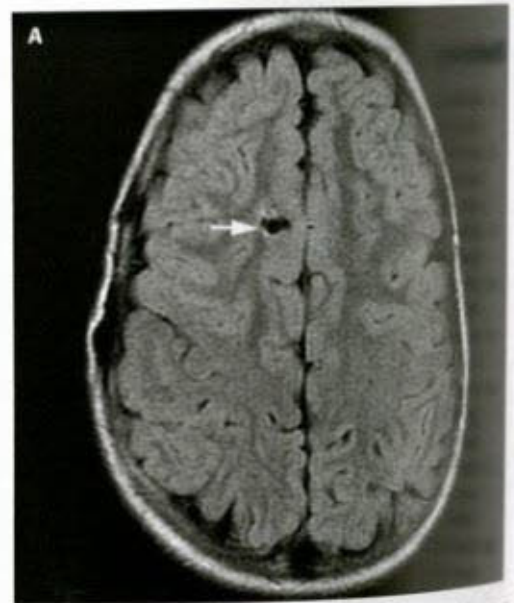


FIG. 8-45. Interstitial edema and cyst formation secondary to shunt malfunction. A. Axial FLAIR image in a shunted 12-year-old hydrocephalic child shows the normal hypointensity of the ventriculostomy tube (arrow) coursing through the cerebrum.

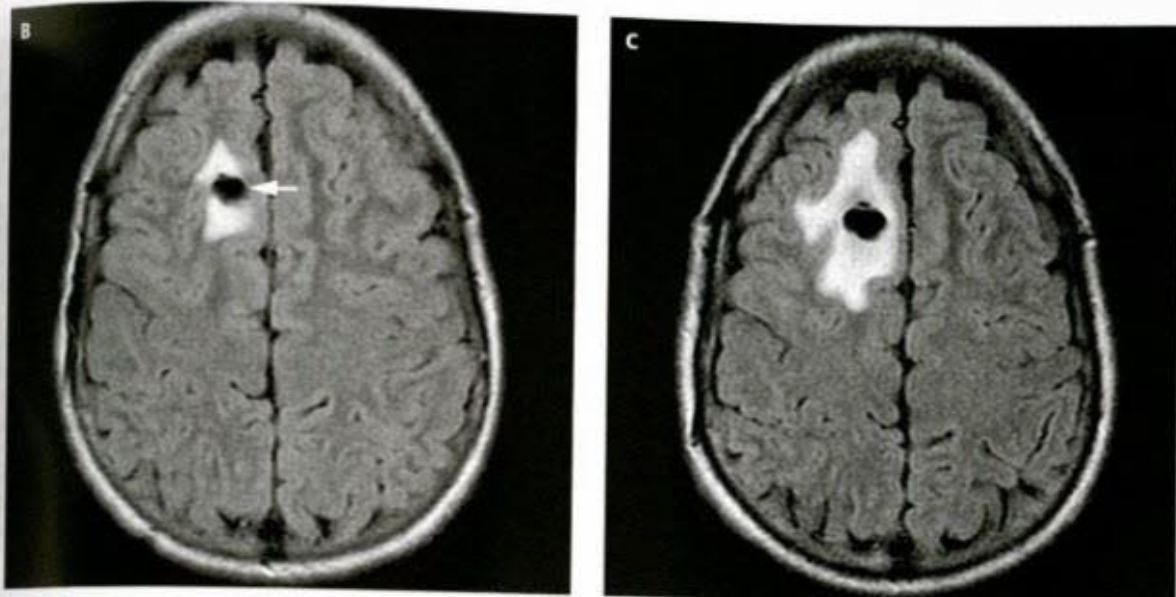


FIG. 8-45. (Continued) B. Two years later, an area of edema surrounds the shunt. The central focus of low signal (arrow) likely represents a cyst forming around the shunt. The child still is asymptomatic. C. At the age of 17, both the edematous area and the cyst have increased in size, leading to a shunt revision.

a irregular, contrast-enhancing masses along the course of the shunt tube. Calcification may be noted within the mass.

One final appearance of shunt malfunction should be mentioned. Rarely, when the ventricular end of the shunt becomes partially occluded, CSF may track along this shunt and enter the interstices of the centrum semiovale. On these occasions, the CT and MR appearance is that of edema (low density in the white matter on CT, prolonged T1 and T2 relaxation time in the white matter on MR) in the area around the shunt. Eventually, an actual cyst may form in the white matter surrounding the ventricular catheter (Fig. 8-45). It should be recognized that the presence of edema in these patients is not the result of infection or tumor but is a sign of shunt malfunction. The edema and cyst will resolve after shunt revision.

References

- Bartelmez GW, Dekaban AS. The early development of the human brain. *Contrib Embryol Carnegie Instn* 1962;37:13–32.
- ten Donkelaar HJ, van der Vliet T. Overview of the development of the human brain and spinal cord. In: ten Donkelaar HJ, Lammens M, Hori S, eds. *Clinical Neuroembryology*. Berlin-Heidelberg: Springer, 2006:1–46.
- Johanson C, Jones H. Promising vistas in hydrocephalus and cerebrospinal fluid research. *Trends Neurosci* 2001;24:631–632.
- Brodbeck A, Stoodley M. CSF pathways: a review. *Br J Neurosurg* 2007;21:510–520.
- McLone DG. The subarachnoid space: a review. *Childs Brain* 1980;6:133–150.
- Osaka K, Handa R, Matsumoto S, Yasuda M. Development of the cerebrospinal fluid pathway in the normal and abnormal human embryos. *Childs Brain* 1980;6:26–38.
- Bruckenhurst G. The development of the human cerebrospinal fluid pathway with particular reference to the roof of the fourth ventricle. *J Anat* 1969;55:40–48.
- Dooling EC, Chi Je G, Gilles FH. Ependymal changes in the human fetal brain. *Ann Neurol* 1977;1:535.
- Kuban ECK, Gilles FH. Human telencephalic angiogenesis. *Ann Neurol* 1985;17:539–548.
- Norman MG, O'Kusky JR. The growth and development of microvasculature in the human cerebral cortex. *J Neuropathol Exp Neurol* 1986;45:222–232.
- Myran JA, Nabiyouni M, Zendah M. Development of the brain: a vital role for cerebrospinal fluid. *Can J Physiol Pharmacol* 2003;81:317–328.
- Cutler RW, Page L, Galichich J, Watters GV. Formation and absorption of cerebrospinal fluid in man. *Brain* 1968;91:707–720.
- McComb JG. Recent research into the nature of cerebrospinal fluid formation and absorption. *J Neurosurg* 1983;59:369–383.
- McComb JG. Cerebrospinal fluid physiology of the developing fetus. *Am J Neuroradiol* 1992;13:595–599.
- Artru AA. Spinal cerebrospinal fluid chemistry and physiology. In: Yaksh TL, ed. *Spinal Drug Delivery*. Amsterdam: Elsevier, 1999:177–238.
- Bulat M, Lupret V, Orekhovic D, Klarica M. Transventricular and transspinal absorption of cerebrospinal fluid into cerebral microvessels. *Coll Antropol* 2008;32(Suppl 41):43–50.
- Olivero WC, Rekate HL, Chizek JH, et al. Relationship between intracranial and sagittal sinus pressure in normal and hydrocephalic dogs. *Pediatr Neurosci* 1988;14:196–201.
- McCormick JM, Yamada K, Rekate HL, Miyake H. Time course of intraventricular pressure change in a canine model of hydrocephalus: its relationship to sagittal sinus elastance. *Pediatr Neurosurg* 1992;18:127–133.
- Worthington, Jr W, Cathcart RS III. Ependymal cilia: distribution and activity in the adult human brain. *Science* 1963;139:221–222.
- Cathcart RS, Worthington, Jr W. Ciliary movement in the rat cerebral ventricles: clearing action and direction of currents. *J Neuropathol Exp Neurol* 1964;23:609–618.
- Welch K, Friedman V. The cerebrospinal fluid valves. *Brain* 1960;83:454–469.
- Bosanovic-Sasic R, Mollanji R, Johnston MG. Spinal and cranial contribution to total cerebrospinal fluid transport. *Am J Physiol Regulatory Integrative Comp Physiol* 2001;281:R909–R916.
- Edsberg M, Tisell M, Jacobsson L, Wikkelso C. Spinal CSF absorption in healthy individuals. *Am J Physiol Regul Integr Comp Physiol* 2004;287:R1450–R1455.
- Zenker W, Bankoul S, Braun J. Morphological indications for considerable diffuse reabsorption of cerebrospinal fluid in spinal meninges particularly in the areas of meningeal funnels. An electronmicroscopical study including tracing experiments in rats. *Anat Embryol (Berl)* 1994;189:243–258.
- Greitz D. Radiological assessment of hydrocephalus: new theories and implication for therapy. *Neurosurg Rev* 2004;27:145–165.
- Greitz D, Hannerz J. A proposed model of cerebrospinal fluid circulation: observations with radionuclide cisternography. *Am J Neuroradiol* 1996;17:431–438.

27. Di Rocco C, Pettorossi VE, Caldarelli M, Mancinelli R, Velardi F. Communicating hydrocephalus induced by mechanically increased amplitude of the intraventricular cerebrospinal fluid pressure: experimental studies. *Exp Neurol* 1978;59:40–52.
28. Greitz D, Greitz T, Hindmarsh T. A new view on the CSF circulation with the potential for pharmacological treatment of childhood hydrocephalus. *Acta Paediatr* 1997;1997:125–132.
29. James AE, Strecker EP, Sperber E, et al. An alternative pathway of cerebrospinal fluid absorption in communicating hydrocephalus. *Radiology* 1974;111:143–146.
30. Greitz D. Thesis: *Cerebrospinal fluid circulation and associated intracranial dynamics. A radiologic investigation using MR imaging and radionuclide cisternography*. [Ph. D.], Karolinska Institute, 1993.
31. Greitz D, Wirestam R, Franck A, Nordell B, Thomsen C, Ståhlberg F. Pulsatile brain movement and associated hydrodynamics studied by magnetic resonance imaging. The Monroe-Kellie doctrine revisited. *Neuroradiology* 1992;34:370–380.
32. Johnston M, Zakharov A, Papaiconomou C, Salmasi G, Armstrong D. Evidence of connections between cerebrospinal fluid and nasal lymphatic vessels in humans, non-human primates and other mammalian species. *Cerebrospinal Fluid Res* 2004;1:2.
33. Papaiconomou C, Zakharov A, Azizi N, Djenic J, Johnston M. Reassessment of the pathways responsible for cerebrospinal fluid absorption in the neonate. *Childs Nerv Syst* 2004;20:29–36.
34. Silver I, Li B, Szalai J, Johnston M. Relationship between intracranial pressure and cervical lymphatic pressure and flow rates in sheep. *Am J Physiol* 1999;277:R1712–R1717.
35. Bradbury MWB, Cole DF. The role of the lymphatic system in drainage of cerebrospinal fluid and aqueous humor. *J Physiol* 1980;299:353–365.
36. McComb JG, Hyman S. Lymphatic drainage of cerebrospinal fluid in the primate. In: Johansson BB, Owman C, Widner H, eds. *Pathophysiology of the Blood-Brain Barrier*. Amsterdam: Elsevier, 1990:421–438.
37. McComb JG, Hyman S, Weiss MH. Lymphatic drainage of cerebrospinal fluid in the cat. In: Shapiro K, Marmarou A, Portnoy H, eds. *Hydrocephalus*. New York: Raven, 1984:83–98.
38. Ludemann W, Berens Von Rautenfeld D, Samii M, Brinker T. Ultrastructure of the cerebrospinal fluid outflow along the optic nerve into the lymphatic system. *Childs Nerv Syst* 2004.
39. Fox RJ, Walji AH, Mielke B, Petrucc K, Aronyk KE. Anatomic details of intradural channels in the parasagittal dura: a possible pathway for flow of cerebrospinal fluid [Report]. *Neurosurgery* 1996;39:84–90.
40. Johnston M, Armstrong D, Koh L. Possible role of the cavernous sinus veins in cerebrospinal fluid absorption. *Cerebrospinal Fluid Res* 2007;4:3.
41. Zervas NT, Lisczak TM, Mayberg MR, et al. Cerebrospinal fluid may nourish cerebral vessels through pathways in the adventitia that may be analogous to systemic vasa vasorum. *J Neurosurg* 1982;56:475–481.
42. Oi S, Di Rocco C. Proposal of “evolution theory in cerebrospinal fluid dynamics” and minor pathway hydrocephalus in developing immature brain. *Childs Nerv Syst* 2006;22:662–669.
43. Davis LE. A physio-pathological study of the choroid plexus with the report of a case of villous hypertrophy. *J Med Res* 1924;44:521–534.
44. Hirano H, Hirahara K, Asakura T, et al. Hydrocephalus due to villous hypertrophy of the choroid plexus in the lateral ventricles. *J Neurosurg* 1994;80:321–323.
45. Welch K, Strand R, Bresnan M, et al. Congenital hydrocephalus due to villous hypertrophy of the telencephalic choroid plexuses. *J Neurosurg* 1983;59:172–175.
46. Friede RL. *Developmental Neuropathology*, 2nd ed. Berlin: Springer-Verlag, 1989.
47. Milhorat TH. Classifications of the cerebral edemas with reference to hydrocephalus and pseudotumor cerebri. *Childs Nerv Syst* 1992;8:301–306.
48. Milhorat TH. Hydrocephaly. In: Myrianthopoulos NC, ed. *Malformations*, vol 50. New York: Elsevier, 1987:285–300.
49. Weller RO, Schulman K. Infantile hydrocephalus, clinical, histological, and ultrastructural study of brain damage. *J Neurosurg* 1972;36:255–260.
50. Del Bigio MR. Neuropathological changes caused by hydrocephalus. *Acta Neuropathol* 1993;85:573–585.
51. Del Bigio MR, Wilson MJ, Enno T. Chronic hydrocephalus in rats: humans: white matter loss and behavior changes. *Ann Neurol* 2002;52:337–346.
52. Shirane R, Sato S, Sato K, et al. Cerebral blood flow and oxygen metabolism in infants with hydrocephalus. *Childs Nerv Syst* 1992;8:118–123.
53. Hill A, Volpe JJ. Decrease in pulsatile flow in the anterior cerebral artery in infantile hydrocephalus. *Pediatrics* 1982;69:4–10.
54. Bannister CM, Chapman SA. Ventricular ependyma of normal and hydrocephalic subjects: a scanning electron microscopic study. *Dev Med Child Neurol* 1980;22:725–731.
55. Greitz D, Greitz T. The pathogenesis and hemodynamics of hydrocephalus. *Int J Neuroradiol* 1997;3:367–375.
56. Greitz D, Franck A, Nordell B. On the pulsatile nature of intracranial spinal CSF-circulation demonstrated by MR imaging. *Acta Radiol* 1993;34:1–8.
57. Du Boulay GH. Pulsatile movements in the CSF pathways. *Br J Radiol* 1966;39:255–262.
58. Huang T-Y, Chung H-W, Chen M-Y, et al. Supratentorial cerebrospinal fluid production rate in healthy adults: quantification with two-dimensional cine phase-contrast MR imaging with high temporal and spatial resolution. *Radiology* 2004;233:603–608.
59. de Marco G, Idy-Peretti I, Didon-Poncelet A, Baledent O, Ozen I, Isgro MC. Intracranial fluid dynamics in normal and hydrocephalic states: systems analysis with phase-contrast magnetic resonance imaging. *J Comp Assist Tomogr* 2004;28:247–254.
60. Luetmer PH, Huston J, Friedman J, et al. Measurement of cerebrospinal fluid flow at the cerebral aqueduct by use of phase-contrast magnetic resonance imaging: technique validation and utility in diagnosing idiopathic normal pressure hydrocephalus. *Neurosurgery* 2002;50:534–543.
61. Mase M, Yamada K, Banjo T, Miyachi T, Ohara S, Matsumoto T. Quantitative analysis of CSF flow dynamics using MRI in normal pressure hydrocephalus. *Acta Neurochir Suppl* 1998;71:350–353.
62. Tsunoda A, Mitsuoka H, Bandai H, Endo T, Arai H, Sato T. Intracranial cerebrospinal fluid measurement studies in suspected idiopathic normal pressure hydrocephalus, secondary normal pressure hydrocephalus or brain atrophy. *J Neurol Neurosurg Psychiatry* 2002;73:552–555.
63. Mori K. Current concept of hydrocephalus: evolutions of new classifications. *Childs Nerv Syst* 1995;11:523–532.
64. Hirsch J-F. Consensus: long term outcome in hydrocephalus. *Childs Nerv Syst* 1994;10:64–69.
65. Levigne D, Trop I, Mehta TS, Barnes PD. MR imaging appearance of cerebral ventricular morphology. *Radiology* 2002;223:652–660.
66. Patel MD, Filly RA, Hersh D, Goldstein RD. Isolated mild fetal cerebral ventriculomegaly: clinical course and outcome. *Radiology* 1995;759–764.
67. Simon EM, Goldstein RB, Coakley FV, et al. Fast MR imaging of fetal anomalies in utero. *Am J Neuroradiol* 2000;21:1688–1698.
68. Rousseau GL, McCullough DC, Joseph AL. Current prognosis in fetal ventriculomegaly. *J Neurosurg* 1992;77:551–555.
69. Garel C, Luton D, Oury JF, Gressens P. Ventricular dilatation. *Childs Nerv Syst* 2003;19:517–523.
70. Cavalheiro S, Moron AF, Zymberg ST, SDastoli P. Fetal hydrocephalus: prenatal treatment. *Childs Nerv Syst* 2003;20:7–8.
71. Laurence KM. The pathology of hydrocephalus. *Am J Clin Pathol* 1959;24:388.
72. Warkany J, Lemire RJ, Cohen MM, Jr. *Mental Retardation and Congenital Malformations of the Central Nervous System*. Chicago: Yearbook, 1972.
73. Yakovlev PI. Paraplegias of hydrocephalics. *Am J Ment Defic* 1972;56:561–577.
74. Muñoz A, Hinojosa J, Esparza J. Cisternography and ventriculogram: gadopentate dimeglumine-enhanced MR imaging in pediatric patients: preliminary report. *Am J Neuroradiol* 2007;28:889–894.
75. Iskandar BJ, Sansone JM, Medow J, Rowley HA. The use of quick fast magnetic resonance imaging in the evaluation of shunt-treated hydrocephalus. *J Neurosurg: Pediatrics* 2004;101:147–151.
76. Bradley WG, Jr, Kortman KE, Burgoine B, Eng D. Flowing cerebrospinal fluid in normal and hydrocephalic states: appearance on MR imaging. *Radiology* 1986;159:611–616.

- Sherman JL, Citrin CM, Gangarosa RE, Bowen BJ. The MR appearance of CSF flow in patients with ventriculomegaly. *Am J Neuroradiol* 1986;7:1025–1031.
- Sherman JL, Citrin CM. Magnetic resonance of normal CSF flow. *Am J Neuroradiol* 1986;7:3–6.
- Atlas SW, Mark AS, Fram EK. Aqueductal stenosis: evaluation with gradient echo rapid MR imaging. *Radiology* 1988;169:449–453.
- Emmrich DR, Pelc NJ. Normal flow patterns of intracranial and spinal cerebrospinal fluid defined with phase-contrast cine MR imaging. *Radiology* 1991;178:467–474.
- Levy LM, Di Chiro G. MR phase imaging and cerebrospinal fluid flow in the head and spine. *Neuroradiology* 1990;32:399–406.
- Kitt WR, Bradley WG, Jr, Watanabe AS, et al. Flow dynamics of cerebrospinal fluid: assessment with phase-contrast velocity MR imaging performed with retrospective cardiac gating. *Radiology* 1992;183:395–405.
- Taylor GA, Madsen JR. Neonatal hydrocephalus: hemodynamic response to fontanell compression—correlation with intracranial pressure and need for shunt placement. *Radiology* 1996;201:685–689.
- Filly RA, Goldstein RB. Fetal ventricular atrium: 4th down and 10 mm to go. *Radiology* 1994;193:315–317.
- Garel C, Chantrel E, Sebag G, Brisse H, Elmalah M, Hussan M. Le développement du cerveau foetal: atlas IRM et biométrie. *Editions Sanramps Medical, Montpellier, France*, 2000.
- Girard N, Raybaud C, Poncet M. In vivo MR study of brain maturation in normal fetuses. *Am J Neuroradiol* 1995;16:407–413.
- Gaglioti P, Danelon D, Bontempo S, Mombro M, Cardaropoli S, Todros T. Fetal cerebral ventriculomegaly: outcome in 176 cases. *Ultrasound Obstet Gynecol* 2005;25:372–377.
- Jain MD, Goldstein RB, Tung S, Filly RA. Fetal cerebral ventricular atrium: difference in size according to sex. *Radiology* 1995;194:713–715.
- Vergani P, Locatelli A, Strobelt N, et al. Clinical outcome of mild fetal ventriculomegaly. *Am J Obstet Gynecol* 1998;178:218–222.
- Garel C. *MRI of the Fetal Brain. Normal Development and Cerebral Pathology*. Berlin: Springer, 2004.
- Girard N, Gire C, Sigaoudy S, et al. MR imaging of acquired fetal brain disorders. *Childs Nerv Syst* 2003;19:490–500.
- Griffiths PD, Reeves RJ, Morris JE, et al. A prospective study of fetuses with isolated ventriculomegaly investigated by antenatal sonography and in utero MR imaging. *Am J Neuroradiol* 2010;31.
- Genn O. MR imaging of the fetal brain. *Pediatr Radiol* 2010;40:68–81.
- Beghey M, Ware J, Soul J, et al. Neurodevelopmental outcome of fetuses referred for ventriculomegaly. *Ultrasound Obstet Gynecol* 2010;35:45–46.
- Baker LL, Barkovich AJ. The large temporal horn: MR analysis in developmental brain anomalies versus hydrocephalus. *Am J Neuroradiol* 1992;13:115–122.
- Heinz ER, Ward A, Drayer BP, DuBois PJ. Distinction between obstructive and atrophic dilatation of ventricles in children. *J Comput Assist Tomogr* 1980;4:320–325.
- Sustad O, Skalpe IO, Engeset A. The width of the temporal horn and the differential diagnosis between pressure hydrocephalus and hydrocephalus ex vacuo. *Neurology* 1969;19:1087–1093.
- LeMay M, Hochberg FH. Ventricular differences between hydrostatic hydrocephalus and hydrocephalus ex vacuo by computed tomography. *Neuroradiology* 1979;17:191–195.
- Childe AE, McNaughton FL. Diverticula of the lateral ventricles extending into the posterior fossa. *Arch Neurol Psychiatry* 1942;47:768–778.
- Ishibashi D, Charest D, Porchet F. Pathogenesis and diagnostic pitfalls of ventricular diverticula: case report and review of the literature. *Neurosurgery* 2003;52:209–212; discussion 212.
- Naidich TP, McLone DG, Hahn YS, Hanaway J. Atrial diverticula in severe hydrocephalus. *Am J Neuroradiol* 1982;3:257–266.
- Otsuka S, Takano S, Enomoto T, Ishikawa E, Tsuboi K, Matsumura A. Endoscopic observation of pathophysiology of ventricular diverticulum. *Childs Nerv Syst* 2007;23:897–900.
- Kim CS, Bennett DR, Roberts TS. Primary amenorrhea secondary to noncommunicating hydrocephalus. *Neurology* 1969;19:533–537.
- Barkovich AJ, Newton TH. Aqueductal stenosis: evidence of a broad spectrum of tectal distortion. *Am J Neuroradiol* 1989;10:471–475.
- El Gammal T, Allen MB, Jr, Brooks BS, Mark EK. MR evaluation of hydrocephalus. *Am J Neuroradiol* 1987;8:591–597.
- Rovira A, Capellades J, Grivé E, et al. Spontaneous ventriculostomy: report of three cases revealed by flow-sensitive phase-contrast cine MR imaging. *Am J Neuroradiol* 1999;20:1647–1652.
- Borit A, Sidman RL. New mutant mouse with communicating hydrocephalus and secondary aqueductal stenosis. *Acta Neuropathol* 1972;21:316–331.
- Williams B. Is aqueductal stenosis the result of hydrocephalus? *Brain* 1973;96:399–412.
- Segev Y, Metser U, Beni-Adani L, Elran C, Reider-Groszasser I-I, Constantini S. Morphometric study of the midsagittal MR imaging plane in cases of hydrocephalus and atrophy and in normal brains. *Am J Neuroradiol* 2001;22:1674–1679.
- Fitz CR, Harwood-Nash DC. Computed tomography of hydrocephalus. *Comput Tomogr* 1978;2:91–108.
- Kleinman PK, Zito JL, Davidson RI, Raptopoulos V. The subarachnoid spaces in children: normal variations in size. *Radiology* 1983;147:455–457.
- Gomori JM, Steiner I, Melamed E, Cooper G. The assessment of changes in brain volume using combined linear measurements. A CT scan study. *Neuroradiology* 1984;26:21–24.
- Hahn FJY, Rim K. Frontal ventricular dimensions on normal computed tomography. *Am J Roentgenol* 1976;126:593–596.
- Haug G. Age and sex dependence of the size of normal ventricles on computed tomography. *Neuroradiology* 1977;14:201–204.
- Evans WA. An encephalographic ratio for estimating ventricular enlargement and cerebral atrophy. *Arch Neurol Psych* 1942;47:931–937.
- Gooskens RHJM, Gielen CCAM, Hanlo PW, Faber JA, Willemse J. Intracranial spaces in childhood macrocephaly: comparison of length measurements and volume calculations. *Dev Med Child Neurol* 1988;30:509–519.
- da Silva MC, Michowicz S, Drake JM, Chumas PD, Tuor UL. Reduced local cerebral blood flow in periventricular white matter in experimental neonatal hydrocephalus—restoration with CSF shunting. *J Cereb Blood Flow Metab* 1995;15:1057–1065.
- Leliefeld PH, Gooskens RHJM, Vincken KL, et al. Magnetic resonance imaging for quantitative flow measurement in infants with hydrocephalus: a prospective study. *J Neurosurg Pediatrics* 2008;2:163–170.
- Braun KPJ, Dijkhuizen RM, de Graaf RA, et al. Cerebral ischemia and white matter edema in experimental hydrocephalus: a combined in vivo MRI and MRS study. *Brain Res* 1997;757:295–298.
- Braun KPJ, Gooskens RHJM, Vandertop WP, Tulleken CAF, van der Grond J. 1-H magnetic resonance spectroscopy in human hydrocephalus. *J Magn Reson Imaging* 2003;17:291–299.
- Assaf Y, Ben-Sira L, Constantini S, Chang LC, Beni-Adani L. Diffusion tensor imaging in hydrocephalus: initial experience. *Am J Neuroradiol* 2006;27:1717–1724.
- Ding Y, McAllister JP, Yao B, Yan N, Canady AI. Neuron tolerance during hydrocephalus. *Neuroscience* 2001;106:659–667.
- Humphreys P, Muzumdar DP, Sly LE, Michaud J. Focal cerebral mantle disruption in fetal hydrocephalus. *Pediatr Neurol* 2007;36:236–243.
- Milhorat TH, Hammock MK, Davis DA, Fenstermacher JD. Choroid plexus papilloma: I. Proof of cerebrospinal fluid overproduction. *Childs Brain* 1977;5:273–277.
- Eisenberg HM, McComb JG, Lorenzo AV. Cerebrospinal fluid overproduction and hydrocephalus associated with choroid plexus papilloma. *J Neurosurg* 1974;40:381–385.
- Cinalli G, Sainte-Rose C, Lellouch-Tubiana A, Sebag G, Renier D, Pierre-Kahn A. Hydrocephalus associated with intramedullary low-grade glioma. Illustrative cases and review of the literature. *J Neurosurg* 1995;83:480–485.
- Turkewitsch N. Die Entwicklung des Aqueductus Cerebri des Menschen. *Morphologisches Jahrbuch* 1935;76:421–477.
- Lapras C, Tommasi M, Bret P. Stenosis of the aqueduct of Sylvius. In: Myrianthopoulos NC, ed. *Malformations*, vol 50. New York: Elsevier, 1987:301–322.

129. Sarnat HB. Ependymal reactions to injury. A review. *J Neuropathol Exp Neurol* 1995;54:1–15.
130. Castro-Gago M, Alonso A, Eiris-Punal J. Autosomal recessive hydrocephalus with aqueductal stenosis. *Childs Nerv Syst* 1996;12:188–191.
131. Gabriel RS, McComb JG. Malformations of the central nervous system. In: Menkes JH, ed. *Textbook of Child Neurology*. Philadelphia: Lea and Febiger, 1985:234–253.
132. Woollam DHM, Millen JW. Anatomical considerations in the pathology of stenosis of the cerebral aqueduct. *Brain* 1953;76:104–112.
133. Russell DS. *Observations on the Pathology of Hydrocephalus*. London: His Majesty's Stationery Office, 1949.
134. Raimondi AJ, Clark SJ, McLone DG. Pathogenesis of aqueductal occlusion in congenital murine hydrocephalus. *J Neurosurg* 1976;45:66–77.
135. Boydston WR, Sanford RA, Mauhlauer MS, et al. Gliomas of the tectum and periaqueductal region of the mesencephalon. *Pediatr Neurosurg* 1991–92;17:234–238.
136. Turnbull I, Drake C. Membranous occlusion of the aqueduct of Sylvius. *J Neurosurg* 1966;24:24–33.
137. Schroeder HWS, Gaab MR. Endoscopic aqueductoplasty: technique and results. *Neurosurgery* 1999;45:508–518.
138. Fritsch MJ, Kienke S, Mehndorn HM. Endoscopic aqueductoplasty: stent or not to stent? *Childs Nerv Syst* 2003.
139. Erkildahin Y. Endoscopic aqueductoplasty. *Childs Nerv Syst* 2007;23:143–150.
140. Bickers DS, Adams RD. Hereditary stenosis of the aqueduct of Sylvius as a cause of congenital hydrocephalus. *Brain* 1949;72:246–262.
141. Willems PJ, Dijkstra I, Van der Auwera BJ, et al. Assignment of X-linked hydrocephalus to Xq28 by linkage analysis. *Genomics* 1990;8:367–370.
142. Willems PJ, Vits L, Raeymaekers P, et al. Further localization of X-linked hydrocephalus in the chromosomal region Xq28. *Am J Hum Genet* 1992;51:307–315.
143. Holmes LB, Nash A, ZuRhein GM, et al. X-linked aqueductal stenosis: clinical and neuropathological findings in two families. *Pediatrics* 1973;51:697–704.
144. Viseskul C, Gilbert EF, Opitz JM. X-linked hydrocephalus. Further observations. *Z Kinderheilk* 1975;119:111–121.
145. Fransen E, Schrandt-Stumpel C, Vits L, Coucke P, Van Camp G, Willems PJ. X-linked hydrocephalus and MASA syndrome present in one family are due to a single missense mutation in exon 28 of the L1CAM gene. *Hum Mol Genet* 1994;3:2255–2256.
146. Basel-Vanagaite L, Straussberg R, Friez M, et al. Expanding the phenotypic spectrum of L1CAM-associated disease. *Clin Genet* 2006;69:414–419.
147. Fransen E, Lemmon V, Van Camp G, Vits L, Coucke P, Willems PJ. CRASH syndrome: clinical spectrum of corpus callosum hypoplasia, retardation, adducted thumbs, spastic paraparesis and hydrocephalus due to mutation in one single gene, L1. *Eur J Hum Genet* 1995;3:273–284.
148. Yamasaki M, Thompson P, Lemmon V. CRASH syndrome: mutations in L1CAM correlate with severity of the disease. *Neuropediatrics* 1997;28:175–178.
149. Weller S, Gartner J. Genetic and clinical spectra of X-linked hydrocephalus (L1 disease): Mutations in the L1CAM gene. *Hum Mutat* 2001;18:1–12.
150. Willems PJ, Brouwer OF, Dijkstra I, Wilmink J. X-linked hydrocephalus. *Am J Med Genet* 1987;27:921–928.
151. Varadi V, Csecsei K, Szeifert GT, Toth Z, Papp Z. Prenatal diagnosis of X linked hydrocephalus without aqueductal stenosis. *J Med Genet* 1987;24:207–209.
152. Wong EV, Kenrick S, Willems P, Lemmon V. Mutations in the cell adhesion molecule L1 cause mental retardation. *Trends Neurosci* 1995;18:168–172.
153. Yamasaki M, Arita N, Hiraga S, et al. A clinical and neuroradiological study of X-linked hydrocephalus in Japan. *J Neurosurg* 1995;83:50–55.
154. Jellinger G. Anatomopathology of non-tumoral aqueductal stenosis. *J Neurosurg Sci* 1986;30:1–16.
155. Bouchard S, Davey MG, Rintoul NE, Walsh DS, Rorke LB, Adzick NS. Correction of hindbrain herniation and anatomy of the vermis after in utero repair of myelomeningocele in sheep. *J Pediatr Surg* 2003;38:451–458.
156. Tulipan N, Sutton LN, Bruner JP, Cohen BM, Johnson M, Adzick NS. The effect of intrauterine myelomeningocele repair on the incidence of dependent hydrocephalus. *Pediatr Neurosurg* 2003;38:27–33.
157. Hirsch JF, Pierre-Kahn A, Renier D, Sainte-Rose C, Hoppe-Best L. The Dandy-Walker malformation: a review of 40 cases. *J Neurosurg* 1984;61:515–522.
158. Raimondi AJ, Sato K, Shimoji T. *The Dandy-Walker Syndrome*. Basel: Karger, 1984.
159. Scotti G, Musgrave MA, Fitz CR, Harwood-Nash DC. The isolated fourth ventricle in children: CT and clinical review of 16 cases. *Am J Roentgenol* 1980;135:1233–1238.
160. James HE. Spectrum of the syndrome of the isolated fourth ventricle: posthemorrhagic hydrocephalus of the premature infant. *Pediatr Neurosurg* 1990–1991;16:305–308.
161. Hall TR, Choi A, Schellinger D, Grant EG. Isolation of the fourth ventricle causing transtentorial herniation: neurosonographic findings in premature infants. *Am J Roentgenol* 1992;159:811–815.
162. Owler BK, Jacobson EE, Johnston IH. Lateral recess cysts in two cases of isolated fourth ventricle. *Childs Nerv Syst* 2001;17:363–365.
163. Hamada H, Hayashi N, Kurimoto M, Endo S. Endoscopic aqueduct stenting via the fourth ventricle under navigating system guidance technical note. *Neurosurgery* 2005;56:E206.
164. Gomori JM, Grossman RI, Goldberg HI, Zimmerman RA, Mani LT. Intracranial hematomas: imaging by high field MR. *Radiology* 1985;157:87–93.
165. Gomori JM, Grossman RI, Goldberg HI, et al. High field spin echo MR imaging of superficial and subependymal siderosis secondary to non-intraventricular hemorrhage. *Neuroradiology* 1987;29:339–342.
166. Unger EC, Cohen MS, Brown TR. Gradient echo imaging of hemorrhage at 1.5T. *Magn Reson Imaging* 1989;7:163–167.
167. Ashwal S, Holshouser BA, Tong K. Use of advanced neuroimaging techniques in the evaluation of pediatric traumatic brain injury. *Dev Neurol* 2006;28:309–326.
168. Rippe DJ, Boyko OB, Friedman HS, et al. Gd-DTPA-enhanced MRI imaging of leptomeningeal spread of primary intracranial CNS tumors in children. *Am J Neuroradiol* 1990;11:329–332.
169. Mathews VP, Kuharit MA, Edwards MK, D'Amour PG, Azarni I, Dreesen RG. Gadolinium enhanced MR imaging of experimental bacterial meningitis: evaluation and comparison with CT. *Am J Neuroradiol* 1988;9:1045–1050.
170. Mathews VP, Broome DR, Smith RR, Bognanno JR, Einhorn LH, Edwards MK. Neuroimaging of disseminated germ cell tumors. *Am J Neuroradiol* 1990;11:319–324.
171. Bagley C. Blood in the cerebrospinal fluid. Resultant functional organic alterations in the central nervous system. A. Experimental in Arch Surg 1928;17:18–38.
172. Hughes CP, Gado M. Pathology of hydrocephalus and brain atrophy. In: Newton TH, Potts DG, eds. *Radiology of the Skull and Brain, Vol III: Anatomy and Pathology*. St. Louis: C.V. Mosby, 1977:Chapter 97.
173. Linscott LI, Osborn AG, Blaser S, et al. Pituitary adenoma: expanding the imaging spectrum. *Am J Neuroradiol* 2008;29:1861–1866.
174. Little JR, Dale AJD, Okazaki H. Meningeal carcinomatosis: clinical manifestations. *Arch Neurol* 1974;30:138–143.
175. Kochi M, Miura Y, Takada A, et al. MRI of subarachnoid dissemination of medulloblastoma. *Neuroradiology* 1991;33:264–267.
176. Rosman NP, Shands KN. Hydrocephalus caused by increased intracranial venous pressure: a clinicopathological study. *Ann Neurol* 1976;14:46–51.
177. Kalbag RM, Woolf AL. *Cerebral Venous Thrombosis*. London: Oxford, 1967.
178. Sainte-Rose C, LaCombe J, Peirre-Kahn A, et al. Intracranial venous hypertension: cause or consequence of hydrocephalus in infants? *J Neurosurg* 1984;60:727–736.
179. Epstein F, Hochwald GM, Ransohoff J. Neonatal hydrocephalus from compressive head wrapping. *Lancet* 1973;1:634.
180. Hochwald GM, Epstein F, Malhan C, et al. The role of skull and brain in experimental feline hydrocephalus. *Dev Med Child Neurol* 1975 (Suppl 27): 65–69.

- Shapiro K, Fried A, Takei F, Kohn L. Effect of the skull and dura on neural tissue pressure-volume relationships and CSF hydrodynamics. *J Neurosurg* 1985;63:76-81.
- Shapiro K, Fried A, Maramou A. Biomechanical and hydrodynamic characterization of the hydrocephalic infant. *J Neurosurg* 1985;63:69-75.
- Hecht JT, Butler JJ. Neurologic morbidity associated with achondroplasia. *J Child Neurol* 1990;5:84-97.
- Kao SCS, Waziri MH, Smith WL, Sato Y, Yuh WTC, Franken EA, Jr. MR imaging of the craniocervical junction, cranium, and brain in children with achondroplasia. *Am J Roentgenol* 1989;153:565-569.
- Pappas CTE, Rekate HL. Cervicomedullary junction decompression in a case of Marshall-Smith syndrome. *J Neurosurg* 1991;75:317-319.
- Moss ML. The pathogenesis of artificial cranial deformation. *Am J Phys Anthropol* 1958;16:269-286.
- Moss ML. Functional anatomy of cranial synostosis. *Childs Brain* 1975;1:22-33.
- Gmili G, Sainte-Rose C, Kollar EM, et al. Hydrocephalus and craniosynostosis. *J Neurosurg* 1998;88:209-214.
- Steinbok P, Hall J, Flodmark O. Hydrocephalus in achondroplasia: the possible role of intracranial venous hypertension. *J Neurosurg* 1989;71:42-48.
- Lundar T, Bakke SJ, Nornes H. Hydrocephalus in an achondroplastic child treated by venous decompression at the jugular foramen. Case report. *J Neurosurg* 1990;73:138-140.
- Martinez-Perez D, Vander Woude DL, Barnes PD, Scott RM, Mulliken JB. Jugular foraminal stenosis in Crouzon syndrome. *Pediatr Neurosurg* 1996;25:252-255.
- McLone DG, Partington MD. Arrest and compensation of hydrocephalus. *Neurosurg Clin North Am* 1993;4:621-624.
- Collmann H, Sørensen N, Krauss J. Hydrocephalus in craniosynostosis: a review. *Childs Nerv Syst* 2005;21:125-131.
- Taylor W, Hayward R, Lasjaunias P, et al. Enigma of raised intracranial pressure in patients with complex craniosynostosis: the role of abnormal intracranial venous drainage. *J Neurosurg* 2001;94:377-385.
- Di Rocco C, McLone DG, Shimoji T, Raimondi AJ. Continuous interventricular cerebrospinal fluid pressure recording in hydrocephalic children during wakefulness and sleep. *J Neurosurg* 1975;42:683-689.
- Di Rocco C, Maira G, Rossi G, Vignati A. Cerebrospinal fluid pressure studies in normal pressure hydrocephalus and cerebral atrophy. *Eur Neurol* 1976;14:119-128.
- Stein BM, Fraser RA, Tenner MS. Normal pressure hydrocephalus: complication of posterior fossa surgery in children. *Pediatrics* 1972;49:50-52.
- Burnett GH, Hahn JF, Palmer J. Normal pressure hydrocephalus in children and young adults. *Neurosurgery* 1987;20:904-907.
- Prassopoulos P, Cavouras D, Golfinopoulos S, Nezi M. The size of the intra- and extraventricular cerebrospinal fluid compartments in children with idiopathic benign widening of the frontal subarachnoid space. *Neuroradiology* 1995;37:418-421.
- Bellon CE. CSF dynamics in hydrocephalus—with special attention to external hydrocephalus. *Brain Dev* 1984;6:119-127.
- Briner S, Bodensteiner J. Benign subdural collections of infancy. *Pediatrics* 1980;67:802-804.
- Carolan PL, McLaurin RL, Tobin RB, Tobin JA, Egelhoff JC. Benign extra-axial collections of infancy. *Pediatr Neurosci* 1986;12:140-144.
- Nickel RE, Gallenstein JS. Developmental prognosis for infants with benign enlargement of the subarachnoid spaces. *Dev Med Child Neurol* 1987;29:181-186.
- Karakas AH, Bakratsi E. Benign enlargement of peripheral subarachnoid spaces in twins. *Comput Med Imaging Graph* 2002;26:47-48.
- Kim D, Choi J, Yoon S, Suh J, Kim T. Hypertrophic arachnoid membrane in infantile external hydrocephalus: neuroradiologic and histopathologic correlation. *Radiology* 1993;189(P):195.
- Gordon N. Apparent cerebral atrophy in patients on treatment with steroids. *Dev Med Child Neurol* 1980;22:502-506.
- Ito M, Takao P, Okuno T, Mikawa H. Sequential CT studies of 24 children with infantile spasms on ACTH therapy. *Dev Med Child Neurol* 1983;25:475-480.
- Barkovich AJ, Edwards MSB. Applications of neuroimaging in hydrocephalus. *Pediatr Neurosurg* 1992;18:65-83.
- Maytal J, Alvarez LA, Elkin CM, Shinnar S. External hydrocephalus: radiologic spectrum and differentiation from cerebral atrophy. *Am J Neuroradiol* 1987;8:271-278.
- Wilms G, Vanderschueren G, Demaezel PH, et al. CT and MR in infants with pericerebral collections and macrocephaly: benign enlargement of the subarachnoid spaces versus subdural collections. *Am J Neuroradiol* 1993;14:855-860.
- Chen C-Y, Chou T-Y, Zimmerman RA, Lee C-C, Chen F-H, Faro SH. Pericerebral fluid collection: differentiation of enlarged subarachnoid spaces from subdural collections with color Doppler US. *Radiology* 1996;201:389-392.
- Mori K, Sakamoto T, Nishimura K, Fujiwara K. Subarachnoid fluid collection in infants complicated by subdural hematoma. *Childs Nerv Syst* 1993;9:282-284.
- McNeely PD, Atkinson JD, Saigal G, O'Gorman AM, Farmer JP. Subdural hematomas in infants with benign enlargement of the subarachnoid spaces are not pathognomonic for child abuse. *Am J Neuroradiol* 2006;27:1725-1728.
- Ravid S, Maytal J. External hydrocephalus: a probable cause for subdural hematoma in infancy. *Pediatr Neurol* 2003;28:139-141.
- Galassi E, Tognetti F, Gaist G, et al. CT scan and metrizamide cisternography in arachnoid cysts of the middle cranial fossa: classification and pathophysiological aspects. *Surg Neurol* 1982;17:363-369.
- Naidich TP, McLone DG, Radkowski MA. Intracranial arachnoid cysts. *Pediatr Neurosci* 1986;12:112-122.
- Morris MW, Smith S, Cressman J, Ancheta J. Evaluation of infants with subdural hematoma who lack external evidence of abuse. *Pediatrics* 2000;105:549-553.
- Yamada H, Yokota A, Furuta A, Horie A. Reconstitution of shunted mantle in experimental hydrocephalus. *J Neurosurg* 1992;76:856-862.
- Wright LC, McAllister JP, II, Katz SD, et al. Cytological and cytoarchitectural changes in the feline cerebral cortex during experimental infantile hydrocephalus. *Pediatr Neurosurg* 1990-1991;16:139-155.
- Greitz D. Paradigm shift in hydrocephalus research in legacy to Dandy's pioneering work: rationale for third ventriculostomy in communicating hydrocephalus. *Childs Nerv Syst* 2007;23:487-489.
- Teo C, Jones R. Management of hydrocephalus by endoscopic third ventriculostomy in patients with myelomeningocele. *Pediatr Neurosurg* 1996;25:57-63.
- Drake JM, Canadian Pediatric Neurosurgery Study Group. Endoscopic third ventriculostomy in pediatric patients: the Canadian experience. *Neurosurgery* 2007;60:881-886.
- Warf BC, Campbell JW. Combined endoscopic third ventriculostomy and choroid plexus cauterization as primary treatment of hydrocephalus for infants with myelomeningocele: long-term results of a prospective intent-to-treat study in 115 East African infants. *J Neurosurg Pediatr* 2008;2:310-316.
- Warf BC, Kulkarni AV. Intraoperative assessment of cerebral aqueduct patency and cisternal scarring: impact on success of endoscopic third ventriculostomy in 403 African children. *J Neurosurg Pediatr* 2010;5:204-209.
- Crosby RM, Henderson CM, Paul RL. Catheterization of the cerebral aqueduct for obstructive hydrocephalus in infants. *J Neurosurg* 1973;38:596-601.
- Miki T, Nakajima N, Wada J, Haraoka J. Indications for neuroendoscopic aqueductoplasty without stenting for obstructive hydrocephalus due to aqueductal stenosis. *Minim Invasive Neurosurg* 2005;48:136-141.
- Fischbein NJ, Ciricillo SF, Barr RM, et al. Endoscopic third ventriculostomy: MR assessment of patency with 2D cine phase-contrast versus T2 weighted fast spin echo technique. *Pediatr Neurosurg* 1998;28:70-78.
- Kim S-K, Wang K-C, Cho B-K. Surgical outcome of pediatric hydrocephalus treated by endoscopic third ventriculostomy: prognostic factors and interpretation of postoperative neuroimaging. *Childs Nerv Syst* 2000;16:161-169.
- St George E, K N, Sgouros S. Changes in ventricular volume in hydrocephalic children following successful endoscopic third ventriculostomy. *Childs Nerv Syst* 2004.

230. Lev S, Bhadelia RA, Estin D, Heilman CB, Wolpert SM. Functional analysis of third ventriculostomy patency with phase contrast MRI velocity measurements. *Neuroradiology* 1997;39:175-179.
231. Hoffmann K, Lehmann T, Baumann C, Felix R. CSF flow imaging in the management of third ventriculostomy with a reversed fast imaging with steady-state precession sequence. *Eur Radiol* 2003;13:1432-1437.
232. Faillace WJ, Canady AJ. Cerebrospinal fluid shunt malfunction signaled by new or recurrent seizures. *Childs Nerv Syst* 1990;6:37-40.
233. Forbes K, Pipe J, Karis J, Farthing V, Heiserman J. Brain imaging in the unsedated pediatric patient: comparison of periodically rotated overlapping parallel lines with enhanced reconstruction and single-shot fast spin-echo sequences. *Am J Neuroradiol* 2003;24:794-798.
234. Patel M, Klufas R, Alberico R, Edelman R. Half-fourier acquisition single-shot turbo spin-echo (HASTE) MR: comparison with fast spin-echo MR in disease of the brain. *Am J Neuroradiol* 1997;18:1635-1640.
235. Pipe J. Motion correction with PROPELLER MRI: application to head motion and free-breathing cardiac imaging. *Magn Reson Med* 1999;42: 963-969.
236. Sugahara T, Korogi Y, Hirai T, et al. Comparison of HASTE and segmented-HASTE sequences with a T2-weighted fast spin-echo sequence in the screening evaluation of the brain. *Am J Roentgenol* 1997;169:1401-1410.
237. Oi S, Matsumoto S. Infantile hydrocephalus and the slit ventricle syndrome in early infancy. *Childs Nerv Syst* 1987;3:145-150.
238. Epstein F, Lapras C, Wisoff JH. "Slit ventricle syndrome": Etiology and treatment. *Pediatr Neurosci* 1988;14:5-10.
239. May CH, Aurisch R, Kornrumpf D, Vogel S. Evaluation of shunt function in hydrocephalic patients with the radionuclide 99m Tc-pertechnetate. *Childs Nerv Syst* 1999;15:239-245.
240. Evans RC, Thomas MD, Williams LA. Shunt blockage in hydrocephalic children. The use of the valvogram. *Clin Radiol* 1976;27:489.
241. Guertin SR. Cerebrospinal fluid shunts. Evaluation, complications, and crisis management. *Pediatr Clin North Am* 1987;34:203-217.
242. Howman-Giles R, McLaughlin A, Johnston I, Whittle I. A radionuclide method of evaluating shunt function and CSF circulation in hydrocephalus. Technical note. *J Neurosurg* 1984;61:604-605.
243. Sweeney LE, Thomas PS. Contrast examination of cerebrospinal fluid malfunction in infancy and childhood. *Pediatr Radiol* 1987;17:177-183.
244. Martin AJ, Drake JM, Lemaire C, Henkelman RM. Cerebrospinal fluid shunts: flow measurements with MR imaging. *Radiology* 1989;173:243-247.
245. Castillo M, Hudgins PA, Malko JA, Burrow BK, Hoffman JC, Jr. Flow-sensitive MR imaging of ventriculoperitoneal shunts: in vitro findings, clinical applications, and pitfalls. *Am J Neuroradiol* 1991;12:667-672.
246. Norbush A, Pelc N, Shimakawa A, Enzmann D. Shunt flow measurement and evaluation of valve oscillation with a spin-echo phase-contrast MR sequence. *Radiology* 1994;190:560-564.
247. Minns RA, Brown JK, Engleman HM. CSF production rate: "real time" estimation. *Z Kinderchir* 1987;47:36-40.
248. Sgouros S, Malluci C, Walsh AR, Hockley AD. Long term complications of hydrocephalus. *Pediatr Neurosurg* 1995;23:127-132.
249. Drake JM, Kestle JRW, Tuli S. CSF shunts 50 years on—past, present and future. *Childs Nerv Syst* 2000;16:800-804.
250. Casey A, Kimmings E, Kleinlugtebeld A, Taylor W, Harkness W, Hayward R. The long term outlook for hydrocephalus in childhood. *Pediatr Neurosurg* 1997;27:63-70.
251. Vinchon M, Lemaitre M, Vallee L, Dhellembes P. Late shunt infection incidence, pathogenesis, and therapeutic implications. *Neurology* 2002;33:160-173.
252. Lewis AJ, Keiper GL, Crone KR. Endoscopic treatment of isolated hydrocephalus. *J Neurosurg* 1995;82:780-785.
253. Lee K, Bae W, Bae H, Yun I. The fate of traumatic subdural hygroma: serial computed tomography scans. *J Korean Med Sci* 2003;18:56-59.
254. Falhauer K, Schmitz P. Overdrainage phenomena in shunt treated hydrocephalus. *Acta Neurochir (Wien)* 1978;45:89-101.
255. Emery JL. Intracranial effects of long-standing decompression of the brain in children with hydrocephalus and meningomyelocele. *Dev Med Child Neurol* 1965;7:302-309.
256. Destian S, Heier LA, Zimmerman RD, et al. Differentiation between venous fibrosis and chronic subdural hematoma after ventricular shunting: value of enhanced CT and MR scans. *Am J Neuroradiol* 1997;18: 1021-1026.
257. Rekate HL. Classification of slit-ventricle syndrome using intraventricular pressure monitoring. *Pediatr Neurosurg* 1993;19:15-20.
258. Hyde-Rowan MD, Rekate HL, Nulsen FE. Reexpansion of previously collapsed ventricles: the slit ventricle syndrome. *J Neurosurg* 1982; 53:536-539.
259. Epstein FJ, Fleisher AS, Hochwald GM, Ransohoff J. Subtemporal craniectomy for recurrent shunt obstruction secondary to mid-ventricular obstruction. *J Neurosurg* 1974;41:29-31.
260. Epstein FJ, Hochwald GM, Wald A, Ransohoff J. Avoidance of dependency in hydrocephalus. *Dev Med Child Neurol* 1975;35:71-7.
261. Bruce DA, Weprin B. The slit ventricle syndrome. *Neurology* 1983;36: 709-717.
262. Serlo W, Heikkilä E, Saukkonen A-L, Wendt L. Classification and management of the slit ventricle syndrome. *Childs Nerv Syst* 1985;1:16-18.
263. Benzel EC, Reeves JD, Kesterson L, Hadden TA. Slit ventricle syndrome in children: clinical presentation and treatment. *Acta Neurochir (Wien)* 1992;117:7-14.
264. Di Rocco C. Is the slit ventricle syndrome always a slit ventricle syndrome? *Childs Nerv Syst* 1994;10:49-58.
265. Forghani R, Farb RI. Diagnosis and temporal evolution of idiopathic intracranial hypotension on MRI of the brain. *Neuroradiology* 2004; 1025-1034.
266. Caldarelli M, Novegno F, Di Rocco C. A late complication of CSF bypass: acquired Chiari I malformation. *Childs Nerv Syst* 2000;16:41-45.
267. Chumas PD, Armstrong DC, Drake JM, et al. Tonsillar herniation through the foramen magnum rather than the exception after lumbo-peritoneal shunting in the pediatric population. *J Neurosurg* 1993;78:568-573.
268. Di Rocco C, Velardi F. Acquired Chiari I malformation managed by supratentorial enlargement. *Childs Nerv Syst* 2003;19:800-807.
269. Davidson RI. Peritoneal bypass in the treatment of hydrocephalus: historical review of abdominal complications. *J Neurol Neurosurg Psychiatry* 1976;39:640-648.
270. Elisevich K, Mattar A, Cheeseman F. Biodegradation of distal shunt catheters. *Pediatr Neurosurg* 1994;21:71-76.
271. Citrin CM, Hammock MK. Computed tomographic representation of granulomatous reaction from intraventricular shunt. *Comput Tomogr* 1979;3:177-180.